THE UNIVERSITY OF CHICAGO

PARTICLE PHYSICS AND COSMOLOGY IN SUPERSYMMETRIC MODELS

A DISSERTATION SUBMITTED TO
THE FACULTY OF THE DIVISION OF THE PHYSICAL SCIENCES
IN CANDIDACY FOR THE DEGREE OF
DOCTOR OF PHILOSOPHY

DEPARTMENT OF PHYSICS

BY

DAVID EDGAR MORRISSEY

CHICAGO, ILLINOIS

AUGUST 2005

To my family.

ABSTRACT

The Standard Model (SM) of particle physics provides an excellent description of the elementary particle interactions observed in particle collider experiments, but the model does less well when it is applied to cosmology. Recent measurements of the Universe over very large distances indicate the existence of non-luminous dark matter and an excess of baryons over anti-baryons. The SM is unable to account for either of these results, implying that an extension of the SM description is needed. One such extension is supersymmetry. Within the minimal supersymmetric version of the SM, the MSSM, the lightest superpartner particle can make up the dark matter, and the baryon asymmetry can be generated by the mechanism of electroweak baryogenesis (EWBG). In this work, we examine these issues together in order to find out whether the MSSM can account for both of them simultaneously. We find that the MSSM can explain both the baryon asymmetry and the dark matter, but only over a very constrained region of the model parameter space. The strongest constraints on this scenario come from the lower bound on the Higgs boson mass, and the upper bound on the electric dipole moment of the electron. Moreover, upcoming experiments will probe the remaining allowed parameter space in the near future. Some of these constraints may be relaxed by going beyond the MSSM. With this in mind, we also investigate the nMSSM, a minimal singlet extension of the MSSM. We find that this model can also explain both the dark matter and the baryon asymmetry.

ACKNOWLEDGEMENTS

This thesis would not have been possible without the help and support of many people. I would especially like to thank my family, to whom this work is dedicated. My supervisor, Carlos Wagner, also played an essential role. His guidance, patience, and deep understanding of particle physics got me started in the field, while his enthusiasm and good humour made my time working with him a lot of fun. I'd also like to thank my friends for the good times, and for reminding me that there is much more to life than physics. Finally, I am grateful the many others who helped me along the way, including my collaborators and my thesis committee.

TABLE OF CONTENTS

LIST OF FIGURES

LIST OF TABLES

CHAPTER 1
INTRODUCTION

The goal of particle physics is to describe the workings of the very small. Indeed, the study of Nature at ever tinier scales has revealed a set of seemingly fundamental building blocks. These *elementary particles* interact with each other to give rise to the world we see. For the past century, the primary way that elementary particles have been studied is through their scattering with each other. As the particle collision energy is increased, shorter and shorter distances can be probed. This had led to the construction of large particle collider machines such as the Tevatron at Fermilab, and the soon-to-be-finished Large Hadron Collider (LHC) at CERN. These gigantic microscopes accelerate particles to energies in excess of 1 TeV (10^{12} *electron Volts*) before smashing them into each other. The resulting debris provides clues about what kinds of particles were involved in the collision, and how these particles interacted with each other.

Based on the results of a great number of particle collider experiments, as well as the data from many smaller scale experiments, a model of elementary particles has been devised. This model, the *Standard Model* (SM) of particle physics, is remarkably successful. It accounts for all known elementary particles, and provides an excellent description of the forces by which they interact. The SM is a *gauge field theory* based on the symmetry group $SU(3)_c \times SU(2)_L \times U(1)_Y$. In gauge theories, forces between the elementary particles are dictated by the symmetry group. In the SM, the $SU(3)_c$ part of the group corresponds to the *strong* force that holds nuclei together, while the $SU(2)_L \times U(1)_Y$ part of the symmetry group describes *electroweak* interactions. These include the *weak* force responsible for beta-decay, as well as the more familiar *electromagnetic* force.

Recent developments in *cosmology*, the study of the Universe over the very largest of scales, have provided new tools with which to study elementary particles. Even though the connections between these two fields have long been important, the very rapid improvement in many cosmological measurements over the past decade has strengthened these bonds even further. In several cases, these measurements have provided information about elementary particles beyond what has been deduced from collider experiments. Two of the most important examples of this are the existence of *dark matter* and the *baryon-antibaryon* asymmetry. Both of these results suggest that there is more to particle physics than what is described by the SM.

Dark matter is matter that doesn't give off light, so it can't be observed directly with telescopes. Instead, its presence has been deduced indirectly in several ways such as by measuring the rotational velocities of galaxies and by studying the *Cosmic Microwave Background Radiation* (CMB). These experiments indicate that dark matter makes up about one-quarter of the energy density of the Universe. The best candidate for the dark matter is a stable, massive, neutral, weakly-interacting particle. The nature of the dark matter is therefore a question of particle physics. Unfortunately, no such particle has yet

been observed in a collider experiment, and none of the species in the SM have the necessary properties.

Of the visible matter in the Universe, nearly all of it (by mass) consists of *baryons*, in the form of protons and neutrons. The total density of baryons has been measured by studying the CMB, and by comparing the light element abundances to the theoretical predictions of *Big Bang Nucleosynthesis* (BBN). In both cases, baryons are found to make up about five percent of the total energy density of the Universe. However, only baryons, not anti-baryons, are observed in large quantities. This imbalance is called the *baryon asymmetry of the Universe*. Within the SM, this asymmetry is curious; the model treats matter and anti-matter on a nearly equal footing, with CP-violation being the only thing that distinguishes between them, and there doesn't seem to be enough CP-violation in the SM to generate such a large matter/anti-matter asymmetry.

There are also good theoretical reasons to extend the Standard Model description of particle physics. Most importantly, the SM has nothing to say about how gravity works, and a consistent quantum theory of gravity has yet to be found. Even so, the effects of gravity are generally believed to be negligible at the energies probed by modern collider experiments. A second more pressing theoretical puzzle is the *gauge hierarchy problem*. This problem arises if we try to extrapolate the SM to energies E above the electroweak scale, of about 100 GeV. At these energies, the model becomes unstable under quantum corrections which tend to push the electroweak scale up to the value $E/4\pi$ unless the parameters of the model are very carefully adjusted. In general, the amount of fine-tuning needed is of order $(4\pi \times 100 \text{ GeV}/E)^2$. While there is nothing wrong with this in principle, it is difficult to understand why it should be the case.

One way to resolve the cosmological and gauge hierarchy problems is to add *supersymmetry* to the Standard Model. Supersymmetry is an extension of the Poincaré symmetries of spacetime that exchanges bosons and fermions. With this symmetry, extensions of the SM can be extrapolated to energies well above the electroweak scale without the need for fine-tuning because of cancellations between the quantum corrections induced by fermions and bosons. Remarkably, the minimal supersymmetric extension of the Standard Model, the MSSM, can also explain the baryon asymmetry, and contains an excellent dark matter candidate. In the MSSM, each type of particle in the SM gets a corresponding *superpartner* particle differing in spin by half a unit. The lightest superpartner particle is stable, and can account for the dark matter provided it is neutral. The MSSM also contains new sources of CP-violation compared to the SM, and these can help generate the baryon asymmetry of the Universe.

In this thesis, we shall investigate the dark matter and the baryon asymmetry within supersymmetric extensions of the Standard Model. The first few chapters contain introductory material relevant to the original work described in the later chapters. In particular, Chapter 2 deals with the main theoretical tools used in particle physics side of this endeavour, and contains a description of the Standard Model and its minimal supersymmetric extension, the MSSM. In Chapter 3, we review some aspects of cosmology. Chapter 4 deals with dark matter, and describes the techniques used to calculate dark matter densities. Baryogenesis is the subject of Chapter 5. Here, we describe the requirements and some

of the mechanisms for generating the baryon asymmetry. We pay special attention to the mechanism of *electroweak baryogenesis*, in which the baryon asymmetry is created during the electroweak phase transition since this is the mechanism that is relevant to the MSSM. The sixth and seventh chapters describe the original research upon which this thesis is based. Chapter 6 consists of an investigation of baryogenesis and dark matter within the MSSM. It is based on the work in reference [1]. In Chapter 7, we investigate the same issues in the nMSSM, an extension of the MSSM containing an additional singlet superfield. This chapter is based on the paper of [2].

CHAPTER 2
PARTICLE PHYSICS AND SUPERSYMMETRY

The language of the SM is quantum field theory (QFT), which combines quantum mechanics and special relativity within a single self-consistent framework. It is precisely what its name suggests: the quantum mechanical theory of a system whose physical degrees of freedom are those of a field. Within QFT, each elementary particle is represented by a quantum field. At first glance, this seems strange. Particles are point-like and discrete, while fields tend to be smooth. But this is only a figment of our intuition about classical fields. When quantum mechanics is included, particles emerge as the quanta of their corresponding fields.

The Standard Model is based on a particular type of QFT, a *gauge field theory* [3]. Gauge theories are intimately linked with symmetry groups. The defining property of a gauge field theory is that it is invariant under spacetime-dependent transformations of a corresponding symmetry group. The requirement of gauge invariance almost completely determines the structure of the field theory, and in particular, fixes the possible interactions between the fields. As a result, the nature of the fundamental forces is dictated by the underlying gauge symmetry. Even though the SM agrees quite well with experiment, there are good reasons to look at theories that extend the SM description. Supersymmetry is a particularly interesting way to do so. By enlarging the SM to include supersymmetry, one obtains a quantum field theory which can be consistently extrapolated to very high energies in a natural way.

In this chapter we will discuss some of the ideas behind and features of the Standard Model and its supersymmetric extensions. Section 2.1 contains a brief outline of gauge field theories, which are the foundation upon which the SM is built. In Section 2.2, we will describe the Standard Model itself. Supersymmetry, and its application to particle physics, including the minimal supersymmetric extension of the SM, will be covered in Section 2.3. More details about the general aspects of quantum field theory can be found in the excellent textbooks [4–8], as well as the review article [9]. An additional discussion of some topics in QFT that we will use later on, as well as a list of our notational conventions, is contained in Appendix A.

2.1 Gauge Field Theories

Gauge field theories have proven to be an invaluable tool for describing the fundamental forces of nature. Indeed, all four of the known forces emerge, at least classically, from gauge theories. A gauge theory is a field theory that is invariant under the action of a spacetime-dependent symmetry group. To maintain invariance under the local *gauge transformations*, it is necessary to introduce a vector *gauge field* that transforms inhomogeneously under the group. These gauge fields are a generalization of the electric and magnetic potentials encountered in electromagnetism. The invariance of the theory under the gauge transformations then fixes (or at least severely restricts) the form of the possible interactions between the fields in the theory.

To construct a field theory with the desired invariance property, it is convenient to define the theory in terms of a *Lagrangian*. (See Appendix A for more details.) The reason why is that if the Lagrangian is invariant under a given symmetry group, it is often the case that the corresponding QFT will be invariant as well. Thus, the first step in constructing gauge field theories is to find a gauge invariant Lagrangian. This will be the subject of Section 2.1.1. Section 2.1.2 will briefly describe a few of the subtleties that arise in formulating a quantum field theory based on a gauge invariant Lagrangian. Finally, in Section 2.1.3 we will cover some of the interesting features of the vacuum structure of gauge theories.

2.1.1 Gauge Invariance

We wish to construct a field theory Lagrangian that is invariant under the spacetime-dependent transformations of a symmetry group G. The most important class of symmetry groups (for particle physics) are the compact Lie groups, so we will focus on these [10]. We will also assume that the fields in the theory transform linearly under finite-dimensional, unitary representations of G. Thus, if ψ is a field multiplet transforming under the representation r of the group, the action of the group on this multiplet is

$$\psi \to U(x)\psi, \tag{2.1}$$

with

$$U(x) = e^{i\alpha^a t_r^a}, \quad \text{and} \quad U^\dagger = U^{-1}, \tag{2.2}$$

where $\alpha^a(x)$ is a spacetime-dependent group parameter, and t_r^a denote the generators of the corresponding representation. Note that the t_r^a must be Hermitian and the $\alpha^a(x)$ real for the representation to be unitary. Since G is a Lie group, these generators satisfy

$$[t_r^a,\ t_r^b] = i\, f^{abc} t_r^c, \tag{2.3}$$

where the f^{abc} are the completely anti-symmetric *structure constants* of the group. We will choose a normalization for the generators such that

$$tr(t_r^a\, t_r^b) = C(r)\delta^{ab}, \tag{2.4}$$

with $C(r) = 1/2$ for the fundamental representation.

The kinetic term in the Lagrangian for a free fermion field is

$$\mathscr{L}_{kin-\psi} = i\bar{\psi}\gamma^\mu\partial_\mu\psi. \tag{2.5}$$

This term is invariant under the group action only when α^a is independent of x. When the α^a do vary with x, the derivative of the fermion field transforms as

$$\begin{aligned} \partial_\mu\psi &\rightarrow \partial_\mu(U\psi) \\ &= (\partial_\mu U)\,\psi + U(\partial_\mu\psi). \end{aligned} \tag{2.6}$$

The first term is the problematic one that doesn't cancel. Instead, to obtain invariance under local group transformations, we need a derivative operator that transforms covariantly, $D_\mu\psi \rightarrow U(D_\mu\psi)$. This is not too hard to construct. Consider the ansatz $D_\mu = \partial_\mu + B_\mu$. This operator, acting on ψ, will be covariant provided

$$B_\mu \rightarrow B'_\mu = U\,B_\mu U^\dagger - (\partial_\mu U)\,U^\dagger. \tag{2.7}$$

It is sufficient for B_μ to take on values in the group representation, so we can write (choosing an arbitrary normalization)

$$B_\mu = i\,g\,A^a_\mu\,t^a_r. \tag{2.8}$$

The factor g is called the *gauge coupling*.

Now, if we are to avoid breaking Lorentz invariance by introducing a fixed four-vector, the quantities A^a_μ must be interpreted as a set of quantum fields. These are the *gauge fields* we alluded to above. For them to be dynamical, they need a kinetic term which should also be gauge-invariant. One way to construct such a kinetic term is to note that, as an operator, D_μ goes to $U\,D_\mu U^\dagger$ under the group action. Thus, so too does the commutator of two D_μ's,

$$[D_\mu,\ D_\nu] \rightarrow U[D_\mu,\ D_\nu]U^\dagger. \tag{2.9}$$

On the other hand, this commutator depends only on the gauge fields,

$$\begin{aligned} [D_\mu,\ D_\nu] &= [\partial_\mu + i\,g\,t^a_r A^a_\mu,\ \partial_\nu + i\,g\,t^a_r A^a_\nu] \\ &= i\,g\,t^a_r\,(\partial_\mu A^a_\nu - \partial_\nu A^a_\mu - g\,f^{abc}A^b_\mu A^c_\nu) \\ &:= i\,g\,t^a_r\,F^a_{\mu\nu}. \end{aligned} \tag{2.10}$$

In the last line, we have introduced the *field strength* $F^a_{\mu\nu}$. It transforms in the same way as the commutator $[D_\mu, D_\nu]$ under gauge transformations, and is an obvious generalization of the field strength tensor encountered in classical electrodynamics. Continuing with this

analogy, a sensible gauge-invariant kinetic term for the A^a_μ gauge fields is

$$\begin{aligned} \mathscr{L}_{kin-A} &= -\frac{1}{4\,C(r)}\; tr(t^a_r F^a_{\mu\nu}\; t^b_r F^{\mu\nu\; b}) \\ &= -\frac{1}{4}\; F^a_{\mu\nu}\; F^{\mu\nu\; a}. \end{aligned} \tag{2.11}$$

Notice that since $F \to UFU^\dagger$, the trace $tr(FF)$ is gauge invariant.

Putting the pieces together, the full Lagrangian is

$$\mathscr{L} = -\frac{1}{4}\; F^a_{\mu\nu}\; F^{\mu\nu\; a} + i\,\bar{\psi}\gamma^\mu D_\mu \psi, \tag{2.12}$$

where

$$\begin{aligned} D_\mu\psi &= (\partial_\mu + ig\,A^a_u t^a_r)\psi, \\ F^a_{\mu\nu} &= \partial_\mu A^a_\nu - \partial_\nu A^a_\mu - g\,f^{abc} A^b_\mu A^c_\nu. \end{aligned} \tag{2.13}$$

With only the fermion and the gauge boson fields, these are the only possible operators with dimension less than or equal to four that respect both Lorentz and gauge invariance.[1] In particular, we see that the interactions between ψ and the gauge fields are fixed by the symmetries. A complex boson field could also be included by adding the kinetic term

$$\mathscr{L}_\phi = (D_\mu\phi)^\dagger D_\mu \phi, \tag{2.14}$$

with a similar expression for the covariant derivative as above. There can also be additional *Yukawa* interactions between the fermions and bosons, of the form $\bar{\psi}\psi'\phi$, provided they are gauge-invariant as well.

2.1.2 The Quantum Gauge Theory

The Lagrangian of Eq. (2.12) defines a classical, gauge invariant field theory. If the gauge group is $U(1)_{em}$ and the ψ field represents the electron, it is simply the Lagrangian for classical electrodynamics (up to a mass term for the electron). However, when it comes to formulating the quantum field theory based on this Lagrangian, one encounters a number related difficulties having to do with gauge invariance. Due to the gauge invariance, it is not possible to write a mass term for the gauge fields, and as a result, the vector boson gauge field corresponds to a massless spin-1 particle. Such a particle has two independent (polarization) degrees of freedom. On the other hand, the gauge field seems to have four Lorentz components. This mismatch causes trouble when one tries to construct the gauge field propagator. To do so, one inverts the portion of the Lagrangian that is quadratic in

[1] Or almost. There's also a term of the form $\tilde{F}F$. This possibility will be discussed below.

the gauge fields. After integrating by parts in the action, this is given by

$$\mathscr{L} \supseteq -\frac{1}{2} A^a_\mu (-\eta^{\mu\nu}\partial^2 + \partial^\mu \partial^\nu) A^a_\nu. \tag{2.15}$$

Unfortunately, this operator has no inverse since it annihilates any gauge field of the form $A^a_\mu = \partial_\mu \Lambda^a$.

Since these problems were the result of gauge invariance, it is perhaps not surprising that gauge invariance also provides a solution. Recall that in (classical) electrodynamics the scalar and vector potentials are not regarded as physical degrees of freedom because they depend on the choice of gauge. Instead, the components of the field strength, the electric and magnetic fields, are the quantities observed experimentally. This suggests that for gauge theories in general, gauge fields that are related by a local gauge transformation should be interpreted as being physically equivalent configurations.

To avoid dealing with this redundancy in the description, it is convenient to work in a particular gauge. A popular choice is the Lorentz gauge,

$$\partial^\mu A^a_\mu = 0. \tag{2.16}$$

This condition doesn't completely fix the gauge, but it is enough to allow us to find a propagator for the gauge fields. Applying the condition to Eq. (2.15), the quadratic operator becomes $-\eta^{\mu\nu}\partial^2$, which is invertible. The most convenient way to accommodate a gauge fixing constraint is to formulate the quantum theory in terms of the path integral formalism. In this formalism, the constraint is incorporated by the *Faddeev-Popov* procedure [11]. From this procedure one obtains an effective gauge-fixed Lagrangian containing additional gauge-fixing terms, as well as new *ghost* fields. The gauge fixing terms enforce the particular gauge condition chosen, while the ghost fields contribute in loop diagrams to maintain gauge invariance [8].

A further bump in the road to construct a quantum gauge theory is the issue of *anomalies*. In most cases, if the Lagrangian defining a field theory is invariant under a particular symmetry group, the full quantum theory based on this Lagrangian will be invariant under that symmetry as well. But this is not always the case, and when the quantum theory doesn't respect a symmetry of the Lagrangian that symmetry group is said to be anomalous. For regular symmetries, this just means that the apparent symmetry isn't really a symmetry at all. For gauge theories, the situation is much more serious because gauge field configurations related by the gauge symmetry are taken to be physically equivalent. If the symmetry is broken by an anomaly, this interpretation is no longer possible, and the whole structure of the gauge theory falls apart. Therefore, the gauge symmetries in a gauge field theory must be anomaly-free for the theory to be self-consistent.

2.1.3 Gauge Theory Vacua and Instantons

Another interesting feature of gauge theories is their vacuum structure. Gauge theories based on *non-Abelian* gauge groups have many physically distinct, degenerate vacua [12].

These vacua are separated by energy barriers of finite height [13–15], which means that in the quantum mechanical theory, a system prepared in one vacuum can pass to another vacuum by tunnelling [16]. The gauge field configurations that describe this tunnelling are called *instantons*. These will be important to us later on because, as we shall see, they provide a means to violate baryon number, an essential ingredient for baryogenesis.

A vacuum state of a field theory is a static field configuration with minimal energy. Consider a pure gauge theory in the gauge $A_0^a = 0$. The energy functional in this gauge is given by [7, 17]

$$E[A] = \int d^3x \, \frac{1}{4} \, F_{ij}^a F^{a\,ij}. \tag{2.17}$$

Since this expression is positive-definite in F, any vacuum solution (in this gauge) must satisfy

$$F_{ij}^a = 0. \tag{2.18}$$

One obvious solution is $A_i^a = 0$, but it is not the only one. Suppose we make a time-independent gauge transformation of the vacuum solution. This will preserve both the gauge, and the $F_{ij}^a = 0$ condition. Using Eqs. (2.7) and (2.8), we obtain

$$A_\mu = 0 \to U A_\mu U^\dagger + \frac{i}{g} (\partial_\mu U) \, U^\dagger, \tag{2.19}$$

where $U(\vec{x})$ is an element of the gauge group, and $A_\mu = A_\mu^a t_r^a$ for some representation r. Thus, any gauge field configuration of the form

$$\begin{aligned} A_0 &= 0, \\ A_i &= \frac{i}{g} \, (\partial_i U) \, U^\dagger. \end{aligned} \tag{2.20}$$

is a vacuum state. It may be shown that this is the most general solution of Eq. (2.18). Note that these configurations are determined entirely by the position-dependent group element $U(\vec{x}) \in G$.

For consistency, $U(\vec{x})$ must have the same limit in all directions as $||\vec{x}|| \to \infty$ [15]. As a result, we may identify all points at spatial infinity. The gauge theory vacua of Eq. (2.20) therefore define maps from position-space to group space,

$$S^3 \to G; \qquad \vec{x} \mapsto U(\vec{x}), \tag{2.21}$$

where S^3 denotes the three-sphere.[2]

Now suppose the gauge group G is $SU(2)$. Since this group is topologically equivalent to S^3, the map corresponding to Eq. (2.21) also defines a map $S^3 \to S^3$. Such maps can be grouped into distinct topological classes characterized by the number of times the map wraps S^3 about itself. This integer-valued wrapping number is called the *Pontryagin index*

[2]Note that $\mathbb{R}^3$ with points at infinity identified is equivalent to the three-sphere S^3.

or *Chern-Simons number*, and is given in terms of $U(\vec{x})$ by the expression [13]

$$N_{cs} = \frac{1}{24\pi^2}\int d^3x\,\epsilon_{ijk}\,\mathrm{Tr}\left[(\partial_\mathrm{i}\mathrm{U})\mathrm{U}^\dagger\,(\partial_\mathrm{j}\mathrm{U})\mathrm{U}^\dagger\,(\partial_\mathrm{k}\mathrm{U})\mathrm{U}^\dagger\right] \in \mathbb{Z}. \tag{2.22}$$

Since N_{cs} is an integer, it is not possible to change this number by continuously deforming the group-valued function $U(\vec{x})$. This will be the reason why the gauge theory has many degenerate vacua.

So far, Eq. (2.20) is just a gauge-transformed version of the trivial vacuum. Since gauge field configurations related by a gauge transformation are physically equivalent, it is not immediately obvious that there exists more than one vacuum. To see that there are many vacua, consider two vacuum configurations defined by U's with different topological indices, and suppose that the first vacuum configuration, U_-, describes the system at time $t \to -\infty$, while the second, U_+, describes the system as $t \to +\infty$. Now, if these two vacua are physically equivalent, it follows that it is possible to pass from one vacuum state to the other while maintaining both the vacuum condition, $F^a_{ij} = 0$, and the choice of gauge, $A^0 = 0$. To do so, there must exist a gauge group valued function $U(t, \vec{x})$ such that

$$\begin{aligned} U(t \to -\infty, \vec{x}) &\to U_-(\vec{x}), \\ U(t \to +\infty, \vec{x}) &\to U_+(\vec{x}). \end{aligned} \tag{2.23}$$

This function must also vary *adiabatically* with t in order to maintain the $A^0 = 0$ gauge, and so $U(t)$ must pass *smoothly* from U_- to U_+. But this is impossible because these configurations belong to different topological classes. Therefore, the configurations U_- and U_+ describe physically distinct vacuum states.

Two more points are worth making. The first is that if U_+ and U_- lie in the same topological class, it is possible to construct a $U(t)$ of the form described above. The second point is that by making a time-independent gauge transformation with U_-^{-1}, the $t \to -\infty$ vacuum becomes the trivial one, $U_- \to \mathbb{I}$ for which $A_i = 0$, while the $t \to \infty$ vacuum becomes $U_+ \to (U_-)^{-1}U_+$. This vacuum has topological index $(n_+ - n_-)$, where n_+ and n_- are the topological indices of U_+ and U_-. Thus, the topological index of a single vacuum is unphysical because it depends on the gauge, but the *difference* in the topological indices of two vacua is gauge-invariant and physical.

In the discussion above we have concentrated on the $G = SU(2)$ case. Things go through in exactly the same way if G is any non-Abelian Lie group because any such group is built of $SU(2)$ subgroups, and it is always possible to reparametrize the group such that the map $S^3 \to G$ is confined completely to one these $SU(2)$ subgroups [14]. On the other hand, if G is an Abelian group it can be shown that all maps $S^3 \to G$ are topologically equivalent. The vacuum of an Abelian gauge theory is therefore unique.

The distinct gauge vacua in non-Abelian gauge theories are separated by energy barriers of finite height [13]. This is illustrated in Fig. 2.1. Because the energy barriers are finite, in the quantum version of the gauge theory a system prepared in one vacuum state can pass to another vacuum state by tunnelling. The gauge field configurations that describe this tunnelling are called *instantons*. These are particularly interesting when the gauge

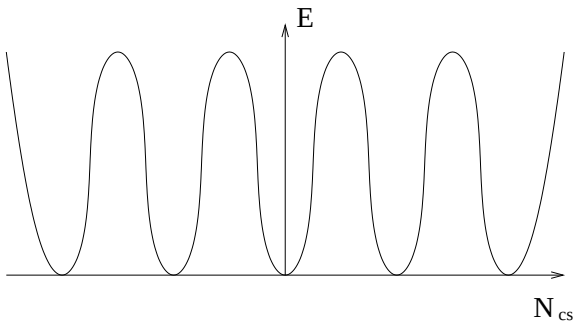

Figure 2.1: Vacuum structure in a non-Abelian gauge theory.

theory includes fermions because each instanton transition is accompanied by the creation or destruction of fermions. This feature will be discussed in more detail in Section 5.2, and will play an essential role in models of baryogenesis.

Even though the degenerate vacua found above have minimal energy, they can't be the true ground states of the theory because they depend on the gauge. In general, if U_m is a gauge transformation with topological index $m \in \mathbb{Z}$, and $|n\rangle$ is a vacuum state with index n, then under the action of the gauge transformation,

$$U_m \, |n\rangle = |m + n\rangle \, . \tag{2.24}$$

Instead, the true ground states should be invariant up to a possible phase. They are therefore given by

$$|\theta\rangle = \sum_{n=-\infty}^{+\infty} e^{-i\theta \, n} \, |n\rangle \, , \tag{2.25}$$

with $0 \leq \theta < 2\pi$. Each value of θ defines a distinct *θ-vacuum*. For a system with vacuum $|\theta\rangle$, the effect of summing over the different topological sectors leads to an additional term in the effective Lagrangian [13],

$$\mathscr{L} \to \mathscr{L} - \frac{\theta}{32\pi^2} F^a_{\mu\nu} \tilde{F}^{\mu\nu \, a}, \tag{2.26}$$

where

$$\tilde{F}^{\mu\nu \, a} = \frac{1}{2} \epsilon^{\mu\nu\alpha\beta} F^a_{\alpha\beta}. \tag{2.27}$$

This term can be shown to be a total divergence which implies that it does not alter the perturbative expansion of theory. As a result, we will (mostly) neglect it in what follows.

2.2 The Standard Model

The Standard Model (SM) is a gauge theory based on the gauge group $SU(3)_c \times SU(2)_L \times U(1)_Y$. (See Ref. [18] and references therein.) The $SU(3)_c$ part of the group describes the *strong* interactions, while the $SU(2)_L \times U(1)_Y$ part corresponds to the *electroweak* interactions. The latter subgroup is reduced to $U(1)_{em}$ by spontaneous symmetry breaking.

2.2.1 Field Content

For each simple subgroup of the gauge group there is a set of gauge bosons:

$$\begin{aligned} G^a_\mu &\leftrightarrow SU(3)_c \\ W^a_\mu &\leftrightarrow SU(2)_L \\ B_\mu &\leftrightarrow U(1)_Y. \end{aligned} \tag{2.28}$$

We will denote the corresponding field strengths by $G^a_{\mu\nu}$, $W^a_{\mu\nu}$, and $B_{\mu\nu}$, and the gauge couplings as g_3, g_2, and g_1.[3] The other fields in the model are the three generations of chiral fermions and a single complex boson doublet. They are listed in Table 2.1, in four-component notation, along with their quantum numbers under the gauge groups. We also list the *baryon* and *lepton* numbers of each species. The chiral fermions all carry a generational index, $i = 1,\ 2,\ 3$. For the leptons, these represent $e^i = (e, \mu, \tau)$ and $\nu_i = (\nu_e, \nu_\mu, \nu_\tau)$, while for the quarks, $u^i = (u, c, t)$ and $d^i = (d, s, b)$ respectively. Φ is the Higgs boson doublet.

	$SU(3)_c \times SU(2)_L \times U(1)_Y$	B	L
$Q^i = \binom{u^i_L}{d^i_L}$	(3, 2, 1/6)	1/3	0
u^i_R	(3, 1, 2/3)	1/3	0
d^i_R	(3, 1, -1/3)	1/3	0
$L^i = \binom{\nu^i_L}{e^i_L}$	(1, 2, -1/2)	0	1
e^i_R	(1, 1, -1)	0	1
$\Phi = \binom{\phi^+}{\phi^0}$	(1, 2, 1/2)	0	0

Table 2.1: Quantum numbers of the SM fields.

The Lagrangian for these fields can be split into three distinct parts:

$$\mathscr{L} = \mathscr{L}_{gauge} + \mathscr{L}_{yuk} + \mathscr{L}_{higgs}. \tag{2.29}$$

[3] We will also sometimes write $\alpha_i = g_i^2/4\pi$.

The first piece, $\mathscr{L}_{gauge}$ contains the gauge boson and matter field kinetic terms. These have the form of Eqs. (2.12) and (2.14), and are completely fixed by gauge invariance. For example, the part involving the Q field reads

$$\begin{aligned}\mathscr{L}_{gauge} &\supseteq i\,\bar{Q}\gamma^{\mu}D_{\mu}Q \\ &= i\,\bar{Q}\gamma^{\mu}(\partial_{\mu}+i\,g_3\,t^a_{SU(3)}G^a_{\mu}+i\,g_2 t^d_{SU(2)}W^d_{\mu}+i\,g_1\,\frac{1}{6}B_{\mu})Q.\end{aligned} \tag{2.30}$$

The second piece, $\mathscr{L}_{yuk}$, describes the Yukawa interactions between the fermion fields and the Higgs bosons. Explicitly,

$$\mathscr{L}_{yuk} = -y_u^{ij}\bar{Q}^i\tilde{\Phi}u_R^j - y_d^{ij}\bar{Q}^i\Phi d_R^j - y_e^{ij}\bar{L}^i\Phi\, e_R^j + h.c., \tag{2.31}$$

where $(h.c.)$ denotes the Hermitian conjugate, and we have defined

$$\tilde{\Phi} = i\sigma^2\Phi = \begin{pmatrix}\phi^{0*}\\ -\phi^-\end{pmatrix}. \tag{2.32}$$

$\mathscr{L}_{yuk}$ contains all possible terms consistent with gauge invariance, and in particular, the Yukawa couplings in this expression, y_f^{ij}, may be complex. The last piece, $\mathscr{L}_{higgs}$, is a potential for the Higgs boson,

$$\mathscr{L}_{higgs} = -V_{higgs} = \mu^2\Phi^{\dagger}\Phi - \frac{\lambda}{4}(\Phi^{\dagger}\Phi)^2. \tag{2.33}$$

2.2.2 Spontaneous Symmetry Breaking and Mass Eigenstates

Even though the SM Lagrangian is invariant under $SU(3)_c \times SU(2)_L \times U(1)_Y$, only a subset of this symmetry is manifest at low energies. This is due to the phenomenon of *spontaneous symmetry breaking* (SSB), in which the vacuum state does not respect the full symmetry of the theory [19]. SSB plays a crucial role in the SM, and among other things, is responsible for generating the masses of all the fermions.

Within the SM, SSB is induced by the Higgs boson. From Eq. (2.33), we see that the potential for the Higgs boson is minimum when

$$\Phi^{\dagger}\Phi = v^2 = \frac{2\mu^2}{\lambda}. \tag{2.34}$$

This condition defines a set of vacuum states which may be transformed into each other by $SU(2)_L \times U(1)_Y$ gauge transformations. To make sense of the model in perturbation theory, it is necessary to expand about a particular vacuum. By an astute choice of the $SU(2)_L \times U(1)_Y$ gauge, we may choose this vacuum configuration of the Higgs doublet to be

$$\langle\Phi\rangle = \begin{pmatrix}0\\ v\end{pmatrix}. \tag{2.35}$$

Since the configuration is not invariant under $SU(2)_L \times U(1)_Y$, this symmetry will be *hidden*

in the low-energy theory. However, not all of the electroweak symmetry is lost. Note that the $U(1)_{em}$ subgroup of $SU(2)_L \times U(1)_Y$ generated by

$$Q = t^3 + Y \tag{2.36}$$

leaves the vacuum invariant. This unbroken subgroup is precisely the symmetry group of electromagnetism, for which the effective coupling constant is

$$e = \frac{g_1 g_2}{\sqrt{g_1^2 + g_2^2}}. \tag{2.37}$$

The effects of expanding about the vacuum of Eq. (2.35) are most obvious in the *unitarity gauge*. Within this gauge,

$$\Phi = \begin{pmatrix} 0 \\ v + h/\sqrt{2} \end{pmatrix}. \tag{2.38}$$

with h a real scalar field describing quantum fluctuations about the vacuum. The corresponding particle is the *Higgs boson*. Using this expansion in $\mathscr{L}_{higgs}$, the Higgs boson mass is

$$m_h = \sqrt{\lambda}\, v. \tag{2.39}$$

Similarly, inserting the expansion for Φ into $\mathscr{L}_{gauge}$, the kinetic term for the Higgs field generates mass terms for the $SU(2)_L$ and $U(1)_Y$ gauge bosons. Upon diagonalizing the resulting mass matrices, the mass eigenstates are found to be

$$\begin{aligned} A_\mu &= \sin\theta_w\, W_\mu^3 + \cos\theta_w\, B^0; & M_A^2 &= 0 \\ Z_\mu^0 &= \cos\theta_w\, W_\mu^3 - \sin\theta_w\, B^0; & M_Z^2 &= \frac{g_1^2 + g_2^2}{2} v^2 \\ W_\mu^\pm &= \frac{1}{\sqrt{2}}(W_\mu^1 \mp i W_\mu^2); & M_W^2 &= \frac{g_2^2}{2} v^2. \end{aligned} \tag{2.40}$$

where we have defined the weak mixing angles

$$\cos\theta_w = \frac{g_2}{\sqrt{g_1^2 + g_2^2}}, \qquad \sin\theta_w = \frac{g_1}{\sqrt{g_1^2 + g_2^2}}. \tag{2.41}$$

The massless A_μ field is the photon, while the Z_μ^0 and $W_\mu^\pm$ states are the massive gauge bosons.

Mass terms for the fermions are generated when the Higgs expansion is inserted in $\mathscr{L}_{yuk}$. If the Yukawa couplings in Eq. (2.32) were real and diagonal, the masses would be given by

$$m_f = y_f\, v \tag{2.42}$$

where y_f is the relevant Yukawa coupling. In practice, the Yukawa couplings turn out to be both non-diagonal and complex. Upon diagonalizing the resulting flavor-space mass matrix, one obtains mass terms of the form of Eq. (2.42), as well as a flavor-changing

coupling between the quarks and the W boson, given by

$$\frac{g_2}{\sqrt{2}} V_{CKM}^{ij} \bar{u}_L^i \gamma^\mu W_\mu^+ d_L^j + (h.c.), \tag{2.43}$$

where V_{CKM} is the *Cabbibo-Kobayashi-Maskawa* mixing matrix [20, 21]. This matrix is unitary, and can be parametrized by three real mixing angle and one complex phase, which provides the only source of CP violation in the SM.[4]

2.3 Supersymmetry

Supersymmetry (SUSY) is a symmetry that relates bosons and fermions. It is the maximal extension of the Poincaré symmetries of spacetime that still produces interesting dynamics [23–25]. In quantum field theory, particles emerge as the quanta of fields, with the spin of the particle corresponding to the particular representation of the Poincaré group under which the field transforms. SUSY extends this idea, combining fields with different spins within a single representation of the symmetry. The particles related to the fields in each of these representations have the same masses and coupling and constants [26]. Moreover, the total number of bosonic degrees of freedom is equal to the net number of fermionic degrees of freedom within each supermultiplet.

There is more than one type of supersymmetry. The types differ in the number N of supersymmetry generators. We will focus on the minimal $N = 1$ variety since this is the only kind of supersymmetry that allows for chiral fermions in four dimensions, an essential ingredient in the SM. The ($N = 1,\ d = 4$) supersymmetry algebra consists of the usual Poincaré generators along with the Grassmann-valued supersymmetry generators Q_α, and $Q^\dagger_{\dot{\beta}}$, where the subscripts are Weyl spinor indices. These obey the anticommutation relations

$$\begin{aligned} \{Q_\alpha, Q_\beta\} &= \{Q^\dagger_{\dot{\alpha}}, Q^\dagger_{\dot{\beta}}\} = 0, \\ \{Q_\alpha, Q^\dagger_{\dot{\beta}}\} &= 2\,\sigma^\mu_{\alpha\dot{\beta}}\, P_\mu, \end{aligned} \tag{2.44}$$

where P_μ is the 4-momentum generator.

As for the Poincaré group, it is possible to represent the supersymmetry algebra on quantum fields. The particular representations are called *supermultiplets*, and are made up of component fields with different spins. Only two kinds of superfields are needed to reproduce the particle content of the SM. The fermions and Higgs bosons of the SM can be embedded in *chiral multiplets*, which consist particles with spins $s = 0$ and $s = 1/2$. The gauge bosons must be placed in *vector multiplets*, which have components of spin $s = 1/2$ and $s = 1$. In both types of multiplets, the component fields transform under the same representation of the gauge group, and have the same mass.

[4]The θ term for the $SU(3)_c$ group provides a second source of CP violation. However, it is constrained to be very small, $\theta \lesssim 10^{-9}$ by the experimental limit on the electric dipole moment of the neutron [22] We will therefore neglect its effects here. (See also Section 2.1.3)

Since degenerate particles with different spins have not been observed, SUSY can't be an exact symmetry. Even so, supersymmetry could still be realized in Nature as a *softly* broken symmetry; one that is hidden at low energies, but present at high energies. The great difficulty in constructing models with broken supersymmetry is that it is not known how the supersymmetry breaking should be induced. The minimal supersymmetric extension of the Standard Model is the MSSM. It contains all the particles of the SM as well as the smallest possible number of superpartners. Supersymmetry breaking is accounted for in the MSSM by including the most general possible set of soft SUSY breaking couplings. Unfortunately, this introduces many undetermined parameters into the model.

In this section, we will give a brief description of those aspects of supersymmetry that we will use later on. For a more detailed account of these topics the reader should consult the many excellent reviews [27–30], as well as the standard textbooks [25, 26].

2.3.1 Chiral Multiplets

Each chiral multiplet can be described by a *chiral superfield*, Φ_i, where i is a flavor index [26, 27]. The components of such a superfield are

$$\Phi_i = (\phi_i,\ \psi_i,\ F_i), \tag{2.45}$$

with ϕ_i a complex scalar, ψ_i a Weyl fermion, and F_i an *auxiliary* complex scalar field with mass dimension 2. As will be seen below, the auxiliary fields are non-dynamical, and do not correspond to any particle. The most general (renormalizable) SUSY-invariant kinetic term for the components of the chiral multiplet is

$$\mathscr{L}_{\chi-kin} = (\partial_\mu \phi_i)^*(\partial^\mu \phi_i) + i\psi_i^\dagger \bar{\sigma}^\mu \partial_\mu \psi_i + F_i^* F_i. \tag{2.46}$$

Since F_i does not have any derivative terms, its equation of motion will be an algebraic constraint. It is in this sense that the F_i are auxiliary; they could be removed from the beginning by imposing the appropriate constraints.

All supersymmetric interactions between chiral superfields, including mass terms, can be encoded in the *superpotential* $W(\Phi_i)$. It must be a holomorphic function of the Φ_i (*i.e.* depending on Φ but not Φ^*). Given a superpotential $W(\Phi)$, the corresponding interaction terms in the Lagrangian are

$$\mathscr{L}_{\chi-int} \ = \ \left.\frac{\partial W}{\partial \phi_i}\right|_\phi F_i \ - \ \frac{1}{2}\left.\frac{\partial^2 W}{\partial \Phi_i \Phi_j}\right|_\phi \psi_i \psi_j \ + \ (h.c.), \tag{2.47}$$

where $|_\phi$ implies the replacement $\Phi_i \to \phi$ in the resulting function.

The total supersymmetric Lagrangian for the chiral superfield components is the sum of the kinetic and the interaction terms. The equation of motion for F_i^* is therefore

$$F_i^* = \left.\frac{\partial W}{\partial \Phi_i}\right|_\phi . \tag{2.48}$$

Applying this constraint to the Lagrangian, the terms involving the F_i fields become

$$F_i^* F_i + \left.\frac{\partial W}{\partial \Phi_i}\right|_\phi F_i + h.c. \;\rightarrow\; \sum_i \left|\frac{\partial W}{\partial \Phi_i}\right|_\phi^2. \tag{2.49}$$

This is a positive-definite potential for the scalars ϕ_i.

2.3.2 Vector Multiplets and Gauge Invariance

A vector multiplet can be represented by a vector superfield V satisfying the constraint $V^\dagger = V$. When V includes a gauge field, its components are [26, 27]

$$V = (\lambda^a,\ A_\mu^a,\ D^a) \tag{2.50}$$

with λ^a a Weyl fermion, A_μ^a the gauge field, and D^a a real scalar auxiliary field of dimension two. The superscript a denotes the adjoint index of the gauge group, and all the components of the supermultiplet transform under this representation. The most general renormalizable, gauge and SUSY invariant Lagrangian involving these component fields is [26] [5]

$$\mathscr{L}_{vec} = -\frac{1}{4} F_{\mu\nu}^a F^{\mu\nu\ a} + i\lambda^{a\dagger}\bar{\sigma}^\mu (D_\mu \lambda)^a + \frac{1}{2} D^a D^a. \tag{2.51}$$

Here, D_μ denotes the gauge-covariant derivative. Its action on the λ field is

$$(D_\mu \lambda)^a = \partial_\mu \lambda^a - g f^{abc} A_\mu^b \lambda^c, \tag{2.52}$$

for a gauge coupling g, and structure constants f^{abc}. Note that for this Lagrangian, the equation of motion for the auxiliary field is just $D^a = 0$.

To reproduce the SM matter fields, we need chiral multiplets that transform under the gauge group. It is easy to modify the chiral superfield Lagrangian, $\mathscr{L}_\chi$, so that it is invariant under gauge transformations. This is done by allowing only gauge-invariant terms in the superpotential and by replacing the ordinary derivatives of the component fields with gauge-covariant derivatives,

$$\partial_\mu \rightarrow D_\mu = \partial_\mu + ig\, A_\mu^a\, t^a, \tag{2.53}$$

where t^a is the generator of the gauge group representation of the field upon which the derivative operator acts. This modification alone produces a Lagrangian that is not invariant under supersymmetry. Supersymmetry can be restored by including additional cross-terms that couple the chiral and vector multiplets. These are [26, 27]

$$\mathscr{L}_{cross} = -\sqrt{2} g \left[(\phi_i^* t_{ij}^a \psi_j)\lambda^a + \lambda^{a\dagger}(\psi_i^\dagger t_{ij}^a \phi_j)\right] + g\,(\phi_i^* t_{ij}^a \phi_j) D^a. \tag{2.54}$$

[5] As in the non-supersymmetric case, we could also add a θ-term here. See Section 2.1.3.

With these cross-terms, the equation of motion for the auxiliary field D^a becomes

$$D^a = -g\,(\phi_i^* t_{ij}^a \phi_j). \tag{2.55}$$

Plugging this in for D^a and including the corresponding F-terms, the bosonic potential becomes

$$\begin{aligned} V_{bosons} &= V_F + V_D \\ &= F_i^* F_i + \frac{1}{2} D^a D^a \\ &= \sum_i \left| \frac{\partial W}{\partial \Phi_i} \right|_\phi^2 + \frac{1}{2}\, g^2\, (\phi_i^* t_{ij}^a \phi_j)^2. \end{aligned} \tag{2.56}$$

Again, this is positive definite.

2.3.3 Supersymmetry Breaking

Using the supersymmetric Lagrangian $\mathscr{L}_{SUSY}$ presented above, one finds that the Weyl fermion *gauginos*, λ^a, are massless, and the chiral field components ϕ_i and ψ_i are degenerate in mass. These features must be avoided in order to construct realistic models, and the only way to do so is to break supersymmetry. Unfortunately, breaking SUSY usually ruins the attractive properties that motivated this symmetry in the first place. However, if the only relevant supersymmetry breaking terms have dimension less than four, and therefore come with a dimensionful coupling of size M_{SUSY}, the nice features of SUSY will be regained at energies above this scale [31]. In particular, if $M_{SUSY} \sim 1$ TeV, supersymmetry will ensure the stability of the electroweak scale. Supersymmetry breaking of this sort is said to be *soft*. Following this rule, the most general set of soft supersymmetry breaking terms is [27, 31] [6]

$$\mathscr{L}_{soft} = -\frac{1}{2}(M_\lambda \lambda^a \lambda^a + h.c.) - m_{\phi\ ij}^2 \phi_i^* \phi_j - (b^{ij}\phi_i\phi_j + a^{ijk}\phi_i\phi_j\phi_k + h.c.). \tag{2.57}$$

The origin of the SUSY breaking terms is a mystery, and while there are many models for how they might emerge, none of them are entirely compelling. Most of them fall into the categories of *gravity mediation* or *gauge mediation* [27, 32]. In both types, the models consist of a *visible sector* containing the particles of the SM, along with a *hidden sector* in which the supersymmetry breaking actually takes place. The hidden and visible sectors only couple weakly with each other, and as a result, the low-energy theory of the visible sector is fairly insensitive to the details of SUSY breaking. Unfortunately, this property also limits the predictivity of these models.

Before describing the gauge and gravity mediation mechanisms, it is worthwhile to point

[6] In addition to those quoted here, terms of the form $\phi^*\phi\phi$ are soft in the absence of gauge singlet fields. However, they are conventionally neglected, and we will follow this trend here [27].

out a couple of general facts about supersymmetry breaking. From the supersymmetry algebra, Eq. (2.44), we see that $\{Q, Q^\dagger\} \sim P^0$. Now, if a state is invariant under SUSY, it must be annihilated by the SUSY generators, $Q\,|\psi\rangle = 0$. It follows that

$$\langle\psi|\, P^0\, |\psi\rangle = \|\, Q\,|\psi\rangle\,\|^2 \geq 0. \tag{2.58}$$

In particular, a non-zero vacuum energy implies that (global) supersymmetry is broken. The tree-level vacuum energy is determined by the bosonic potential, and for a theory built from chiral and vector superfields, it is given by

$$V_{tree} = F_i^* F_i + \frac{1}{2} D^a D^a, \tag{2.59}$$

which is positive-definite in both F_i and D^a, and shows that SUSY is broken if and only if

$$\langle F_i\rangle \neq 0, \quad \text{or} \quad \langle D^a\rangle \neq 0. \tag{2.60}$$

These two possibilities are called F- and D-term breaking, respectively. Most phenomenologically viable models rely on F-term breaking.

Gravity mediated models are based on supergravity, the supersymmetric generalization of general relativity. Supergravity emerges automatically if one promotes global supersymmetry to a local (gauge) symmetry [26, 29, 33]. The corresponding gauge field is the spin-2 *graviton*, and is accompanied by a spin-3/2 superpartner, the *gravitino*. The supergravity Lagrangian for the graviton and gravitino is necessarily non-renormalizable, involving operators of dimension greater than four suppressed by powers of the Planck mass, $M_{\rm Pl}$. Thus, there is no reason not to include higher dimensional ($d > 4$) operators, also suppressed by powers of $M_{\rm Pl}$, for the visible and hidden sector fields as well. The key feature of gravity mediated models is that the visible and hidden sectors interact with each other only through these higher dimensional, M_{Pl}-suppressed operators. If SUSY is broken in the hidden sector by an F-term VEV, soft (and only soft) supersymmetry breaking interactions of order

$$m_{soft} \sim \frac{\langle F\rangle}{M_{Pl}} \tag{2.61}$$

are generated in the visible sector. This SUSY breaking also generates a gravitino mass of the same size,

$$m_{3/2} \sim \frac{\langle F\rangle}{M_{Pl}}. \tag{2.62}$$

To get $m_{soft} \sim 1000$ GeV, $\sqrt{\langle F\rangle}$ should be of order 10^{10} GeV.

Due to the large number of possible operators connecting the visible and hidden sectors, gravity mediation models do not give very definite predictions for the soft breaking terms. A much more predictive variant of gravity-mediated models is *anomaly mediation* [34, 35] in which the visible and hidden sectors are completely separated from each other, at least to a very high order. SUSY breaking in the hidden sector is communicated to the visible sector through the *superconformal anomaly* of supergravity. This contribution is already present

in gravity-mediated models, but its effects are usually suppressed relative to the others. Unfortunately, one of the definite predictions of anomaly mediation is negative masses for the scalar superpartners of the lepton fields, which tend to induce the breaking of $U(1)_{em}$.

In gauge mediated models of SUSY breaking, the visible and hidden sectors interact through ordinary gauge interactions [36, 37]. In this case, SUSY breaking in the hidden sector is transferred to the visible sector by loop diagrams that connect the two sectors. If the hidden sector masses are at scale M_h, the soft masses in the visible sector are of order [27]

$$m_{soft} \sim \frac{g^2}{16\pi}\frac{\langle F\rangle}{M_h}. \tag{2.63}$$

For $\langle F\rangle \sim M_h$, we need $\sqrt{\langle F\rangle} \sim 10^5$ GeV to get $m_{soft} \sim 1000$ GeV. Models with gauge mediation tend to be somewhat more predictive than gravity mediated models, but there is still a considerable freedom in specifying the hidden sector. Furthermore, if we assume that supergravity is present at high energies, these lower values for $\langle F\rangle$ lead to very light gravitinos, whose masses are still given by Eq. (2.62), which can be problematic phenomenologically.

2.4 The MSSM

Given the success of the Standard Model, it is expected that any extension of the SM should reproduce the particle content and the gauge structure of the model at low energies. The simplest supersymmetric model that accomplishes this is the *Minimal Supersymmetric Standard Model* (MSSM). This model is also consistent with the current experimental data.

In the MSSM, the Standard Model fermions are embedded in chiral multiplets, while the gauge bosons become members of vector multiplets. As a result, the MSSM contains bosonic *sfermion* superpartners of the fermions, and Weyl fermion *gaugino* superpartners for the gauge bosons. The Higgs sector can't be extended quite so easily. Instead, the single Higgs doublet of the SM must be replaced by a pair of Higgs doublets with $Y = \pm 1/2$. Each of these are members of a chiral superfield, and are therefore accompanied by Weyl fermion *higgsinos*. There are two reasons why a pair of Higgs doublets are needed. First, if there was only a single Higgs doublet, the corresponding *higgsino* would generate a gauge anomaly. Second, the Yukawa interactions in the MSSM are determined by the superpotential, which must be holomorphic in the superfields. Consequently, it is no longer possible to use a single Higgs doublet to give masses to both the up and down type quarks since this would require complex conjugating the Higgs field, as in Eq. (2.32).

2.4.1 Field Content

The chiral superfield content of the MSSM is shown in Table 2.2. We have omitted the flavor indices, but just like the SM there are three generations of fermions, and now sfermions as well. This table also shows the notation used for the component fermions and sfermions, and for the Higgs bosons and higgsinos. Here, the c superscript and the L and R subscripts are a part of the names of the particles. For instance, the U^c is a superfield whose Weyl

fermion component is the *left-handed* spinor $u_R^\dagger$, and whose complex boson component is $\tilde{u}_R^*$. However, since $(u_R^\dagger)^\dagger := u_R$ is a right-handed spinor, this name is apt. Table 2.3 shows the vector superfield content of the MSSM, as well as the notation used for the component gauge bosons and Weyl fermion gauginos.

	$SU(3)_c \times SU(2)_L \times U(1)_Y$	Fermions	Bosons	B	L
$Q = \binom{U_L}{D_L}$	(3, 2, 1/6)	u_L, d_L	$\tilde{u}_L, \tilde{d}_L$	1/3	0
U^c	($\bar{3}$, 1, -2/3)	$u_R^\dagger$	$\tilde{u}_R^*$	-1/3	0
D^c	($\bar{3}$, 1, 1/3)	$d_R^\dagger$	$\tilde{d}_R^*$	-1/3	0
$L = \binom{\nu_L}{E_L}$	(1, 2, -1/2)	ν_L, e_L	$\tilde{\nu}_L, \tilde{e}_L$	0	1
E^c	(1, 1, 1)	$e_R^\dagger$	$\tilde{e}_R^*$	0	-1
$H_2 = \binom{H_2^+}{H_2^0}$	(1, 2, 1/2)	$\tilde{h}_2^+, \tilde{h}_2^0$	h_2^+, h_2^0	0	0
$H_1 = \binom{H_1^0}{H_1^-}$	(1, 2, -1/2)	$\tilde{h}_1^0, \tilde{h}_1^-$	h_1^0, h_1^-	0	0

Table 2.2: Chiral superfields in the MSSM.

	$SU(3)_c \times SU(2)_L \times U(1)_Y$	Fermions	Bosons	B	L
G^a	(8, 1, 0)	$\tilde{G}^a$	G_μ^a	0	0
W^d	(1, 3, 0)	$\tilde{W}^d$	W_μ^d	0	0
B	(0, 0, 1)	$\tilde{B}$	B_μ	0	0

Table 2.3: Vector superfields in the MSSM.

Because of the joint requirements of gauge invariance and supersymmetry, the supersymmetric part of the Lagrangian is completely determined once we specify the superpotential.[7] It is given by

$$W_{MSSM} = -y_u^{ij} H_2 \cdot Q_i \, U_j^c + y_d^{ij} H_1 \cdot Q_i D_j^c + y_e^{ij} H_1 \cdot L_i \, E_j^c - \mu \, H_1 \cdot H_2, \tag{2.64}$$

where $i, j = 1, 2, 3$ are generational indices, and $A \cdot B = \epsilon^{ab} A_a B_b$ denotes the antisymmetric contraction of $SU(2)_L$ indices.[8]

[7] We are implicitly neglecting non-renormalizable terms.

[8] ϵ^{ab} is the completely antisymmetric tensor with $\epsilon^{12} = 1$.

Unlike the SM Lagrangian, the MSSM superpotential of Eq. (2.64) does not contain every possible operator consistent with gauge invariance. The gauge invariant operators that are not included in the superpotential, such as $L\cdot Q\, U^c$, are omitted because they would be inconsistent with experimental observations. All of these dangerous operators can be formally forbidden in the MSSM by imposing an additional symmetry on the Lagrangian, called *R-parity* [38]. This is a $\mathbb{Z}_2$ symmetry under which each species has charge

$$R = (-1)^{(3B-L)+2s}, \tag{2.65}$$

where s is the spin of the particle. Thus, the fermions of the SM as well as the gauge and Higgs bosons all have $R = +1$, while the sfermions, higgsinos, and gauginos have $R = -1$. Because of R-parity, the $R = -1$ *superpartner* particles can only be created or destroyed in pairs. This implies that the lightest superpartner, the LSP, is absolutely stable if R-parity is an exact symmetry.

Since supersymmetry must be broken, soft-supersymmetry-breaking terms have to be included in the Lagrangian. These are

$$\begin{aligned}
\mathscr{L}_{soft} \;=\; & -m_1^2 H_1^\dagger H_1 - m_2^2 H_2^\dagger H_2 - (B\mu H_1\cdot H_2 + h.c.) \\
& - (m_Q^2)^{ij}\, \tilde{Q}_i^\dagger \tilde{Q}_j - (m_U^2)^{ij}\, \tilde{U}_i^{c\dagger} \tilde{U}_j^c - (m_D^2)^{ij}\, \tilde{D}_i^{c\dagger} \tilde{D}_j^c \\
& - (m_L^2)^{ij}\, \tilde{L}_i^\dagger \tilde{L}_j - (m_E^2)^{ij}\, \tilde{E}_i^{c\dagger}\, \tilde{E}_j^c \\
& - (-a_U^{ij}\, H_2\cdot \tilde{Q}_i\, \tilde{U}_j^c + a_D^{ij}\, H_1\cdot \tilde{Q}_i\, \tilde{D}_j^c + a_E^{ij}\, H_1\cdot \tilde{L}_i\, \tilde{E}_j^c + h.c.) \\
& - \frac{1}{2}(M_3\, \tilde{G}^a \tilde{G}^a + M_2\, \tilde{W}^d \tilde{W}^d + M_1\, \tilde{B}\tilde{B}).
\end{aligned} \tag{2.66}$$

The terms in the first line of this equation contribute to the potential for the Higgs bosons. The squared masses in the second line and the trilinear couplings on the third and fourth lines generate masses and mixings for the sfermions. The final line contains mass terms for the gauginos.

As they stand, the soft terms can be problematic. Without a concrete model of supersymmetry breaking, they must be regarded as (a large number of) new unknown parameters in the model. The soft breaking terms are also dangerous for phenomenology because they can generate unacceptably large amounts of flavor mixing and CP-violation. Because of these difficulties, several simplifying assumptions are often made about the soft parameters. To reduce the amount of flavor mixing, it is common to take

$$\begin{aligned}
(m_Q^2)^{ij} &= (m_Q^2)^i \delta^{ij}, \quad (m_U^2)^{ij} = (m_U^2)^i \delta^{ij}, \quad etc\ldots \\
a_U^{ij} &= y_U^{ij} A_U^i, \quad a_D^{ij} = y_D^{ij} A_D^i, \quad a_E^{ij} = y_E^{ij} A_E^i.
\end{aligned} \tag{2.67}$$

CP-violation can be avoided by requiring that the potentially complex couplings μ, B, A_f, and M_i, be real. We shall assume the flavor structure of Eq. (2.67) in our subsequent analysis, although we will allow for complex phases in the μ-term and the soft-breaking parameters.

2.4.2 Electroweak Symmetry Breaking and Particle Masses

As in the SM, the $SU(2)_L \times U(1)_Y$ electroweak symmetry is spontaneously broken to its $U(1)_{em}$ subgroup by the vacuum expectation value of a Higgs boson field. In this case, both Higgs doublets develop VEV's,

$$\langle H_1 \rangle = \begin{pmatrix} v_1 \\ 0 \end{pmatrix}, \qquad \langle H_2 \rangle = \begin{pmatrix} 0 \\ v_2 \end{pmatrix}. \tag{2.68}$$

These VEV's can also be taken to be real and positive. It is conventional to define

$$v = \sqrt{v_1^2 + v_2^2}, \qquad \tan\beta = \frac{v_2}{v_1}. \tag{2.69}$$

In terms of v, the gauge boson masses are given by the same expressions as in the SM, Eq. (2.40). The SM fermion masses are given by

$$m_u = y_u\, v \sin\beta, \quad m_d = y_d\, v \cos\beta, \quad m_e = y_e\, v \cos\beta, \tag{2.70}$$

for the up-type quarks, the down-type quarks, and the charged leptons. The mass matrices of the corresponding sfermions are complicated by the appearance of soft-breaking parameters. With the simplifying assumptions in Eq. (2.67), the mass matrix for the up-type sfermions $(\tilde{u}_L, \tilde{u}_R^*)^t$ is given by

$$\mathcal{M}_{\tilde{u}}^2 = \begin{pmatrix} m_Q^2 + m_u^2 + D_L & m_u(A_u - \mu^* \cot\beta) \\ m_u(A_u^* - \mu \cot\beta) & m_U^2 + m_u^2 + D_R \end{pmatrix}, \tag{2.71}$$

where m_u is the fermion mass, m_Q^2, m_U^2, and A_u are the soft-breaking terms corresponding to each appropriate generation, and D_L and D_R are given by

$$\begin{aligned} D_L &= (t_{SU(2)}^3 - Q\, \sin^2\theta_w)\, M_Z^2 \cos 2\beta, \\ D_R &= Q\, \sin^2\theta_w\, M_Z^2 \cos 2\beta. \end{aligned} \tag{2.72}$$

For a down-type sfermion, the mass matrix is

$$\mathcal{M}_{\tilde{d}}^2 = \begin{pmatrix} m_Q^2 + m_d^2 + D_L & m_d(A_d - \mu^* \tan\beta) \\ m_d(A_d^* - \mu \tan\beta) & m_D^2 + m_d^2 + D_R \end{pmatrix}, \tag{2.73}$$

with a similar expression for the slepton masses.

The physical Higgs bosons of the MSSM consist of two real CP-even states, one real CP-odd state, and one complex charged state. Their tree-level masses can be expressed in terms of v, β, μ and M_a^2, where M_a^2 is a function of the soft parameters. For the CP-odd Higgs boson, A^0, and the charged Higgs boson, $H^\pm$, the tree-level masses are [39]

$$\begin{aligned} A^0: \qquad m_A^2 &= M_a^2, \\ H^\pm: \qquad m_{H^\pm} &= M_a^2 + M_W^2. \end{aligned} \tag{2.74}$$

The mass matrix for the two CP-even states is given by [39]

$$\mathcal{M}_0^2 = \begin{pmatrix} M_a^2 \sin^2\beta + M_Z^2 \cos^2\beta & -(M_a^2 + M_Z^2)\sin\beta\cos\beta \\ -(M_a^2 + M_Z^2)\sin\beta\cos\beta & M_a^2\cos^2\beta + M_Z^2\sin^2\beta \end{pmatrix}. \tag{2.75}$$

The lighter and heavier states are denoted h^0 and H^0, respectively.

In addition to the SM fermions, sfermions, and Higgs bosons, the MSSM also contains gauginos and higgsinos. The $SU(3)_c$ gaugino is the *gluino*. It transforms as an adjoint under the gauge group, and has mass M_3. The $SU(2)_L$ and $U(1)_Y$ gauginos, the *Wino* and the *Bino*, mix with the higgsinos once these symmetries are broken. The resulting mass eigenstates then consist of four neutral Majorana fermion *neutralinos*, and two Dirac fermion *charginos*. The chargino mass matrix, in the (Weyl fermion) basis $(\tilde{W}^+, \tilde{H}_2^+, \tilde{W}^-, \tilde{H}_1^-)$, [9] is

$$M_{\chi^\pm} = \begin{pmatrix} 0 & X^t \\ X & 0 \end{pmatrix}, \tag{2.76}$$

where

$$X = \begin{pmatrix} M_2 & \sqrt{2}s_\beta M_W \\ \sqrt{2}c_\beta M_W & \mu \end{pmatrix}. \tag{2.77}$$

For the neutralinos, the mass matrix in the (Weyl fermion) basis $\psi_i^0 = (\tilde{B}, \tilde{W}^3, \tilde{H}_1^0, \tilde{H}_2^0)$ reads

$$\mathcal{M}_{\tilde{N}} = \begin{pmatrix} M_1 & 0 & -c_\beta s_w M_Z & s_\beta s_w M_Z \\ 0 & M_2 & c_\beta c_w M_Z & -s_\beta c_w M_Z \\ -c_\beta s_w M_Z & c_\beta c_w M_Z & 0 & -\mu \\ s_\beta s_w M_Z & -s_\beta c_w M_Z & -\mu & 0 \end{pmatrix}. \tag{2.78}$$

2.4.3 Predictions of the MSSM

Like the Standard Model, the MSSM agrees fairly well with the results of particle collider experiments. But, in addition to the SM, the MSSM stabilizes the electroweak scale, and as we shall discuss below, can also account for the dark matter and the baryon asymmetry of the Universe. Another attractive feature of the MSSM is that it leads to an excellent unification of gauge couplings [40]. This suggests that MSSM could be the low energy limit of a *grand unified theory*, in which the gauge groups of the SM are embedded in a larger and possibly simple gauge group.

The downside of the MSSM compared to the SM is that it contains a much larger number of undetermined parameters. They arise from our lack of understanding of how supersymmetry is broken, and they limit the predictivity of the model. At the same time, many of these parameters are very constrained by limits on the amount of flavor mixing and CP violation seen in experiments. In fact, for a generic set of soft supersymmetry breaking terms of order $m_{SUSY} \sim 1$ TeV, as required to solve the gauge hierarchy problem,

[9] We have implicitly defined $\tilde{W}^\pm = (\tilde{W}^1 \mp i\tilde{W}^2)/\sqrt{2}$ in analogy with the gauge bosons.

one would expect much more flavor mixing and CP violation than is seen.

Despite our ignorance of the soft breaking terms, the MSSM does make a definite prediction for the mass of the lightest CP-even Higgs boson, h^0. From Eq. (2.75) it follows that the tree-level mass of the h^0 state is bounded by

$$m_h^2 \leq M_Z^2 \cos^2 2\beta. \tag{2.79}$$

When this bound is saturated, the h^0 state behaves nearly identically to the Higgs boson of the SM. However, the current LEP II limit on a SM-like Higgs is [41]

$$m_h \gtrsim 114 \text{ GeV}, \tag{2.80}$$

which exceeds the tree-level upper bound. This limit does not rule out the MSSM because the h^0 mass receives large radiative corrections from the top squarks, and for stop masses below 2 TeV, the h^0 mass can be as high as 130 GeV [42]. Upcoming particle collider experiments will probe this this Higgs boson mass range.

CHAPTER 3
COSMOLOGY

Just as there exists a standard model of particle physics, there is also a standard model of cosmology that provides a very good description of what has been observed over the very largest scales [43]. The model is based on two assumptions, namely, that gravity is described by classical general relativity, and that the contents of the Universe obey the rules of statistical mechanics and particle physics. In both cases this is an extrapolation from small to large. General relativity has been experimentally tested only within the solar system [44], while the laws of particle physics have been deduced from laboratory experiments. Even so, the many successful predictions of the model indicate that these assumptions are reasonable.

Having made these assumptions, much of the standard cosmological model then follows directly from three observational results: the Universe is homogeneous and isotropic over very large scales [45]; distant points in the Universe are moving away from each other [46]; the Universe is uniformly filled with photons obeying a thermal distribution with a temperature of about 2.75 K [45, 47]. The collection of these photons is called the cosmic microwave background (CMB) radiation.

Since distant points are receding, the Universe must be expanding. As we'll show below, the energy of a free particle decreases with time in an expanding Universe. For a thermal distribution of particles, this implies that their temperature also decreases with the expansion. Starting with the present CMB temperature and extrapolating backwards in time, the early Universe must therefore have been much more hotter and denser in its youth. At very high temperatures, the early Universe would have consisted of a plasma of elementary particles. The standard model of cosmology describes how this plasma subsequently evolved as it cooled to form the Universe we see today.

In the model, the Universe begins with a brief but violent period of *inflation*, in which a small but causally connected region of space rapidly expands to a size large enough to encompass all of the presently observed Universe [48]. Inflation seems to be the only way to explain why the CMB is as uniform as it is, and it makes several other predictions that all remarkably consistent with the measured CMB spectrum as well [45]. Following the inflationary expansion, the Universe *reheated* to a thermal plasma of elementary particles with temperature T_{RH}, which in many models is of order $10^8 - 10^{12}$ GeV [49]. This reheating can be identified with the "Big Bang" [50].

After reheating, the Universe steadily expanded and cooled, with unstable massive particles decaying into lighter species. This smooth expansion was punctuated by phase transitions along the way. At temperatures of order 10^2 GeV, the $SU(2)_L \times U(1)_Y$ electroweak symmetry of the SM was broken to the $U(1)_{em}$ symmetry of electromagnetism [51]. When the temperature cooled below about 1 GeV, the QCD phase transition took place, in which free quarks and gluons in the plasma combined into baryons and mesons. At a temperature

close to 10^{-3} GeV, the remaining long-lived baryons, protons and neutrons, combined to form light elements in a process called *Big Bang Nucleosynthesis* (BBN). The predictions of BBN agree very well with the primordial light element abundances seen today [52]. At still lower temperatures, of order 10^{-6} GeV, free nuclei and electrons combined to form atoms. Once this *reionization* took place, the rate of photon scattering dropped sharply, and the Universe effectively became transparent since photons could now propagate freely. The photons observed in the CMB are those that have not scattered since, so the CMB gives an excellent way to probe this epoch. The stars and galaxies were formed much later and over much longer time scales. In this work, we will primarily be interested in the very early Universe, when the temperature was in excess of 1 GeV.

In this chapter, we will outline the basic tools used to describe these phenomena. In Section 3.1, we shall outline how the expansion of the Universe emerges from general relativity. Section 3.2 deals with the contents of the Universe, and how for much of its history, they can be well described in terms of equilibrium statistical mechanics. Finally, departures from equilibrium, and their description in terms of the Boltzmann equation, are the subject of Section 3.3. More detailed accounts of cosmology can be found in the textbooks [43, 54], as well as the review articles [55, 56].

3.1 An Expanding Universe

Gravity is the most important force over the very large distances encountered in cosmology. The evolution of the Universe is therefore determined by Einstein's equations which relate the spacetime metric to the local energy-momentum density. Because of the observed isotropy and homogeneity of the Universe the form of the metric is highly constrained. The most general form of the metric consistent with these two requirements is [57]

$$\begin{aligned} ds^2 &= g_{\mu\nu} dx^\mu dx^\nu \\ &= dt^2 - a^2(t) \left[\frac{dr^2}{1-kr^2} + r^2 d\Omega^2 \right]. \end{aligned} \tag{3.1}$$

Here, $a(t)$ is a dimensionless scale factor, and k describes the spatial curvature. Following the usual convention, we will use the subscript 0 to denote quantities evaluated at the present time, and choose spatial coordinates such that the current scale factor is equal to unity, $a(t = t_0 = \text{now}) = a_0 = 1$. With this normalization, the CMB data [45] indicates that the spatial curvature k is negligibly small, and so the spatial geometry is locally identical to $\mathbb{R}^3$. We will therefore neglect k in most of what follows.

To find the functional form of $a(t)$, it is necessary to solve Einstein's equations [57]

$$R^{\mu\nu} - \frac{1}{2} g^{\mu\nu} R = T^{\mu\nu}, \tag{3.2}$$

where R and $R^{\mu\nu}$ are curvature terms constructed from the metric, and $T^{\mu\nu}$ is the energy

momentum tensor. Because of isotropy and homogeneity, it must have the form

$$T^{\mu}_{\ \nu} = diag(\rho, -p, -p, -p), \tag{3.3}$$

which is that of a perfect fluid with energy density ρ and pressure p. The relationship between these is given by the equation of state, which usually takes the form

$$p = w(t)\rho. \tag{3.4}$$

For Einstein's equations to be self-consistent, the energy momentum must be covariantly conserved, $\nabla_\mu T^{\mu\nu} = 0$. In terms of the metric of Eq. (3.1), this will be true if and only if

$$\begin{aligned} 0 &= \frac{d}{dt}(\rho\, a^3) + p\,\frac{d}{dt}(a^3) \\ &= \left[\dot{\rho} + (\rho + p)\frac{\dot{a}}{a}\right]. \end{aligned} \tag{3.5}$$

Here, the overdot implies differentiation with respect to the time coordinate t. The Einstein equations themselves give the relations

$$\left(\frac{\dot{a}}{a}\right)^2 + \frac{k}{a^2} = \frac{8\pi\, G}{3}\rho, \tag{3.6}$$

and

$$\frac{\ddot{a}}{a} = -\frac{4\pi\, G}{3}(\rho + 3p). \tag{3.7}$$

Only two of these three equations are independent, but it is useful to have them all written out explicitly.

Since the universe is currently expanding, we know that $\dot{a}(t = t_0) > 0$. Furthermore, provided $w(t) > -1/3$ in the past, the Universe has been decelerating, $\ddot{a} < 0$. Together, these imply that there must have been a time t_* in the finite past at which $a(t_*) = 0$, usually called the "Big Bang". However, we hasten to point out that the description of gravity by classical Einstein relativity is expected to break down before this happens. Even so, we should still be able to trust our picture of an expanding Universe well into the distant past.

Consider now the Einstein equations for the simple case of $w(t) = constant$ and $k = 0$. Energy-momentum conservation, in the form of Eq. (3.5), then implies

$$\rho = \rho_o \left(\frac{a}{a_0}\right)^{-r}, \tag{3.8}$$

where $r = 3(1 + w)$. Putting this result into Eq. (3.6), we find

$$a(t) = \left(\frac{r}{2}\right)^{2/r} \left(\frac{8\pi\, G\rho_0}{3}\right)^{1/r} t^{2/r}. \tag{3.9}$$

For future use, it will be convenient to rewrite Eq. (3.6) in terms of the Hubble parameter H. This parameter provides a measure of the expansion rate of the Universe, and is defined by the relation

$$H(t) := \frac{\dot{a}(t)}{a(t)}. \tag{3.10}$$

The measured value of H in the present is [45]

$$H(t = t_0) := H_0 = 100\, h\, \mathrm{km\, s^{-1} Mpc^{-1}} = 2.1332\, \mathrm{h} \times 10^{-42}\ \mathrm{GeV}, \tag{3.11}$$

with h in the range

$$h = 0.71 \pm 0.06. \tag{3.12}$$

In terms of H, Eq. (3.6) becomes

$$\Omega = 1 - \frac{k}{a^2 H^2}, \tag{3.13}$$

where we have defined

$$\Omega = \frac{\rho}{(3H^2/8\pi\, G)}. \tag{3.14}$$

The denominator is sometimes called the critical density, $\rho_c = (3H^2/8\pi\, G)$. The energy density, ρ in the numerator, receives contributions from many sources including massive particles and radiation. For each contribution ρ_i to the energy density, we will write $\Omega_i = \rho_i/\rho_c$. Thus,

$$\Omega = \sum_i \Omega_i = 1 - \frac{k}{a^2 H^2}. \tag{3.15}$$

A crucial property of an expanding Universe is that both the momentum of a particle and the wavelength of radiation decrease with the expansion. This follows from the geodesic equation, which describes the motion of free particles in a curved background. If $x^\mu(\xi)$ is the trajectory of a particle parametrized by the affine parameter ξ, this equation reads

$$\frac{d^2 x^\mu}{d\xi} + \Gamma^\mu_{\ \alpha\beta} \frac{dx^\alpha}{d\xi} \frac{dx^\beta}{d\xi} = 0. \tag{3.16}$$

Putting the Christoffel symbols for the RW metric into the zero component of this equation, and identifying $dx^\mu/d\xi$ with the momentum (up to a proportionality factor), one obtains that the magnitude of the three momentum scales as

$$\|\vec{p}\| \propto a^{-1}. \tag{3.17}$$

For radiation, this momentum is inversely proportional to the wavelength, and so photons get red-shifted by the expansion of the Universe.

This redshifting effect is of great importance to observational cosmology since it allows one to determine the age of distant objects. In fact, it was the observation of the redshift of

light from distant galaxies by Hubble that gave the first evidence for an expanding Universe. The amount by which an object is redshifted is usually expressed in terms of the quantity z, given by [43]

$$z = \frac{\lambda_i - \lambda_0}{\lambda_i} = 1 - \frac{a_0}{a_i}, \tag{3.18}$$

where λ_i and a_i are the initial wavelength and scale factor, and λ_0 and a_0 are at present. Very old, distant objects correspond to large z.

3.2 Equilibrium Thermodynamics in the Early Universe

For much of the evolution of the Universe, the rate of Hubble expansion was much less than the rate at which elementary particles interacted with each other. Because of this, these particles are very well described by equilibrium statistical mechanics, and we may assign a temperature T to the Universe. At a given temperature, those particles with masses well below T are called *radiation*, while those with masses greater than T are referred to as *matter*.

The grand canonical ensemble is the most convenient way to describe this system of particles. In this ensemble, all thermodynamic quantities of interest can be obtained from the free-energy (really the grand canonical potential) defined by [58, 59]

$$F = -T \ln Z_{GCE}, \tag{3.19}$$

with Z_{GCE} the grand canonical partition function,

$$Z_{GCE} = tr[e^{-\beta(\mathscr{H} - \mu_a Q_a)}], \tag{3.20}$$

where $\beta = 1/T$, $\mathscr{H}$ is the Hamiltonian for the system, and $\{Q_a\}$ are a set of conserved charges. In terms of F, the expectation values of these are

$$\begin{aligned} E &= \langle \mathscr{H} \rangle = \left. \frac{\partial F}{\partial \beta} \right|_{\mu_a} \\ Q_a &= \left. \frac{\partial F}{\partial \mu_a} \right|_{\beta} \\ p &= -\left. \frac{\partial F}{\partial V} \right|_{\mu_a, \beta} \end{aligned} \tag{3.21}$$

Using elementary thermodynamics, we also have

$$F = -pV = E - TS - \mu_a Q_a. \tag{3.22}$$

It is usually a good approximation to treat the particles in the early Universe as a weakly-interacting dilute gas consisting of several species. Recall that particles are described by quantum fields. This approximation then amounts to neglecting interactions between the

fields, and introducing a chemical potential for each particle species when computing its contribution to the free energy. The effect of interactions is included in two ways. First, in writing Eq. (3.20), we have implicitly assumed that elastic collisions are sufficiently fast to ensure kinetic equilibrium. Second, the effects of rapid inelastic interactions are included by assuming chemical equilibrium. This implies that if the reaction $(a+b+\ldots) \leftrightarrow (x+y+\ldots)$ goes, then the chemical potentials add:

$$\mu_a + \mu_b + \ldots = \mu_x + \mu_y + \ldots . \tag{3.23}$$

The dilute gas picture works well provided the mean free-paths of the constituent particles are large compared to the time-scale over which they interact (so that a particle picture makes sense). On the other hand, kinetic and chemical equilibrium only hold provided the corresponding reaction rates are fast compared to the expansion rate of the Universe. Corrections to this picture can be computed in perturbation theory.

At lowest order in the dilute-gas approximation, the contribution of a single species to the free-energy is

$$F \supseteq V\,T\,g \int \frac{d^3p}{(2\pi)^3} \eta \left(\ln[1 + \eta\, e^{-(E-\mu)/T}] + \ln[1 + \eta\, e^{-(E+\mu)/T}] \right), \tag{3.24}$$

where $E = \sqrt{\vec{p}^{\,2} + m^2}$, $\eta = \pm 1$ for fermions and bosons respectively, and g is the total number of internal degrees of freedom. The first term is interpreted as being due to particles, and the second from anti-particles. Using this result in Eq. (3.21), the number density, energy density, and pressure due to a given species can be written as

$$\begin{aligned} n &= g \int \frac{d^3p}{(2\pi)^3}\, f(E,t) \\ \rho &= g \int \frac{d^3p}{(2\pi)^3}\, E\, f(E,t) \\ p &= g \int \frac{d^3p}{(2\pi)^3}\, \frac{\vec{p}^{\,2}}{3E}\, f(E,t) \end{aligned} \tag{3.25}$$

where the distribution function $f(E,t)$ is given by

$$f(E,t) = \left[e^{-(E-\mu)/T} \pm 1 \right]^{-1}, \tag{3.26}$$

and the $(\pm)$ corresponds to fermions and bosons respectively. This description in terms of distribution functions is also useful when there are deviations from the thermodynamic equilibrium.

Particles whose masses are much smaller than T are called *radiation*. If $\mu \ll T$ as well,

the number density, energy density, and pressure of radiation are given by

$$\begin{aligned} n &= \left\{ \begin{matrix} 7/8 \\ 1 \end{matrix} \right\} \frac{\pi^2}{30} g\, T^4, \\ \rho &= \left\{ \begin{matrix} 3/4 \\ 1 \end{matrix} \right\} \frac{\zeta(3)}{\pi^2}\, g T^4, \\ p &= \rho/3. \end{aligned} \tag{3.27}$$

Here, $\zeta(3) \doteq 1.202$ is the Riemann zeta-function, g is the degeneracy of the species (spins, internal quantum numbers), and the upper (lower) bracketed values are for fermions (bosons).

Heavy particles, with $m \gg T$, are called *matter*. The corresponding expressions in this case are

$$\begin{aligned} n &= g \left(\frac{mT}{2\pi} \right)^{3/2} e^{-(m-\mu)/T}, \\ \rho &= m\, n, \\ p &= n\, T \ll \rho. \end{aligned} \tag{3.28}$$

These expressions show that, except in the case of degenerate particles with large μ, the relativistic species tend to give a much larger contribution to the energy density due to the Boltzmann suppression of heavy particles. The total energy density due to all species is therefore well approximated by

$$\rho_{tot} = \frac{\pi^2}{30}\, g_* T^4, \tag{3.29}$$

with g_* defined to be

$$g_* = \sum_b g_b \left(\frac{T_b}{T} \right)^4 \theta(T_b - m_b) + \frac{7}{8} \sum_f g_f \left(\frac{T_f}{T} \right)^4 \theta(T_f - m_f), \tag{3.30}$$

where the first sum runs over bosons and the second over fermions. In this expression we have allowed for the possibility that not all particles have the same temperature. This is a slight generalization of the situation discussed above in which all particles interact with each other, to the case in which there are several subsets of particles which interact only with members of their subset. In this more general situation, equilibrium will be maintained within each subset but not between different subsets, and so each subset can have a different temperature. The system temperature T is then taken to be the temperature of that subset which includes the photon.

For much of the early Universe, and at the temperatures relevant for the creation of dark matter and the generation of the baryon asymmetry in particular, radiation provides the dominant component of the energy density. Inserting $w = 1/3$ into Eqs. (3.8) and (3.9),

we obtain

$$\begin{aligned} \rho &\propto a^{-4}, \\ a(t) &= a_0 \left(\frac{t}{t_0}\right)^{1/2}. \end{aligned} \tag{3.31}$$

If g_* remains constant, this implies that the Universe cools as it expands according to $T \propto a^{-1}$. Putting the energy density into Eq. (3.6) we find

$$\begin{aligned} H(T) &= \sqrt{\frac{4\pi^3}{45}}\, g_*^{1/2} \frac{T^2}{M_{\rm Pl}}, \\ t &= \frac{1}{2} H^{-1} = \sqrt{\frac{45}{16\pi^3}}\, g_*^{-1/2} \frac{M_{\rm Pl}}{T^2}. \end{aligned} \tag{3.32}$$

Entropy is another useful quantity with which to describe the early Universe because it is conserved. From the usual thermodynamic relations, we have

$$S = \frac{(\rho + p)\, V}{T} \tag{3.33}$$

as well as the First Law of thermodynamics,

$$T\, dS = dE + p\, dV. \tag{3.34}$$

Applying these relations to a volume of unit coordinate size (and thus a physical size a^3), and using Eq. (3.5), we find

$$\frac{dS}{dt} = \frac{1}{T}\left[\frac{d}{dt}(\rho\, a^3) + p\, \frac{d}{dt}(a^3)\right] = 0, \tag{3.35}$$

Entropy is therefore conserved as the Universe expands. An important exception to this occurs when there are departures from thermodynamic equilibrium.

The entropy density is taken to be

$$s = S/V = \frac{\rho + p}{T}. \tag{3.36}$$

It decreases like a^{-3} with the expansion. As for the energy density, the entropy density is dominated by the relativistic species in the thermal bath. Thus, to an excellent approximation, we can write

$$s = \frac{2\pi^2}{45} g_{*S}\, T^3, \tag{3.37}$$

where

$$g_{*S} = \sum_b g_b \left(\frac{T_b}{T}\right)^3 \theta(T_b - m_b) + \frac{7}{8} \sum_f g_f \left(\frac{T_f}{T}\right)^3 \theta(T_f - m_f). \tag{3.38}$$

Eq. (3.37) implies that, when relativistic species give the largest contribution to the energy and entropy densities, the temperature decreases as

$$T \propto g_{*S}^{-1/3} a^{-1}. \tag{3.39}$$

This confirms our previous estimate when g_{*S} is constant. When g_{*S} decreases, due to the temperature cooling below the mass of a particular species, the temperature decreases less quickly than it would otherwise.

3.3 Departures from Equilibrium: the Boltzmann Equation

While equilibrium thermodynamics describes much of the evolution of the Universe, the most interesting events usually involve a departure from equilibrium. This is the case both for the generation of the dark matter and the baryon asymmetry. Such departures can be described by the Boltzmann equation [43], a differential equation relating the rate of change of the distribution function for a given species, x_1 say, to the scattering and decay processes that change the number of x_1 particles. It has the form

$$L[f_1] = C[f_1], \tag{3.40}$$

where the Liouville operator $L[f]$ is essentially the total time derivative of the distribution function $f_1(\vec{x}, \vec{p}, t)$, and the collision operator $C[f]$ accounts for processes that change the number of the given particle. More precisely, the (covariantly generalized) Liouville operator is [43]

$$L[f] = \left(p^\mu \frac{\partial}{\partial x^\mu} - \Gamma^\mu_{\alpha\beta}\, p^\alpha p^\beta \frac{\partial}{\partial p^\mu} \right) f(\vec{x}, \vec{p}, t). \tag{3.41}$$

Here, $\Gamma^\mu_{\alpha\beta}\, p^\alpha p^\beta$ is the Christoffel symbol derived from the metric. In the case of a Robertson-Walker metric and $f_1 = f_1(E, t)$, this simplifies to

$$L[f_1] = E_1 \frac{\partial f_1}{\partial t} - H \, \|\vec{p}_1\| \, E_1 \frac{\partial f_1}{\partial \|\vec{p}_1\|}. \tag{3.42}$$

Dividing by E_1, integrating over momentum space, and finally integrating the last term by parts, the Boltzmann equation becomes

$$\frac{dn_1}{dt} + 3\, H\, n_1 = g_1 \int \frac{d^3 p_1}{(2\pi)^3} \frac{1}{E_1} C[f_1]. \tag{3.43}$$

When considering baryogenesis, we will need to generalize these equations to include local (position-dependent) fluctuations of the distribution functions. However, the simplified form presented here is sufficient for most cases of interest, including the decoupling of dark matter.

The collision term on the right hand side of Eq. (3.43) receives contributions from all processes that change the number of x_1 particles. For the reaction $(x_1 + x_2 \leftrightarrow y_a + y_b + \ldots)$,

it is given by

$$g_1 \int \frac{d^3p_1}{(2\pi)^3}\frac{1}{E_1}\,C[f_1] \;\supseteq\; -\int \tilde{d}p_1\tilde{d}p_2\tilde{d}k_a\ldots\,(2\pi)^4\,\delta^{(4)}(p_1+p_2-k_a-\ldots)\cdot \\ \cdot\left[(g_1g_2)|\mathcal{M}_{12\to ab\ldots}|^2\,f_1f_2(1\pm f_a)(1\pm f_b)\ldots\right. \\ \left.-\,(g_ag_b\ldots)|\mathcal{M}_{ab\ldots\to 12}|^2 f_af_b\ldots(1\pm f_1)(1\pm f_2)\right], \tag{3.44}$$

where $\tilde{d}p = d^3p/2E(2\pi)^3$, and $|\mathcal{M}|^2$ is the squared matrix element, *averaged* over initial states and *summed* over final states. The total collision operator will be the sum of all such contributions. Note that the contribution from elastic scattering processes vanishes.

Eq. (3.44) can usually be simplified considerably. It is often the case that $f_i(E,t) \ll 1$, and $(1\pm f) \simeq 1$. If the i-th species is in thermal equilibrium, $f_i(E,t) \simeq e^{-E/T}$ as well. This is usually true for the decay products (y_i's). If so, and using conservation of energy, we also get $f_af_b\ldots \simeq f_1^{eq}f_2^{eq}\ldots$, where the subscripts denote the equilibrium distributions. Since CP-violating effects are generally small, we have $(g_1g_2)\,|\mathcal{M}_{12\to ab\ldots}|^2 \simeq (g_ag_b\ldots)\,|\mathcal{M}_{ab\ldots\to 12\ldots}|^2$ as well.[1]

If these approximations are valid, the contribution to the collision operator becomes

$$-\int \tilde{d}p_1\tilde{d}p_2\left[\int \tilde{d}k_a\ldots\tilde{d}k_b\ldots(2\pi)^4\,\delta^{(4)}(p_1+p_2-k_a+k_b+\ldots)\cdot\right. \\ \left.\cdot\,(g_1g_2\ldots)|\mathcal{M}_{12\to ab\ldots}|^2\right]\,(f_1f_2-f_1^{eq}f_2^{eq})\,. \tag{3.45}$$

The term within the square brackets is just the scattering cross-section times $(p_1\cdot p_2) = (2E_1)(2E_2)\,v_{rel}$. The factors of $2E$ cancel with those in $\tilde{d}p_1\tilde{d}p_2$, and we obtain a thermal average of $\sigma_{12\to ab\ldots}v_{rel}$. The final contribution to the collision operator is therefore

$$\langle\sigma_{12\to ab\ldots}v\rangle\,(n_1n_2-n_1^{eq}n_2^{eq})\,, \tag{3.46}$$

where the thermal average of the operator $A(p_1,\ldots,p_N)$ is defined to be

$$\langle A\rangle = \frac{1}{n_1\ldots n_N}\int g_1\frac{d^3p_1}{(2\pi)^3}\ldots g_N\frac{d^3p_N}{(2\pi)^3}\;A(p_1,\ldots,p_N)\;f_1\ldots f_N. \tag{3.47}$$

It is straightforward to generalize Eq. (3.46) to decays of the x_1 particle. The decay contribution to the collision operator is simply

$$\Gamma_{1\to ab\ldots}\,(n_1-n_1^{eq})\,. \tag{3.48}$$

Our final form for the Boltzmann equation for a species x_1 is therefore

$$\frac{dn_1}{dt}+3\,H\,n_1 = -\Gamma_{\rm eff}(n_1-n_1^{eq}), \tag{3.49}$$

[1]The additional g factors cancel those due to averaging over initial states.

where $\Gamma_{\rm eff} \sim n \langle \sigma\, v \rangle$ or Γ_{decay} is the net effective rate of processes that change x_1 number.

Eq. (3.49) indicates the necessary condition for a particle species to remain in thermodynamic equilibrium; the interaction rate be much larger than the rate of Hubble expansion. If so, the number density relaxes to its equilibrium value. On the other hand, if $\Gamma \ll H$, the number density decreases as a^{-3}, simply being diluted by the expansion of space. The momentum distribution of a species after it has decoupled may also be deduced from this result. For a massless particle that has decoupled, the energy of a given momentum mode is $E = p$, and redshifts as a^{-1}. Thus, the momentum space distribution function for such a particle keeps the same form as in equilibrium, but with an effective temperature

$$T_{\rm eff}(t) = T_D \left(\frac{a_D}{a(t)} \right), \tag{3.50}$$

where T_D and a_D are the values of the temperature and the scale factor at decoupling. For a massive particle we can play a similar game, but it is less useful. The important point in this case is that the number density of the decoupled massive species decreases as a^{-3}.

CHAPTER 4
DARK MATTER

There seems to be much more matter in the Universe than what we can see. The best determination of the total matter density in the Universe comes from measurements of the CMB spectrum, in which the relative height of the peaks is sensitive to this density. These indicate a total matter density of [45]

$$\Omega_m h^2 = 0.14 \pm 0.02. \tag{4.1}$$

On the other hand, the density of luminous matter in the Universe is much smaller than this. Recent estimates give [60]

$$\Omega_{lum} h^2 \simeq 0.003. \tag{4.2}$$

By mass, the luminous matter consists mostly of baryons. Some of the non-luminous matter also contains baryons, but baryons can't account for it all since a baryon density approaching the total matter density would be wildly at odds with the both the predictions of BBN, as well as the CMB spectrum [45]. Most of the non-luminous matter must therefore be non-baryonic. We shall reserve the term *dark matter* for the non-baryonic component of the non-luminous matter.

The evidence for dark matter comes from a number of different sources [61, 62]. For example, the measured rotational velocities of galaxies indicate that the matter density associated with the galaxy extends well beyond the light-emitting part [63]. The gravitational lensing of galaxy clusters points towards the presence of dark matter over much larger scales, and suggests a value $\Omega_m \sim 0.3$ [64]. Furthermore, simulations of structure formation require a significant density of non-baryonic matter to reproduce the amount of small scale structure we see today.

Many explanations have been proposed for the dark matter. For the most part, attempts to explain the dark matter by astrophysical mechanisms fail. Indeed, the evidence for dark matter comes from many different length scales, from that of galaxies to the much larger scales probed by measurements of the CMB, making such explanations implausible. A much more successful explanation for the dark matter is given by the existence of a stable, massive particle. Since a stable species can't decay, it can only change its number by inelastic scattering processes. When the temperature falls below the mass of the particle, the number density of the particle will decrease exponentially, as described by Eq. (3.28), provided it is still in equilibrium. Since the scattering rate is proportional to this number density, Eq. (3.49), it will fall quickly as well. Eventually, the scattering rate becomes so small that $\Gamma_{\text{eff}} < H$, and the species falls out of equilibrium. Thus, massive stable particles tend to *freeze out* shortly after the temperature falls below their mass. After freezing out, the number density of the massive species will fall off as a^{-3} due to the expansion of the Universe. Since this is much slower than the exponential drop that would occur if the

particle were in equilibrium, the number density of a *relic* particle that has frozen out can be a great deal larger than its equilibrium value. The contribution of such a particle to the energy density of the Universe is

$$\rho_{relic} = m_1\, n_1, \tag{4.3}$$

where m_1 is the mass of the particle, and n_1 is its number density.

For the relic particle density to be significant, the species must be weakly-interacting (*i.e.* uncharged). It must also be non-relativistic at decoupling to avoid washing out structure over small scales [61]. which usually requires that the particle mass be greater than about 1 keV.[1] The SM has no particle with these properties. On the other hand, many extensions of the Standard Model contain new particles of this sort. Very often, these extensions contain a new sector of particles all carrying a conserved quantum number. The lightest particle in this sector will therefore be stable because of the conservation law. A well known example of this is the lightest superpartner particle in supersymmetric models with conserved R-parity.

In this chapter we will describe the methods used to calculate the relic density of a stable massive particle. The primary tool for this will be the Boltzmann equation introduced in the previous chapter. In Sections 4.1 and 4.2 we will apply this equation to the freeze-out of a massive stable particle. Section 4.3 describes a generalization of these techniques to *coannihilation*, in which the light stable particle also annihilates with other heavy particles in the thermal bath.

4.1 Solutions to the Boltzmann Equation

Let us now apply the Boltzmann equation, in the form of Eq. (3.46), to the freeze out of a massive stable particle. The inelastic cross-section is usually dominated by annihilations between the particle and its antiparticle, so we'll focus on this process. It is convenient to make a change of variables and replace time by the variable

$$x = m_1/T, \tag{4.4}$$

and rewrite the number density in terms of

$$Y_1 = \frac{n_1}{s}, \tag{4.5}$$

where s is the entropy density. In terms of these new variables, the Boltzmann equation becomes

$$\frac{dY_1}{dx} = -\frac{2\pi^2}{45}\frac{m_1^3}{H(m_1)} g_{*S}\,\langle\sigma\, v\rangle\; x^{-2}\left(Y_1^2 - Y_1^{eq2}\right), \tag{4.6}$$

[1] An important exception to this occurs when the particle species was produced non-thermally and was never in equilibrium. This is the case for axion dark matter.

where we have used Eq. (3.33) to relate time and temperature. This change of variables is useful because $Y(x)$ remains constant in the absence of collisions. The function $Y_1^{eq}(x)$ follows from the equilibrium expressions for s and n:

$$\begin{aligned} Y_1^{eq}(x) &= \frac{45}{4\pi^4}\frac{g}{g_{*S}}\, x^2\, K_2(x) \\ &\simeq \frac{45}{2\pi^2}\left(\frac{1}{2\pi}\right)^{3/2}\frac{g}{g_{*S}}\, x^{3/2}\, e^{-x}, \qquad \text{for } x \gg 1. \end{aligned} \tag{4.7}$$

On the other hand, $\langle \sigma\, v\rangle$ is usually a complicated function of x.

Eq. (4.6) can't be solved exactly, but it is possible to obtain a very accurate approximate solution. The method is outlined in [43, 65], and involves solving the differential equations in the limits $x \ll x_f$ and $x \gg x_f$, where x_f is the freeze-out temperature, the temperature at which the species falls out of equilibrium. The two solutions are matched at $x \sim x_f$, and then used to find $Y_1(x \to \infty)$, the value at the present time where $T = T_0 \simeq 0$.

The freeze-out temperature is defined by the relation

$$[Y(x_f) - Y^{eq}(x_f)] = C\, Y^{eq}(x_f), \tag{4.8}$$

for C a constant of order unity. (The value $C \sim (1+\sqrt{2})$ appears to optimize the approximation compared to numerical evaluations.) It then follows that

$$x_f = \ln\left[C(C+2)\sqrt{\frac{45}{32\pi^6}}\,\frac{g}{g_*^{1/2}} m_1 M_{\rm Pl}\, x^{-1/2}\,\langle\sigma\, v(x_f)\rangle\right]. \tag{4.9}$$

This equation can be solved iteratively. In terms of x_f, the approximate solution to the Boltzmann equation is

$$Y_1(x \to \infty) = \sqrt{\frac{45}{\pi}}\frac{1}{m_1 M_{\rm Pl}}\left[\int_{x_f}^{\infty} dx\, \frac{g_{*S}}{g_*^{1/2}}\,\frac{\langle\sigma\, v\rangle}{x^2}\right]^{-1}. \tag{4.10}$$

This result is usually re-expressed as the contribution of the relic particle density to $\Omega\, h^2$, which is just a matter of multiplying $Y_1(x \to \infty)$ by the constant conversion factor of Eq. (3.14). The final result is

$$\Omega_1 h^2 \simeq (1.07 \times\ 10^9\, {\rm GeV}^{-1})\frac{1}{M_{\rm Pl}}\left[\int_{x_f}^{\infty} dx\, \frac{g_{*S}}{g_*^{1/2}}\,\frac{\langle\sigma\, v\rangle}{x^2}\right]^{-1}. \tag{4.11}$$

4.2 The Thermally Averaged Cross-Section

In order to evaluate the relic density, we need an explicit expression for the thermally averaged cross-section, $\langle\sigma\, v\rangle$, as a function of x. This function is usually very complicated, but can be reduced to a much simpler form by expanding the cross section in powers of

the relative velocity, v, which is a small quantity for a massive particle that decouples when it is non-relativistic. Upon performing the thermal average, $v^2 \to 3/2x$, one obtains an expansion in inverse powers of x. However, this expansion becomes unreliable in many cases of interest such as when the annihilation cross-section is enhanced by a resonance [65]. Thus, it is safer and usually more accurate to stick with the exact expression for $\langle \sigma\, v \rangle$.

Recall that for the process $1 + 2 \to a + b + \ldots$, the thermally averaged cross-section is given by

$$\langle \sigma\, v \rangle = \int d^3p_1 d^3p_2\; \sigma v\; e^{-E_1/T} e^{-E_2/T} \Big/ \int d^3p_1 d^3p_2\, e^{-E_1/T} e^{-E_2/T} \tag{4.12}$$

with

$$\sigma\, v = \frac{1}{4E_1E_2} \tilde{W}(s), \tag{4.13}$$

where

$$\tilde{W}(s) = \int \tilde{dk}_a \tilde{dk}_b \ldots (2\pi)^4\, \delta^{(4)}(p_1 + p_2 - k_a - k_b - \ldots)\, |\mathcal{M}|^2. \tag{4.14}$$

Again, $|\mathcal{M}|^2$ is the corresponding squared matrix element, *averaged* over initial states and *summed* over final states. It also includes the appropriate $1/n!$ symmetry factors for identical particles in the final state. The dominant contribution to $\langle \sigma\, v \rangle$ usually comes from $2 \to 2$ processes. In this case $\tilde{W}(s)$ simplifies to

$$\tilde{W}_{2\to 2}(s) = \frac{p_{ab}}{16\pi^2\, \sqrt{s}} \int d\Omega\, |\mathcal{M}|^2, \tag{4.15}$$

with $s = (p_1 + p_2)^2$, and p_{ab} given by

$$p_{ab} = \frac{1}{2} \sqrt{\frac{[s - (m_a - m_b)^2][s - (m_a + m_b)^2]}{s}} \tag{4.16}$$

for final state masses m_a and m_b. The quantity $d\Omega$ is the solid angle for the outgoing particle direction.

The integrations in the thermal average can be rewritten as a single integral over the center-of-mass invariant, s. The denominator of Eq. (4.12) becomes [66]

$$(n_1^{eq})^2 = \left[\frac{T}{2\pi^2} g_1 m_1^2 K_2(x) \right]^2, \tag{4.17}$$

where $K_2(x)$ is the modified Bessel function of degree two. Similarly, the numerator becomes

$$\frac{T}{32\pi^2} \int_{4m_1^2}^{\infty} ds \frac{1}{2} \sqrt{s - 4m_1^2}\, \tilde{W}(s) K_1(\sqrt{s}/T). \tag{4.18}$$

Putting these together and changing the integration variable to $\hat{s} = s/4m_1^2$, we find

$$\langle \sigma\, v \rangle (x) = \frac{x}{2m_1^2} \int_1^\infty d\hat{s}\, \sqrt{\hat{s}-1}\, \tilde{W}\, K_1(2x\sqrt{\hat{s}}) \big/ K_2^2(x). \tag{4.19}$$

4.3 Coannihilations

In the previous sections we only considered the annihilation of a massive stable particle with itself or its antiparticle. This is usually the most important mode since other more massive particles will have already decoupled from the plasma or decayed away. However, in some cases the annihilations of the lightest particle with the heavier ones can be very important, especially when the next-to-lightest particle carrying a conserved charge is close in mass to the lightest one, but has much stronger annihilation couplings. This *coannihilation* of particles is what we consider here.

Consider the SM along with a set of heavy "X" particles, each with conserved charge -1 under a global $\mathbb{Z}_2$ symmetry. The SM particles will be assumed to have charge $+1$. Charge conservation implies that the product of the initial state charges must be equal to those of final state. Thus, the lightest of the X particles will be stable, and will contribute to the dark matter density. An example of this situation is supersymmetry with conserved R-symmetry in which case the X sector consists of the superpartner particles. We'll label the X sector species by $i = 1, \ldots, N$, such that $m_1 < m_2 < \ldots, m_N$. Particle X_1 is therefore our dark matter candidate.

Besides annihilation processes, there will be elastic and inelastic scatterings between the X sector particles and the SM, such as

$$X_i + a \leftrightarrow X_j + b. \tag{4.20}$$

These scatterings will be much faster than the annihilation reactions because the SM particles are much more abundant in the plasma than the X particles at temperatures below m_1. The standard assumption for treating coannihilations is that this scattering with SM species is sufficiently fast to maintain the equilibrium ratio of the X sector number densities:

$$\frac{n_i}{n} = \frac{n_i^{eq}}{n^{eq}}, \tag{4.21}$$

where

$$n = \sum_i^N n_i \tag{4.22}$$

is the total number density of X sector particles. Notice that if $m_1 \ll m_2$, Eq. (3.28) implies that the number density of the heavier X particles will be exponentially small. Thus, coannihilation is only important when the lightest and the next-to-lightest X sector species are close in mass.

Since all the X particles will eventually decay into particle X_1 and SM particles (by

assumption), it suffices to calculate the total X sector number density after freeze out. By generalizing the previous result and using Eq. (4.21), the Boltzmann equation for n becomes

$$\frac{dn}{dt} + 3\,H\,n = \langle\sigma\,v\rangle_{\rm eff}\,(n^2 - n^{eq\,2}), \tag{4.23}$$

where

$$\langle\sigma\,v\rangle_{\rm eff} = \sum_{i,j=1}^{N} \langle\sigma_{ij} v_{ij}\rangle \left(\frac{n_i^{eq} n_j^{eq}}{n^{eq\,2}}\right) \tag{4.24}$$

The cross-section σ_{ij} corresponds to the reaction $X_i + X_j \to$ (SM *particles*). Contributions from scatterings of the form $X_i + a \leftrightarrow X_j + b$ cancel out in the sum over the X species.

The calculation of $\langle\sigma\,v\rangle_{\rm eff}$ goes through in nearly the same way as in the simpler case without coannihilations. The final result is [67]

$$\begin{aligned}\langle\sigma\,v\rangle_{\rm eff} \;&=\; \frac{x}{2m_1^2}\left[\int_1^\infty d\hat{s}\,\sqrt{\hat{s}-1}\,K_1(2x_1\sqrt{\hat{s}})\sum_{i,j=1}^{N}\frac{p_{ij}}{p_{11}^2}\frac{g_i g_j}{g_1^2}\tilde{W}_{ij}\right] \\ &\qquad \Big/\left[\sum_{i=1}^{N}\frac{g_i}{g_1}\frac{m_i^2}{m_1^2}K_2(\frac{m_i}{m_1}x)\right]^2,\end{aligned} \tag{4.25}$$

where $\hat{s} = s/4m_1^2$, and

$$p_{ij} = \frac{1}{2}\sqrt{\frac{[s-(m_i-m_j)^2][s-(m_i+m_j)^2]}{s}}. \tag{4.26}$$

The quantity $\tilde{W}_{ij}$ corresponds to $\tilde{W}$ in Eq. (4.14) for the reaction $X_i + X_j \to$ SM. Using Eqs. (4.25) and (4.11), the solution for the final relic density follows as before.

CHAPTER 5
BARYOGENESIS: ELECTROWEAK AND OTHERWISE

About five percent of the energy density of the Universe consists of baryons. These take the form of atomic nuclei, mostly hydrogen and helium, and account for nearly all the visible mass in the Universe. The most accurate determination of the density of baryons comes from measurements of the CMB, which find [45]

$$\Omega_b h^2 = 0.024 \pm 0.001. \tag{5.1}$$

This value is consistent with the one obtained by comparing the primordial abundances of light elements with the predictions of Big Bang Nucleosynthesis (BBN) [52]. The baryon density is often re-expressed in terms of a baryon-to-photon ratio,

$$\eta = \frac{n_b}{n_\gamma} = (6.5^{+\,0.4}_{-\,0.3}) \times 10^{-10}. \tag{5.2}$$

The baryon density is made up almost entirely of baryons, not anti-baryons. This is curious because the Standard Model (of particle physics) treats baryons and anti-baryons in nearly the same way. Only CP violation, whose effects tend to be weak, distinguishes between them, and so one would naïvely expect roughly equal numbers of baryons and anti-baryons. This *baryon asymmetry of the Universe* therefore presents an interesting puzzle. To explain the asymmetry, we need a mechanism to generate an excess of baryons. Such a mechanism must operate below the reheating scale of inflation since any initial state asymmetry would be completely diluted by the inflation.

Several mechanisms for such a *baryogenesis* have been proposed [68]. In Section 5.1 we will briefly describe a few of the most popular ones. All of these mechanisms are affected by baryon-number changing *sphaleron* transitions associated with the $SU(2)_L$ part of the SM gauge group which we will discuss in Section 5.2. In Section 5.3, we will focus on a particular mechanism, *electroweak baryogenesis*, in which the baryon asymmetry is generated during the electroweak phase transition in the early Universe. This mechanism is the only known way to generate the baryon asymmetry within the SM or the MSSM.

5.1 Mechanisms for Baryogenesis

While there are many proposals for how the baryon asymmetry was created, nearly all of them share three common features. They were pointed out in 1967 by Sakharov [69], and are called the *Sakharov Conditions*:

1. Baryon number violation.

2. C and CP violation.

3. Departure from thermal equilibrium.

By baryon number (B), we mean the total number of baryons minus the total number of anti-baryons. The first condition is therefore fairly obvious. The second Sakharov condition is a bit less so. C and CP violation are essential because without them, baryon number violating processes that increase the baryon number would be just as probable as those that decrease it. This follows from baryon number being odd under both of these charges. Finally, a departure from equilibrium is needed to provide an arrow of time, since otherwise, the net baryon number will remain constant.

The three Sakharov conditions are met by the SM in an expanding Universe. Baryon number is violated in the SM by topology-changing transitions between different $SU(2)_L$ gauge vacua. These *sphaleron* transitions violate B+L, and in the absence of other conserved charges, they tend to cause any net $B+L$ charge to relax to zero. C and CP violation are also present; C is violated because of the chiral fermion structure of the SM, and CP is violated by the CKM phase present in the Yukawa couplings. The third condition, a departure from equilibrium, is induced by the expansion of the Universe, and even larger departures can arise during first-order phase transitions. Even though the SM has all the essential ingredients for baryogenesis, it doesn't seem to be possible to generate a large enough baryon asymmetry within the model. To understand why, we must examine particular mechanisms for baryogenesis. Of the numerous mechanisms proposed, the three most popular and best-motivated are electroweak baryogenesis, GUT baryogenesis, and leptogenesis.

In electroweak baryogenesis, the baryon asymmetry is generated during the *electroweak phase transition*. At high temperatures, as are expected to arise in the very early Universe, the full $SU(2)_L \times U(1)_Y$ symmetry of the Standard Model is restored. This symmetry is broken to $U(1)_{em}$ as the Universe cools below about $T \simeq 100$ GeV. If this phase transition is first-order, it proceeds by the nucleation of bubbles of broken phase within the surrounding symmetric phase. As the bubbles expand, CP-violating reactions in and around the bubble walls can generate an excess of chiral fermions in front of the walls. This net chiral fermion charge then biases the B-violating sphaleron transitions towards producing more baryons than anti-baryons.

GUT baryogenesis assumes that the Standard Model gauge structure becomes embedded in a larger gauge group, such as $SU(5)$ or $SO(10)$, at very high energies [70,71]. A common feature of many of these *grand unified theories* (GUT's) is that baryons and leptons are combined within the same representation. Because of this, the heavy gauge and Higgs bosons in these models will mediate interactions that violate baryon and lepton number. In GUT baryogenesis, the CP-violating, out-of-equilibrium decays of these heavy bosons can generate a net baryon number [72]. Unfortunately, these models are constrained by the fact that the reheating temperature in most inflationary models isn't high enough to produce enough of the heavy bosons to create the current baryon asymmetry. Furthermore, in many GUT models the heavy boson decays only violate $B+L$. Since the sphaleron transitions tend to drive the net B+L charge to zero, they will erase the baryon asymmetry produced in this way. Instead, the GUT decays must violate $B-L$ if the baryon asymmetry is to be preserved.

The leptogenesis mechanism of baryogenesis is very similar to the GUT mechanism [73–75] In this scenario, the CP-violating out-of-equilibrium decays of a heavy right-handed Majorana neutrino generate a net lepton number (L), and therefore a net $B-L$. Some of this lepton number is subsequently converted to a non-zero baryon number by the sphaleron transitions. Leptogenesis is attractive because a heavy right-handed neutrino can also explain, through the seesaw mechanism, the very small neutrino masses seen in experiments [75].

5.2 Electroweak Baryon Number Violation

An essential feature in all three of the baryogenesis mechanisms presented above is the baryon number violation induced by sphalerons. At first glance, it is surprising that baryon number is violated in the SM. B appears to be conserved in collider experiments, and is a classical symmetry of the Lagrangian defining the SM, as well as those of many SM extensions including the MSSM. However, this apparent symmetry is *anomalous* because it is broken by quantum corrections. The way in which B this violation occurs is a bit subtle. The only B violating processes in the SM are transitions between different $SU(2)_L$ vacuum states, as discussed in Section 2.1.3). Each transition violates both B and L by n_g units, where n_g is the number of fermion generations. At zero temperature these transitions proceed by tunnelling, the rate for which is unobservably small. This explains why B appears to be conserved in laboratory and collider experiments. The situation is very different at high temperatures. Here, the rate is much larger because the transitions are induced by classical thermal fluctuations. These thermal vacuum transitions are often called *sphaleron* transitions. The purpose of this section is to examine them in more detail.

We will formally define baryon number, B, as the charge that generates the $U(1)$ symmetry under which all SM quark fields are assigned $B = +1/3$, while leptons and Higgs bosons have $B = 0$. (See Table 2.1.) In other words,

$$\psi_i \to e^{iQ_i}\psi_i \tag{5.3}$$

under the $U(1)_B$ transformation. In the same way, lepton number, L, is the charge generating the $U(1)_L$ under which the lepton fields are assigned $L = +1$, and quarks and Higgs bosons have $L = 0$. Like baryon number, lepton number is a classical symmetry of the Standard Model, but is violated by quantum corrections. The Noether currents corresponding to these symmetries are given by

$$J^\mu_Q = \sum_i \left(\bar{\psi}_i \gamma^\mu \psi_i\right) Q_i, \tag{5.4}$$

where the sum runs over all SM Dirac fermions, and $Q_i = B_i$ or L_i is the charge of fermion i. If we were to add Weyl fermions to the model, they would contribute to the sum with terms identical to these but with the appropriate insertion of P_L or P_R. If there were complex bosons charged under B or L as well, such as in the MSSM, their contribution to

the current would be

$$J^\mu_Q \supseteq \sum_i i(\phi_i^* \overleftrightarrow{\partial} \phi_i)\, Q_i. \tag{5.5}$$

The time and space components of these currents correspond to the charge density and the spatial current for Q. In particular, $\bar{\psi}\gamma^0\psi$ is the net number density (number of fermions minus number of anti-fermions) for the Dirac fermion ψ. Thus, our formal definition of B coincides with our previous definition of the baryon number as being the number of baryons minus the number of anti-baryons.

The classical Lagrangian of the SM is invariant under both $U(1)_B$ and $U(1)_L$ transformations. In fact, with only the fields present in the SM there are no possible renormalizable operators operators that violate these symmetries. For this reason, B and L are said to be accidental symmetries of the SM. The violation of these symmetries by quantum corrections can be seen in a couple of ways. Either by calculating the expectation value of the current at one-loop order between two $SU(2)_L$ or $U(1)_Y$ gauge boson states [76], or by carefully computing the change in the path integral measure due to a B or L transformation [77], one obtains

$$\partial_\mu J^\mu_B = \partial_\mu J^\mu_L = \frac{n_g}{32\pi^2}\left(g_2^2 \tilde{W}^a_{\mu\nu} W^{a\,\mu\nu} - g_1^2 \tilde{B}_{\mu\nu} B^{\mu\nu}\right), \tag{5.6}$$

where $W^a_{\mu\nu}$ and $B_{\mu\nu}$ are the $SU(2)_L$ and $U(1)_Y$ field strengths, and $\tilde{F}_{\mu\nu} = \frac{1}{2}\epsilon_{\mu\nu\alpha\beta}F^{\alpha\beta}$. Recall that $\partial_\mu J^\mu_Q \neq 0$ signals the non-conservation of the charge Q.

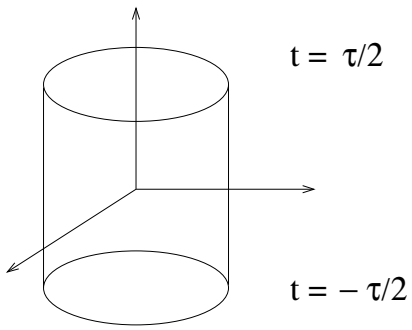

Figure 5.1: Integration region used in the analysis.

While Eq. (5.6) shows that baryon and lepton number are not conserved in the SM, it says nothing about how these charges are violated. To see how, consider integrating both sides of the equation over the spacetime cylinder depicted in Fig. 5.1, with symmetry axis along the time direction, height τ, and infinite spatial radius. We will assume that the system is in a vacuum state on the boundary of the cylinder. The left-hand side of Eq.

(5.6) then gives

$$\begin{aligned} L.S. &= \int_V d^4x\, \partial_\mu J^\mu_Q \\ &= \int_{\tau/2}^{\tau/2} dt \int d^3x\, (\partial_0 J^0_Q + \vec{\nabla}\cdot\vec{J}_Q) \\ &= \int_{\tau/2}^{\tau/2} dt \left(\frac{d}{dt}\int d^3x J^0_Q + \int_{sides} d\vec{a}\cdot\vec{J}_Q \right) \\ &= Q(\tau/2) - Q(-\tau/2), \end{aligned} \tag{5.7}$$

where in the last line we've used $Q(t) = \int d^3x\, J^0_Q(t,\vec{x})$, the total charge at time t, and the fact that $\psi(\|\vec{x}\| \to \infty) = 0$ to eliminate the spatial term. For the right-hand side of Eq. (5.6) we can rewrite these terms as total divergences,

$$\begin{aligned} \tilde{W}^a_{\mu\nu} W^{a\,\mu\nu} &= \partial_\mu K^\mu_2, \\ \tilde{B}^a_{\mu\nu} B^{a\,\mu\nu} &= \partial_\mu K^\mu_1, \end{aligned} \tag{5.8}$$

with

$$\begin{aligned} K^\mu_2 &= 2\epsilon^{\mu\nu\alpha\beta}\left(\partial_\nu W^a_\alpha\, W^a_\beta - \frac{g}{3} f^{abc} W^a_\nu W^b_\alpha W^c_\gamma\right), \\ K^\mu_1 &= 2\epsilon^{\mu\nu\alpha\beta}\partial_\nu B_\alpha\, B_\beta. \end{aligned} \tag{5.9}$$

It is now convenient to choose a gauge in which $W^a_0 = B_0 = 0$. Inserting the general gauge theory vacuum solutions given in Eq. (2.20), and integrating these terms over the cylinder (and using the divergence theorem), we get

$$\begin{aligned} R.S. &= \frac{n_g}{32\pi^2}\int_V d^4x\, \partial_\mu (K^\mu_2 + K^\mu_1) \\ &= \frac{n_g}{32\pi^2}\int_{\partial V} dS_\mu (K^\mu_2 + K^\mu_1) \\ &= \frac{n_g}{32\pi^2}\int_{t=\tau/2} d^3x\, K^0_2 \;+\; \frac{n_g}{32\pi^2}\int_{t=-\tau/2} d^3x\, K^0_2 + 0, \end{aligned} \tag{5.10}$$

where in the last line we've made use of the fact that the integral over the sides of the cylinder vanishes for the vacuum solution in our choice of gauge, and that $K^0_1 = 0$ in the vacuum. Now, using Eq. (2.20) in Eq. (5.9) we find

$$N_{cs}(t) = \frac{1}{32\pi^2}\int_t d^3x\, K^0_2, \tag{5.11}$$

where N_{cs} is the Chern-Simons number of the $SU(2)_L$ vacuum configuration at time t, as

defined in Eq. (2.22). Combining Eqs. (5.6), (5.10), and (5.11), we obtain

$$Q(\tau/2) - Q(-\tau/2) = n_g \left(N_{cs}(\tau/2) - N_{cs}(-\tau/2) \right), \tag{5.12}$$

where $Q = B$ or L. Therefore a change in baryon or lepton number requires a transition between different $SU(2)_L$ gauge vacua, and in each transition, both B and L are violated by n_g units.

Since the $SU(2)_L$ gauge vacua are separated from each other by energy barriers (of finite height), the only way to change the Chern-Simons index at zero temperature is by *instanton* tunnelling. The tunnelling rate was computed in [16], and is proportional to $e^{-2S_{inst}} = e^{-16\pi^2/g_2^2} \sim 10^{-160}$. Because of this enormous suppression, the instanton transitions are much too slow to be observed. At non-zero temperature, on the other hand, the system can pass from one vacuum to another by classical thermal fluctuations, which bump the system over the barrier. For very large temperatures, approaching the height of the energy barrier, these transitions occur very quickly.

The precise rate for the B and L violating thermal transitions depends on whether the electroweak symmetry is broken or not. In both cases, the rate is determined by a Boltzmann factor, $e^{-E_{sp}/T}$, where E_{sp} corresponds to the height of the smallest energy barrier separating distinct vacua. When the electroweak symmetry is broken, the static field configuration corresponding to this barrier is called the *sphaleron*. It has energy [78]

$$E_{sp}(T) = \frac{4\pi \left\langle \phi(T) \right\rangle}{g_2} B(\lambda/g_2), \tag{5.13}$$

where $\langle \phi(T) \rangle$ is the symmetry breaking VEV (or their orthogonal sum if there are several, as in the MSSM), λ is the effective scalar quartic self-coupling, and $B(x)$ is complicated function which ranges between $B(x = 0) \simeq 1.52$ and $B(x \to \infty) \simeq 2.72$. A careful calculation of the transition rate yields [79]

$$\Gamma_{sp} = \kappa \left(2.8 \times 10^5\right) T^4 \left(\frac{\alpha_2}{4\pi}\right)^4 \left(\frac{E_{sp}(T)}{B}\right)^7 e^{-E_{sp}(T)/T}. \tag{5.14}$$

Here, κ is a constant estimated to be of order $\kappa \simeq 10^{-1}$ [80].

For temperatures above the electroweak phase transition, where the Higgs VEV vanishes, the barrier for classical transitions goes to zero and the analysis must be modified. In this case the rate is dominated by nearly static, non-perturbative field configurations. From Eq. (5.9), it follows that in order to produce an order one change in the Chern-Simons number, a gauge field configuration of spatial extent R must be of size $1/g_2 R$, which corresponds to an energy of order $1/g_2^2 R$. The total rate should be dominated by the smallest configurations that aren't overly Boltzmann suppressed since they are the most numerous. By these rough arguments the rate per unit volume is expected to be of order $(\alpha_2 T)^4$. This crude estimate is modified by screening effects, and a more careful calculation for the rate gives [81]

$$\Gamma_{sp} = \kappa' \alpha_2^5 T^4, \tag{5.15}$$

with $\kappa' \simeq 20$ [82]. These thermal transitions are called sphaleron transitions as well, even though, strictly speaking, the sphaleron configuration no longer exists when the electroweak symmetry is unbroken.

Compared to the expansion rate of the Universe, the sphaleron transitions occur rapidly for a wide range of temperatures. In Chapter 3 we found that when the Universe is radiation-dominated, the Hubble rate is of order

$$H \simeq M_{\rm Pl}/T^2. \tag{5.16}$$

This is smaller than the sphaleron rate in the electroweak symmetric phase provided $T \lesssim 10^{12}$ GeV. In the electroweak broken phase, the sphaleron rate is much smaller. Even so, this rate exceeds the Hubble rate provided [83]

$$v/T \lesssim 1. \tag{5.17}$$

Thus, the sphaleron transitions cease to occur shortly after the electroweak phase transition.

Even though the sphaleron transitions violate both B and L, they do not create a baryon asymmetry on their own. This is because, in the absence of CP violating charge asymmetries, transitions that increase B are just as likely as those that decrease B. Even worse, if the only CP violating charge asymmetry is $B + L$, the sphaleron transitions will tend to drive the value of this asymmetry to zero. As a result, several models of GUT baryogenesis based on $SU(5)$ in which a B+L asymmetry is created by heavy boson decays have been ruled out. On the other hand, sphaleron transitions do not erase a $B-L$ charge, but they can alter the ratio of B to L. This is essential for leptogenesis, in which an initial L charge is converted to B by the sphalerons. The sphalerons can also be induced to create a baryon asymmetry in the presence of a net chiral fermion charge, which is the source of baryon production during electroweak baryogenesis.

So far we have only considered $SU(2)_L$ sphalerons. In addition to these, there are sphaleron transitions associated with the $SU(3)_c$ colour group. These *strong sphalerons* don't violate B or L, but they do violate some of the (classical) chiral symmetries of QCD, and as we shall see, play an important role in electroweak baryogenesis. The rate for the strong sphaleron transitions is given by [82]

$$\Gamma_{ss} = \kappa_{ss} \frac{8}{3} \alpha_3 \, T^4 \tag{5.18}$$

with $\kappa_{ss} = \mathcal{O}(1)$.

5.3 Electroweak Baryogenesis

Electroweak baryogenesis (EWBG) is a mechanism for creating the baryon asymmetry during the electroweak phase transition. The mechanism relies only on electroweak-scale physics, and for this reason, it will be tested directly in future particle collider experiments. This feature is not shared by the GUT and leptogenesis models. There are in fact sev-

eral related mechanisms by which the baryon asymmetry could be produced during the electroweak phase transition. We will focus on the particular version that applies to the SM and the MSSM. However, the techniques described here are generally applicable to the other cases as well.

At very high temperatures, the full $SU(2)_L \times U(1)_Y$ electroweak symmetry is restored by thermal corrections to the Higgs boson potential. As the Universe expands and the temperature falls, these corrections become less important and the Higgs boson develops a non-vanishing vacuum expectation value breaking the electroweak symmetry to its $U(1)_{em}$ subgroup. Successful EWBG requires that this *electroweak phase transition* be first order. If so, the transition proceeds by the nucleation of bubbles of broken phase, in which the Higgs expectation value is non-zero, within the surrounding symmetric phase where the Higgs expectation value vanishes. As the bubbles expand in size, CP violating interactions between the plasma and the bubble walls can generate a net chiral asymmetry in front of the bubble wall. This asymmetry tends to bias the sphaleron transitions towards producing more baryons than anti-baryons. Once produced, these baryons are swept up by the passage of the bubble or diffuse, into the broken phase. It is essential that the electroweak phase transition be *strongly* first order. Quantitatively, the necessary condition from Eq. (5.17) is

$$\frac{v_c}{T_c} \gtrsim 1, \tag{5.19}$$

where T_c is the critical temperature, and v_c is the electroweak symmetry breaking VEV at temperature T_c. If this condition holds, the sphaleron transitions are effectively turned off within the broken phase and the net baryon number that has diffused into the bubble is conserved. On the other hand, for a less strongly first-order phase transition, $v_c/T_c \lesssim 1$, the baryon number inside the broken phase will be washed out by the sphalerons. If the phase transition is strongly first order, and if there is enough CP violation in the bubble walls, this mechanism can generate the observed baryon asymmetry.

5.3.1 Dynamics of the EWPT

The details of the electroweak phase transition are essential to electroweak baryogenesis. As described above, the phase transition must be strongly first order. The subsequent formation and evolution of bubbles of broken phase within the surrounding symmetric phase determines how much of a baryon asymmetry is actually generated. Nearly all of this information is encoded in the finite-temperature effective potential, which is a generalization of the zero-temperature effective potential discussed in Appendix A.

For a theory with the scalars $\{\varphi_i\}$, $i = 1, 2, \ldots$, this potential has the form

$$V(\varphi_i, T) = V_0(\varphi_i) + V_1(\varphi_i, T) + V_{daisy}(\varphi_i, T) + \ldots \tag{5.20}$$

where V_n is the n-loop contribution, and the additional term, V_{daisy}, will be discussed below. In particular, V_0 is just the potential appearing in the Lagrangian used to define the theory. We will confine ourselves to one-loop order in this analysis.

The precise form of the loop terms depends on how the theory is renormalized. In

the $\overline{DR}$ renormalization scheme, appropriate for supersymmetric theories, the one-loop contribution reads

$$V_1(\varphi_i, T) = \sum_b g_b\, f_B(m_b^2, T) + \sum_f g_f\, f_F(m_f^2, T), \tag{5.21}$$

where b runs over bosons, f runs over Weyl fermions, and g_i is the number of (on-shell) degrees of freedom. To a very good approximation, the functions $f_B,\ f_F$ are given by [84, 85]

$$f_B(m^2, T) = \begin{cases} -\frac{\pi^2}{90}T^4 + \frac{1}{24}m^2\,T^2 - \frac{1}{12\pi}(m^2)^{3/2}\,T - \frac{m^4}{64\pi^2}\ln(\frac{Q^2}{\tilde{a}_B T^2}) & ; m/T \lesssim 2.2 \\ \frac{m^4}{64\pi^2}\left[\ln(\frac{m^2}{Q^2}) - \frac{3}{2}\right] - (\frac{m}{2\pi T})^{3/2}T^4 e^{-m/T} & ; m/T \gtrsim 2.2 \end{cases} \tag{5.22}$$

$$f_F(m^2, T) = \begin{cases} -\frac{7\pi^2}{720}T^4 + \frac{1}{48}m^2T^2 + \frac{m^4}{64\pi^2}\ln(\frac{Q^2}{\tilde{a}_F T^2}) & ; m/T \lesssim 1.9 \\ -\frac{m^4}{64\pi^2}\left[\ln(\frac{m^2}{Q^2}) - \frac{3}{2}\right] - (\frac{m}{2\pi T})^{3/2}T^4 e^{-m/T} & ; m/T \gtrsim 1.9 \end{cases}$$

Here, $\tilde{a}_B = (4\pi e^{-\gamma_E})^2,\ \tilde{a}_F = (\pi e^{-\gamma_E})^2$, m^2 is the field-dependent mass at zero temperature. We neglect V_2 and terms of higher order. The third contribution to the potential, V_{daisy}, is a finite-temperature effect [58, 85, 86]. To extend the validity of the perturbative loop expansion to high temperatures, it is necessary to resum the temperature-dependent corrections to the bosonic self-energies. These generate a thermal mass $m^2 \to \overline{m}^2 = m^2 + \alpha\, T^2$ for the bosons in theory. The effect of this resummation is to modify the effective potential by the amount

$$V_{daisy} = -\frac{1}{12\pi}\sum_b\ g_b\ \left(\overline{m}_b^2 - m_b^2\right)^{3/2}, \tag{5.23}$$

where $\overline{m}_b^2$ is the thermal mass. This sum includes gauge bosons, although only the longitudinal modes of these develop a thermal contribution to their mass at leading order.

As in the zero-temperature case, the vacuum states at finite temperature are determined by the minima of the effective potential. The location of these minima depend on the temperature, and at very high temperatures the absolute minimum is usually located at the origin of the background field space. This is true in the SM and the MSSM, and is the reason why the electroweak symmetry is restored at high temperature. In both models, as the temperature decreases, a second symmetry breaking minimum develops away from the origin. The phase transition, from symmetric phase to broken phase, will be first order provided the second minimum is separated from the minimum at the origin by a potential barrier. This is illustrated in Fig. 5.2. If there is no barrier, the transition will be second order. For both a first or a second order phase transition, we define the *critical temperature*, T_c, to be temperature at which the symmetry-breaking minimum becomes degenerate with the broken phase one.

To illustrate how the order of the PT is determined, consider the effective potential for the SM with a small scalar quartic coupling. Because the quartic is small we can neglect

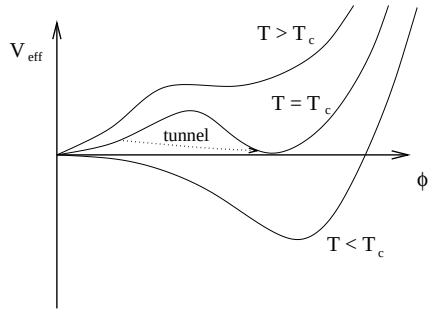

Figure 5.2: The effective potential for a first order phase transition.

the Higgs contribution to $V_{\rm eff}$. Similarly, we can ignore all the fermions except for the top quarks since they couple very weakly to the scalar background on account of their small Yukawa couplings. The relevant degrees of freedom are therefore

$$\begin{array}{ccc} W^{\pm}: & m_W^2 = \frac{g_2^2}{2}\varphi^2 & g_W = 6 \\ Z^0: & m_Z^2 = \frac{g_1^2+g_2^2}{2}\varphi^2 & g_Z = 3 \\ t: & m_t^2 = y_t^2\varphi^2 & g_t = 12. \end{array}$$

The tree-level (zeroth order) part of the potential is

$$V_0 = -\mu^2\varphi^2 + \frac{\lambda}{4}\varphi^4. \tag{5.24}$$

Combining this with the high-temperature form of the loop corrections, we can write the one-loop effective potential in the generic form

$$V_{\rm eff} \simeq (-\tilde{\mu}^2 + A\,T^2)\,\varphi^2 - E\,T\,\varphi^3 + \frac{\tilde{\lambda}}{4}\varphi^4, \tag{5.25}$$

where $\tilde{\lambda}$ and $\tilde{\mu}^2$ are the loop-corrected versions of λ and μ^2. They are related to the Higgs boson mass by

$$\begin{aligned} v^2 &= \frac{2\tilde{\mu}^2}{\tilde{\lambda}}, \\ m_h^2 &= \tilde{\lambda}\,v^2. \end{aligned} \tag{5.26}$$

For simplicity, we will also ignore the corrections due to resumming the thermal propagator, the V_{daisy} term of Eq. (5.23), in this example.

It is now a matter of straightforward algebra to find the critical temperature and the

value of the symmetry breaking minimum. At $T = T_c$ the necessary conditions are

$$\begin{aligned} \frac{\partial V_{\rm eff}}{\partial \varphi}(\varphi_c,\, T_c) &= 0, \\ V_{\rm eff}(\varphi_c,\, T_c) &= 0. \end{aligned} \tag{5.27}$$

The first condition is that φ_c be a minimum, while the second comes from demanding that the minimum at φ_c and the one at the origin are degenerate. Together, these equations imply

$$\frac{\varphi_c}{T_c} = \frac{2\,E}{\tilde{\lambda}}. \tag{5.28}$$

In the SM, the cubic coefficient E is generated at one-loop order by the electroweak gauge bosons. Comparing with equation (5.23), we see that

$$E_{SM} = \frac{3}{12\pi}\left[2\left(\frac{g_2^2}{2}\right)^{3/2} + \left(\frac{g_1^2+g_2^2}{2}\right)^{3/2}\right]. \tag{5.29}$$

When the daisy contribution is included, it turns out that only the transverse modes contribute, and this result picks up a factor of 2/3.

To avoid washing out the baryon asymmetry after the phase transition, the condition $\varphi_c/T_c > 1$ must be satisfied. Within the SM, with E given by Eq. (5.29), this requires the Higgs boson mass to be smaller than about 45 GeV. A more careful analysis including two-loop corrections increases this upper bound to 60 GeV. Either way, these values are well below the current LEP II Higgs mass lower bound of 114 GeV [41]. Things are better in the MSSM because this model has additional bosonic degrees of freedom. Specifically, a light scalar top quark can give a large contribution to the cubic coefficient. This contribution will be considered in more detail in Section 6. For appropriate values of the stop mass parameters, it is enough to make the EWPT strongly first order for Higgs boson masses up to about 120 GeV [87–95].

If the phase transition is first order, it proceeds by the formation of bubbles of broken phase within the surrounding symmetric phase. These arise because of the potential barrier separating the phases. As the temperature falls below T_c the system becomes trapped in the symmetric phase, even though the broken phase minimum is thermodynamically favoured. This situation is disrupted by tunnelling, which allows small regions to spontaneously pass to the broken phase. The result of each tunnelling event is the nucleation of a bubble of broken phase. At some temperature $T_n < T_c$, the tunnelling rate overcomes the Hubble expansion rate, and the Universe fills with expanding bubbles. In the SM and MSSM, T_n is very close to T_c [96].

Once these bubbles are formed, they expand and grow. This growth is rapid at first, but is very quickly slowed by interactions with the surrounding plasma, and as a result it is a good approximation to treat the bubbles as expanding with constant radial velocity v_w.

In this steady state, the width w of the bubbles in the MSSM is approximately [96]

$$w \simeq 20 - 30/T, \tag{5.30}$$

while typical values for the wall velocity are

$$v_w \simeq 0.01 - 0.1. \tag{5.31}$$

5.3.2 Baryon Number Generation

As the bubbles sweep through the plasma, they disturb the local thermodynamic equilibrium. The passage of a bubble is characterized by a rapid change in the local expectation values of the Higgs fields, which go from zero in the symmetric phase to non-zero values in the broken phase. This change is communicated to the other particles in the plasma by their couplings to the Higgs fields. Since the particle mass matrices generally depend on the Higgs expectation values, both the masses and the mass eigenstates will vary across the wall. These mass matrices typically also depend on CP violating phases. If so, the passage of the bubble wall will affect particles and anti-particles differently, which can lead to the generation of (CP violating) charge asymmetries in front of the bubble wall.

If the charge created in this way is approximately conserved in the symmetric phase, it will persist long enough to diffuse away from the bubble wall into the symmetric phase where the sphaleron transitions are active. The presence of this CP violating charge then biases the sphaleron transitions towards producing more baryons than antibaryons. Shortly after these baryons are produced, they are swept up by the passage of the bubble wall. Once inside the bubbles, the baryons are stable provided the phase transition is strongly first order, with the precise condition being Eq. (5.17). Since the baryon number violating interactions are spread over an extended region, this mechanism is sometimes called *non-local* electroweak baryogenesis. The diffusion of the charges enhances the amount of baryon number produced because the sphaleron transitions are induced to create baryons over a much larger volume [97].

To describe the time evolution of the charge densities, n_X, due to the passage of the bubble wall, we need a slightly more complicated form of the Boltzmann equation than was treated in Section 3.3. Consider a reaction that changes the charge X by ΔX units. Let Γ_+ be the forward rate per unit volume, and Γ_- be the backward rate. The time rate of change of the charge density n_X (assuming spatial homogeneity) is thus

$$\dot{n}_X = \Delta X \, (\Gamma_+ - \Gamma_-). \tag{5.32}$$

The ratio of the rates $\Gamma_\pm$ is given by [98]

$$\Gamma_+/\Gamma_- = e^{-(F_+ - F_-)/T}, \tag{5.33}$$

where $F_\pm$ are the free-energies corresponding to the initial states of each reaction. If the

free energy difference between the initial and final states is small, it follows that

$$\dot{n}_X \simeq -\Delta X \left(\frac{\Delta F}{T}\right) \Gamma_+. \tag{5.34}$$

Now suppose the initial and final states differ only in the number of particles which they contain. In this case,

$$\Delta F = F_+ - F_- = \sum_i \xi_i \, \mu_i, \tag{5.35}$$

where ξ is the change in the number of particle species i in each transition.

From Eq. (3.21), the net particle number density (number of particles minus antiparticles) for the species i is given by

$$n_i = g_i \int \frac{d^3p}{(2\pi)^3} \left[\frac{1}{e^{-(E-\mu_i)/T} + \eta} - (\mu_i \to -\mu_i)\right]. \tag{5.36}$$

If $\mu_i \ll T$, this simplifies to

$$n_i = k_i(m/T)\frac{T^2}{6}\,\mu_i. \tag{5.37}$$

Here, $k_i(x)$ is function that vanishes as e^{-x} for $x \gg 1$, and has $k_i(0) = g_i$.[1] Combining this with our previous results, we obtain

$$\dot{n}_X = -\Delta X \left(\sum_i \xi_i \frac{n_i}{k_i}\right) \tilde{\Gamma}, \tag{5.38}$$

where

$$\tilde{\Gamma} = \frac{6\Gamma_+}{T^3}. \tag{5.39}$$

If there are several processes that change the X charge density, the expression for $\dot{n}_X$ would involve a sum of terms of this form.

The second extension of the Boltzmann equations that we need to make is the inclusion of spatial inhomogeneities. These are induced by the passage of the bubble wall, which, in the presence of CP violation, generates charge asymmetries as it goes. This effect can be accounted for by adding position-dependent source terms for these charges in the Boltzmann equations. Once produced, the inhomogeneities in the charge densities get smoothed out by elastic scattering, the net effect of which can be modelled by adding a diffusion term to the Boltzmann equations. For the special case where the charge X corresponds to a

[1] This applies to Weyl fermions or real scalars. For Dirac fermions and complex scalars, a factor of two should be included in g_i.

particle number asymmetry, the Boltzmann equation becomes [99, 100]

$$\dot{n}_X = D_X \nabla^2 n_X - \Delta X \left(\sum_i \xi_i \frac{n_i}{k_i} \right) \tilde{\Gamma} + \gamma_X(x), \tag{5.40}$$

where γ_X is the source term, and D_X is the diffusion constant for the species.

The source term in Eq. (5.40) is related to the net X charge current, j^μ_X, computed in the position-dependent Higgs background, but in the absence of particle number changing reactions like those in Eq. (5.38). The expression for this current in terms of quantum fields is given by Eqs. (5.4) or (5.5). In terms of the current, the source is given by [101]

$$\gamma_X = \partial_0 j^0_X - D_X \nabla^2 j^0_X. \tag{5.41}$$

With this source, the actual number density reduces to j^0_X as $\tilde{\Gamma} \to 0$, which is the correct boundary condition.

Because of diffusion, the charge density created by the source will move away from the bubble wall. The typical distance travelled is the diffusion length, which after a time t is approximately $\sqrt{D_X t}$. In the same time interval the bubble wall will have advanced by an amount $v_w\, t$, where v_w is the wall velocity. Equating these two distances, we see that the charge density will persist in front of the bubble wall for a time

$$t_D \simeq D_X / v_w^2, \tag{5.42}$$

before getting swept up by the bubble. This persistence time ignores the effects of particle number changing reactions. These will be relevant only if the reaction time scale, Γ^{-1}, is less than t_D. If so, the actual persistence time of the charge can be much smaller than t_D since the charge is destroyed before the bubble arrives.

Consider Eq. (5.40) applied to the baryon number asymmetry, n_B. The only processes that change n_B are the weak sphaleron transitions. Each transition alters B by three units and produces three quarks and one lepton for each generation. The relevant Boltzmann equation, assuming all baryons have roughly the same diffusion constant D_q, is therefore [100–103]

$$\dot{n}_B = D_q \nabla^2 n_B - \Theta(-x - v_w t) \left[\frac{n_g T^2}{6} \sum_i (3\mu_{q_i} + \mu_{l_i}) + \mathcal{R}\, n_{B+L} \right] \tilde{\Gamma}_{ws}, \tag{5.43}$$

where n_g is the number of generations, and μ_{q_i} and μ_{l_i} are the chemical potentials for the left-handed quark and lepton doublets. We have also assumed that the weak sphalerons are active only in the symmetric phase, which we take to be $x < -v_w\, t$ for a bubble moving in the $-x$ direction. This is illustrated in Fig. 5.3. The second term in this equation was not present in Eq. (5.38), and is the result of the change in topological number in the sphaleron transition [83, 104]. For the SM and MSSM, the corresponding *relaxation coefficient* $\mathcal{R}$ has

value [102]

$$\mathcal{R} = \frac{9}{4}\left(1 + \frac{n_{\tilde{q}}}{6}\right)^{-1} + \frac{3}{2}, \tag{5.44}$$

where $n_{\tilde{q}}$ is the number of light squark flavors. ($n_{\tilde{q}} = 0$ gives the SM.)

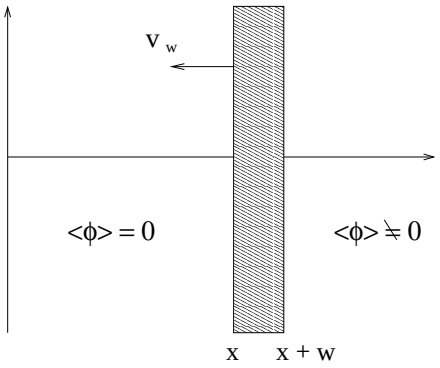

Figure 5.3: Expansion of a bubble wall. The wall has width w and is moving to the left with speed v_w. The region to left of the wall is the symmetric phase, while the region to the right is the broken phase.

Compared to the persistence time t_D over which the the bubble disturbs the particle number asymmetries, the weak sphaleron rate is quite slow. As a result, we can ignore the weak sphalerons when calculating the asymmetries that generate non-zero values of μ_{q_i} and μ_{l_i}, and treat them as specified background sources in Eq. (5.43). The evolution of the baryon asymmetry is then simple to see. In the absence of a chiral asymmetry, $\mu_{q_i} = \mu_{l_i} = 0$, and any initial baryon number in the symmetric phase relaxes to zero as $e^{-\Gamma_{ws}t}$. On the other hand, a non-zero chiral asymmetry acts as a source for baryon number. This is what drives electroweak baryogenesis.

Let us now give an example of how the non-zero chiral asymmetry is generated. We will specialize to the case of the MSSM, and assume that the only CP violating sources arise from the charginos and the third generation squarks. This treatment follows that of [100]. The bubble-wall timescale is given in Eq. (5.42), and is fast relative to the weak sphalerons, but quite slow compared to the $SU(3)_c$ and $SU(2)_L$ gauge interactions in the symmetric phase. It is also slow compared to the top Yukawa interactions, the supersymmetric gauge and Higgs interactions, but fast relative to the other Yukawas. The reactions that are fast relative to the wall timescale can be treated as being in chemical equilibrium allowing us to relate many of the chemical potentials. In particular, we have

- $SU(3)_c \Rightarrow \mu_q$ is the same for all colours.
- $SU(2)_L \Rightarrow \mu_{t_L} = \mu_{b_L}$.
- SUSY Higgs $\Rightarrow \mu_{h_2^0} = \mu_{h_2^+} = \mu_{h_1^0} = \mu_{h_1^-}$.

- SUSY Gauge $\Rightarrow \mu_q = \mu_{\tilde{q}},\ \mu_h = \mu_{\tilde{h}}$.
- Top Yukawa $\Rightarrow \mu_{t_L} - \mu_{h_2^0} - \mu_{t_R} = 0$.
- Strong Sphaleron $\Rightarrow \sum_i (\mu_{u_L^i} + \mu_{d_L^i} - \mu_{u_R^i} - \mu_{d_R^i})$.

Here, $h_2^0,\ h_2^+,\ \ldots$ are the components of the Higgs bosons, $\tilde{q}$ are squarks, and $\tilde{h}$ are higgsinos. The other interactions that we will consider in computing the chiral asymmetry are the top mass and the Higgs VEV interactions. If these were in equilibrium they would imply $\mu_{t_L} = \mu_{t_R}$, and $\mu_h = 0$ respectively. Both reaction rates are fast in the broken phase, but being proportional to the Higgs vacuum expectation value, they vanish in the symmetric phase. We will therefore include them explicitly in the relevant Boltzmann equations. We will also include reactions due to the strong sphalerons, $\tilde{\Gamma}_{ss}$, and the top Yukawa interactions, $\tilde{\Gamma}_y$. All other reactions will be treated as being too slow to be relevant.

By assumption, only the higgsinos and the third generation squarks are sourced by the bubble wall. Since the only reaction that produces first and second generation particles are the strong sphalerons, we can relate their number densities to those of the third generation. The effect of the strong sphalerons can be represented by the effective operator [105]

$$\mathcal{O}_{ss} \sim \prod_{i=1}^{n_g} (u_L^i d_L^i u_R^c d_R^c). \tag{5.45}$$

Thus, one u_L is always produced with one anti-u_R so that

$$q_L^1 = q_L^2 = -2u_R = -2d_R = -2c_R = -2s_R = -2b_R, \tag{5.46}$$

where $f_{L,R}$ is the number asymmetry for fermion f, $q_L^i = (u_L^i + d_L^i)$, and the superscript i labels generations. Barring an initial asymmetry, we also have $B+L \simeq B \simeq 0$. Applying this constraint and using Eq. (5.46), we get

$$b_R + \tilde{b}_R = -(q_L^3 + \tilde{q}_L^3 + t_R + \tilde{t}_R) \tag{5.47}$$

Putting these constraints together, we see that there are only three independent particle densities:

$$\begin{aligned} Q &= t_L + b_L + \tilde{t}_L + \tilde{b}_L = \mu_Q (k_{t_L} + k_{b_L} + k_{\tilde{t}_L} + k_{\tilde{b}_L}) \frac{T^2}{6} := \mu_Q k_Q \frac{T^2}{6}; \\ T &= t_R + \tilde{t}_R := \mu_T (k_{t_R} + k_{\tilde{t}_R}) \frac{T^2}{6} := \mu_T k_T \frac{T^2}{6}; \\ H &= h + \tilde{h} = \mu_H (k_h + k_{\tilde{h}}) \frac{T^2}{6} := \mu_H k_H \frac{T^2}{6}. \end{aligned} \tag{5.48}$$

For EWBG within the MSSM, it is usually the case that the one Higgs boson and the all Higgsinos are light, but the squarks other than a mostly right-handed stop are heavy. If so, then

$$k_Q = 3 + 3 = 6, \qquad k_T = 3 + 3 \cdot 2 = 9, \qquad k_H = 4 + 2 \cdot 4 = 12. \tag{5.49}$$

Also, $k_B = k_U = \ldots = 3$ for the corresponding right-handed quark/squark densities, and $k_{Q_1} = k_{Q_2} = 6$ for the left-handed first and second generation quark/squark doublets.

The Boltzmann equations for these particle asymmetries can be simplified somewhat by making two well-motivated approximations. The first is that the bubble walls are nearly planar, so that we need only concentrate on the spatial coordinate normal to the wall. The second approximation is that all the quarks and squarks have nearly equal diffusion constants, D_q, as do the Higgs bosons and Higgsinos, D_h. Calculations of these quantities find $D_q \simeq 10/T$, $D_h \simeq 100/T$ [99]. On top of these approximations, it helps to work in the bubble wall frame and re-express all of the equations in terms of the distance from the bubble wall, $z = x + v_w t$. In doing so, we will implicitly assume that the particle densities depend only on this coordinate. In the bubble wall frame, the Boltzmann equations for the relevant particle asymmetries then read

$$\begin{aligned} v_w Q' &= D_q\, Q'' - \tilde{\Gamma}_y\,(Q/k_Q - H/k_H - T/k_T) - \tilde{\Gamma}_m\,(Q/k_Q - T/k_T) \\ &\qquad - 2\tilde{\Gamma}_{ss}\,[2Q/k_Q - T/k_T + 9(Q+T)/k_B] + \gamma_Q, \\ v_w T' &= D_q\, T'' + \tilde{\Gamma}_y\,(Q/k_Q - H/k_H - T/k_T) + \tilde{\Gamma}_m\,(Q/k_Q - T/k_T), \\ &\qquad + \tilde{\Gamma}_{ss}\,[2Q/k_Q - T/k_T + 9(Q+T)/k_B] + \gamma_T \\ v_w H' &= D_q\, H'' + \tilde{\Gamma}_y\,(Q/k_Q - H/k_H - T/k_T) + \tilde{\Gamma}_h\, H/k_H + \gamma_h. \end{aligned} \tag{5.50}$$

Here, the prime denotes differentiation with respect to the bubble wall coordinate, z, and Eq. (5.46) was used to simplify the form of the strong sphaleron terms.

Since $\tilde{\Gamma}_m$ and $\tilde{\Gamma}_h$ are proportional to the Higgs VEV's, they tend to be much smaller than $\tilde{\Gamma}_{ss}$ and $\tilde{\Gamma}_y$. Thus, we may use these to further relate the particle densities. Together, they imply

$$\begin{aligned} T &= -\frac{k_T}{k_H}\left(\frac{2k_B + 9k_Q}{k_B + 9k_Q + 9k_T}\right) H, \\ Q &= \frac{k_Q}{k_H}\left(\frac{9k_T - k_B}{k_B + 9k_Q + 9k_T}\right) H. \end{aligned} \tag{5.51}$$

Corrections to these values will be $\mathcal{O}(1/\tilde{\Gamma}_{ss})$ or $\mathcal{O}(1/\tilde{\Gamma}_y)$. Taking the linear combination of Eqs. (5.50) that is independent of $\tilde{\Gamma}_s$ and $\tilde{\Gamma}_y$, we obtain the following reduced diffusion equation:

$$0 = -v_w\, H' + \bar{D} H'' - \bar{\Gamma}\, H + \bar{\gamma}, \tag{5.52}$$

where the barred coefficients are given by

$$\begin{aligned} \bar{\gamma} &= (\gamma_h - 2\gamma_T - \gamma_Q) k_H (k_B + 9k_Q + 9k_T)/\mathscr{D} \\ \bar{\Gamma} &= (\tilde{\Gamma}_h + \tilde{\Gamma}_m)\,(9k_Q + 9k_T + k_B)/\mathscr{D} \\ \bar{D} &= [k_H(k_B + 9k_Q + 9k_T)\, D_h + (k_T k_B + 9 d_T k_Q + k_Q k_B)\, D_q]/\mathscr{D} \end{aligned} \tag{5.53}$$

with the denominator $\mathscr{D} = [k_H(k_B + 9k_Q + 9k_T) + 9k_Tk_Q + 4k_Tk_B + k_Qk_B]$.

In general, k_i, $\bar{D}$, $\bar{\gamma}$, and $\bar{\Gamma}$ all depend on z due to the varying Higgs background. Once a Higgs profile is specified, these functions are determined, and it is straightforward to integrate Eq. (5.52) numerically to obtain the particle asymmetries, $H(z)$, $Q(z)$, and $T(z)$. However, in order to be able to show an analytic solution we will make the following approximations:

$$\begin{aligned} k_i,\ \bar{D} &= \textit{constant} \\ \bar{\gamma} &= \begin{cases} \bar{\gamma}_0; & 0 < z < w \\ 0; & \text{otherwise} \end{cases} \\ \bar{\Gamma} &= \begin{cases} \bar{\Gamma}_0; & z > 0 \\ 0; & z < 0 \end{cases} \end{aligned} \tag{5.54}$$

In other words, we fix $\bar{D}$, k_i which depend only weakly on the Higgs background, take the CP-violating sources to be non-zero only within a finite bubble wall width, and assume the Higgs and top mass interactions are active only in the broken phase. Compared to a more precise numerical evaluation, these approximations work well except for the CP-violating source term, which depends sensitively on the Higgs VEV profile in the bubble wall. The solution for $H(z)$ in the symmetric phase ($z < 0$) is then

$$H(z) = \mathscr{A}\, e^{z v_w/\bar{D}}, \tag{5.55}$$

with the constant $\mathscr{A}$ given by

$$\mathscr{A} = \left(\frac{\gamma_0}{\Gamma_0}\right)\left(1 - e^{-2w\sqrt{\Gamma_0/\bar{D}}}\right). \tag{5.56}$$

Using Eqs. (5.46), (5.51), and the above expression for the Higgs density, we solve for the quark densities. These provide the chiral fermion source term for the weak sphalerons, Eq. (5.43):

$$\begin{aligned} \frac{T^2}{6}\sum_{i=1}^{3}(3\mu_{q_i} + \mu_{l_i}) &= 3\left(\frac{Q}{k_Q} + \frac{Q_1}{k_{Q_1}} + \frac{Q_2}{k_{Q_2}}\right), \\ &= \frac{1}{2}(5Q + 4T) \\ &:= \frac{1}{2}\, n_L(z), \end{aligned} \tag{5.57}$$

The quantity $n_L(z)$ represents the net chiral fermion charge created by the bubble wall.

We can now solve for the baryon asymmetry generated by this mechanism. In the broken phase, the asymmetry is independent of position, and equal to [103]

$$n_B = -\frac{n_g\tilde{\Gamma}_{ws}}{2\, v_w}\int_{-\infty}^{0} dz\; n_L(z)\, e^{z\mathcal{R}/v_w}. \tag{5.58}$$

This equation exhibits all three Sakharov conditions. The weak sphaleron rate corresponds to B violation, the appearance of the chiral fermion asymmetry $n_L(z)$ indicates C and CP violations, and the presence of v_w implies departure from equilibrium. We should also point out that this result relies on the inequalities $D/v_w^2 \ll \tilde{\Gamma}_{ws}^{-1}$, as well as $D/v_w^2 \gg \tilde{\Gamma}_{ss}^{-1},\ \tilde{\Gamma}_y^{-1}$. As a result, it no longer holds if these inequalities are violated.

CHAPTER 6
EWBG AND DM IN THE MSSM

The Standard Model of particle physics fails to explain both the baryon asymmetry of the Universe, and the nature of the dark matter. Thus, despite its great success in collider experiments, an extension of the SM description is needed. Both shortcomings of the SM can be overcome if the model is extended to include supersymmetry. For example, within the minimal supersymmetric extension of the SM, the MSSM, the baryon asymmetry can be generated by electroweak baryogenesis, and the dark matter can be made up of the lightest neutralino.

In this section we will investigate whether the MSSM is able to account for both the dark matter and the baryon asymmetry simultaneously. Compared to previous work along these lines [106], we include the effect of CP violating phases, which are essential to electroweak baryogenesis. In Section 6.1 we will discuss the conditions that must be fulfilled within the MSSM for EWBG to generate the baryon asymmetry. The constraints on these conditions, especially those on CP violating phases, will be discussed in Section 6.2. Section 6.3 deals with the neutralino dark matter relic density subject to conditions needed for EWBG. In particular, we shall consider the effect of CP violating phases and a light stop. Section 6.4 examines the prospects for direct detection of the neutralino dark matter in laboratory experiments, again including CP violating phases. Finally, Section 6.5 is reserved for our conclusions. The material in this section is based on Ref. [1].

6.1 Electroweak Baryogenesis in the MSSM

The MSSM has two crucial ingredients compared to the SM that allow electroweak baryogenesis to be successful: additional bosonic degrees of freedom; and new sources of CP-violation. The extra bosons in the model, a light stop in particular, can make the electroweak phase transition strongly first-order. Furthermore, the model has many CP violating phases in addition to the CKM phase of the SM. These phases originate from the soft supersymmetry breaking terms, and the μ parameter.

6.1.1 A First-Order Electroweak Phase Transition

As far as the electroweak phase transition is concerned, the most important new contribution in the MSSM comes from a light stop. This particle interacts with the Higgs field with a coupling equal to the top-quark Yukawa, and its six degrees of freedom further enhances the effect on the Higgs potential. While there are two stop mass eigenstates in the MSSM, only one of the two can be light. There are two reasons for this. First, one stop must be

heavy in order to raise the mass of the lightest CP-even Higgs boson above the current experimental limit. And second, a light state with a large left-handed component ($\tilde{t}_L$) would generate too large of a correction to the electroweak observables such as $\Delta\rho$ [107].

The mass matrix for the stop quarks in the MSSM is given by

$$\mathcal{M}^2_{\tilde{t}} = \begin{pmatrix} m^2_{Q_3} + m^2_t + D_L & m_t X_t \\ m_t X_t^* & m^2_{U_3} + m^2_t + D_R \end{pmatrix}, \tag{6.1}$$

where $m_t = y_t \varphi \sin\beta$, $D_L = (t^3 - Q\sin^2\theta_w) M_Z^2 \cos 2\beta$, $D_R = Q\sin^2\theta_w M_Z^2 \cos 2\beta$, and $X_t = (A_t - \mu^* \cot\beta)$. Since the mostly left-handed state must be fairly heavy, we consider the limit $m^2_{Q_3} \gg |m^2_{U_3}|$, $|X_t|^2$, D_L, D_R. The mass of the mostly right-handed state in this limit is then

$$m^2_{\tilde{t}_1} \simeq m^2_{U_3} + D_R^2 + m_t^2 \left(1 - \frac{|X_t|^2}{m^2_{Q_3}}\right). \tag{6.2}$$

Studies of the EWPT within the MSSM indicate that the ratio of the vacuum expectation values, $\tan\beta = \varphi_2/\varphi_1$, remains relatively constant over the course of the phase transition. As a result, we may treat β as being fixed and focus on the potential as a function of $\varphi = \sqrt{{\varphi_2}^2 + {\varphi_1}^2}$ for the purposes of finding the order of the phase transition. The one-loop effective potential therefore has the generic form of Eq. (5.25), with $\lambda = (g_1^2 + g_2^2)\cos^2 2\beta/2$ at tree-level, but with a significant one-loop correction [108]. The effective cubic coefficient, E, is greatly enhanced relative to the MSSM due to the light stop states. Using Eqs. (5.21) and (5.23), the portion that gives rise to this cubic term is

$$\begin{aligned} (cubic) \;&\simeq\; T\, E_{SM} \varphi^3 \\ &\quad + T \frac{6}{12\pi} \left[m^2_{U_3} + D_R + y_t^2 \sin^2\beta \left(1 - \frac{|X_t|^2}{m^2_{Q_3}}\right) \varphi^2 + \Pi_{\tilde{t}_1}(T) \right]^{3/2}, \end{aligned} \tag{6.3}$$

where $\Pi_{\tilde{t}_1}(T)$ is the thermal correction to the mass from Eq. (5.23). If the gluino and all the squarks are except for the light stop are heavy (compared to the temperature), it is given by [109]

$$\Pi_{\tilde{t}_1}(T) = \frac{4}{9} g_3^2\, T^2 + \frac{1}{6} y_t^2 \left[1 + \sin^2\beta (1 - \frac{|X_t|^2}{m^2_{Q_3}})\right] T^2 + \frac{1}{18}(6 + \cos 2\beta)\, T^2. \tag{6.4}$$

The effect of the term in Eq. (6.4) will be greatest if it is exactly cubic. This is the case only for a negative soft mass-squared equal to

$$m^2_{U_3} = -\left(D_R + \Pi_{\tilde{t}_1}\right). \tag{6.5}$$

However, if $m^2_{U_3}$ is too negative it will induce a vacuum expectation value for the right-handed stop field. This vacuum state is ruled out experimentally because in it, the Higgs fields do not get a VEV and the $SU(3)_c$ gauge symmetry is broken. To avoid this situation

altogether, the necessary condition is [109]

$$m_{U_3}^2 \gtrsim -(80 \text{ GeV})^2. \tag{6.6}$$

This condition can be relaxed somewhat if one allows for the usual MSSM vacuum state to be metastable with a lifetime much longer than the age of the Universe..

With the enhancement of the cubic term due to a light stop, the electroweak phase transition can be made strongly first order. However, more detailed calculations show that this is only possible if the Higgs boson involved in breaking the electroweak symmetry is lighter than 120 GeV [87–95], only slightly above the present experimental bound [41],

$$m_h \gtrsim 114 \text{ GeV}, \tag{6.7}$$

which is valid for a Higgs boson with SM-like couplings to the gauge bosons.[1]

The combined requirements of a first-order electroweak phase transition, strong enough for EWBG, and a Higgs boson mass above the experimental limit severely restrict the allowed values of the stop parameters. Since the stops generate the most important radiative contribution to the Higgs boson mass in the MSSM [42], the other stop must be considerably heavier in order to raise the Higgs mass above the experimental bound (Eq. (6.7)). For the stop soft supersymmetry-breaking masses, this implies [91]

$$\begin{aligned} m_{U_3}^2 &\lesssim 0 \,, \\ m_{Q_3}^2 &\gtrsim (1 \text{ TeV})^2 \,. \end{aligned} \tag{6.8}$$

A similar tension exists for the combination of soft SUSY breaking parameters defining the stop mixing, $|A_t - \mu^* \cot\beta|/m_{Q_3}$, and $\tan\beta$. Large values of these quantities tend to increase the Higgs mass at the expense of weakening the phase transition or the amount of baryon number produced. The allowed ranges have been found to be [91]

$$\begin{aligned} 5 &\lesssim \tan\beta \lesssim 10 \,, \\ 0.3 &\lesssim |A_t - \mu^*/\tan\beta|/m_{Q_3} \lesssim 0.5 \,. \end{aligned} \tag{6.9}$$

6.1.2 CP Violation

In addition to a strongly first-order EWPT, new sources of CP violation beyond the CKM phase of the SM are needed to generate the baryon asymmetry. These sources induce a net chiral fermion charge that causes the sphaleron transitions to produce baryons. Within the MSSM, the most efficient source for generating a chiral fermion charged is generated by the charginos, and to a lesser extent the neutralinos [120].

---

[1] The requirements of a light stop and a light Higgs boson may be relaxed in non-minimal supersymmetric extensions. See, for instance, Refs. [113]– [119].

Recall that the chargino mass matrix is given by

$$M_{\chi^\pm} = \begin{pmatrix} 0 & X^t \\ X & 0 \end{pmatrix}, \tag{6.10}$$

where

$$X = \begin{pmatrix} M_2 & g_2\, v_2 \\ g_2\, v_1 & \mu \end{pmatrix}. \tag{6.11}$$

During the passage of the bubble wall, both v_1 and v_2 become functions of position. Furthermore, each of M_2 and μ can have CP violating phases. Together, these properties give rise to a source term for the (charged) Higgsino density [Eq. (5.49)]. This source is obtained from the Higgsino current computed in the position-dependent background using Eq. (5.41). The value of the resulting source term is proportional to $\mathrm{Im}(\mu\, \mathrm{M}_2)$ [101, 120, 121].

In order for the source to be significant, this phase must be fairly large, and the charginos must be abundant in the plasma which requires that they not be too much heavier than the temperature of the plasma, $T \sim T_c$. In the recent analysis of Ref. [101], the authors found the bounds

$$\begin{aligned} |\mathrm{Arg}(\mu\, \mathrm{M}_2)| &\gtrsim 0.1\ , \\ \mu,\ M_2 &\lesssim 500\ \mathrm{GeV}\ . \end{aligned} \tag{6.12}$$

The need for a large CP violating phase implies that there is a danger of violating the experimental bounds on the electric dipole moments (EDM) of the electron, neutron, and ^{199}Hg atom since such phases generate new contributions to these EDM's. Similarly, the branching ratio for $b \to s\gamma$ decays is also sensitive to this phase, and therefore imposes a further constraint on the EWBG mechanism. These constraints will be investigated below.

6.2 Constraints on CP Violating Phases

The only phase that we consider in this work is the one directly related to EWBG, namely $\mathrm{Arg}(\mu\, \mathrm{M}_2)$. We will assume further that this phase is the result of a common phase for the electroweak gaugino soft mass parameters. With this assumption, all CP violating effects are confined to the chargino and neutralino sectors, or the loop corrections induced by them.[2] By means of a $\mathrm{U}(1)_R$ transformation, we may transfer the gaugino phase into the μ parameter and the trilinear A_f terms. Under this transformation, the effective values of these parameters are shifted according to

$$\begin{aligned} M_\lambda &\to M_\lambda\, e^{-i\,\varphi}, \\ \mu &\to \mu\, e^{i\,\varphi}, \\ A_f &\to A_f\, e^{-i\,\varphi}, \end{aligned} \tag{6.13}$$

[2] We do not consider the effects of a gluino phase. For the parameters considered in the present work, we expect that such a phase would only have a very small effect.

with the remaining MSSM parameters left unchanged. For consistency of notation with Ref. [101], we will implicitly make a $U(1)_R$ rotation such that the gaugino masses are all real and positive, and the μ parameter and the A_f terms have equal and opposite phases, up to a possible relative sign.

As a further simplification, we will neglect the mixing between CP-even and CP-odd Higgs bosons due to these phases. While this mixing can be significant in some regions of the MSSM parameter space, especially for large values of $\tan\beta$, we have checked that the mixing induced by chargino and neutralino loop corrections is small ($\lesssim 3\%$) for the parameters considered here, where $\tan\beta$ takes only moderate values. We also note that in Ref. [122] the effect of Higgs mixing [123] on the neutralino relic density was found to be small, even in the large $\tan\beta$ regime. The supersymmetric corrections to the bottom mass [124] are also suppressed in the region of parameter space considered here, and thus all relevant CP violating effects are associated with the tree-level effect on the neutralino masses and couplings.

6.2.1 Electron EDM Constraints

The MSSM can accommodate many new CP violating phases in addition to the CKM phase present in the SM. Such phases, however, are very highly constrained by the experimental limits on the electric dipole moments (EDM) of the electron, neutron, and ^{199}Hg atom. Of these, we will focus our attention on the electron EDM since it is the best measured, the least plagued by theoretical uncertainties, and for the phases relevant to the model under study gives the strongest constraint. The upper bound on the electron EDM comes from measurements of the EDM of the ^{205}Tl atom. For the phases considered here and in the absence of Higgs mixing, the CP-odd electron-neutron operator studied in Ref. [125] vanishes, and the ^{205}Tl EDM is due almost entirely to the electron EDM. This translates into a limit on the electron EDM of [126]

$$|d_e| < 1.6 \times 10^{-27}\, e\, cm, \tag{6.14}$$

at 90% CL.

In the MSSM, the leading order contributions to the electron EDM come from one-loop diagrams containing an intermediate selectron or sneutrino. For $\mathcal{O}(1)$ phases, these loops generate an EDM well above the experimental limit unless these sfermions are taken to be quite heavy, $m_{\tilde{f}} \gtrsim 10$ TeV [127]. The neutron and ^{199}Hg EDM constraints require that the other first and second generation sfermions be very heavy as well. This feature arises in several models considered in the literature [119, 128–130]. Such large first and second generation sfermion masses present no problem for EWBG since they couple very weakly to the Higgs bosons, and have only a minor effect on the final CP asymmetry [120]. With respect to EWBG, a much more dangerous contribution arises at two loops.

At the two-loop order, there are contributions to the electron EDM from loops containing intermediate charginos and Higgs bosons. Since EWBG demands that the charginos be fairly light, $m_\chi \lesssim 500$ GeV, these contributions cannot be suppressed by taking large chargino masses. On the other hand, these terms can be reduced by taking large M_a or

small $\tan\beta$. The phase associated with this contribution comes primarily from the chargino mass matrix, which is the same phase that generates the baryon asymmetry. Consequently, the electron EDM bound presents a particularly severe constraint on EWBG within the MSSM.

We have examined whether it is possible for EWBG to generate the observed baryon asymmetry while obeying the electron EDM bounds. The two-loop contributions to the electron EDM due to loops with charginos and Higgs bosons were calculated following Refs. [125, 131]. The method of Ref. [101] was used to calculate the baryon asymmetry generated by EWBG. In our analysis, we have fixed $M_2 = 200$ GeV, and have varied μ, $\mathrm{Arg}(\mu)$, $\tan\beta$, and M_a. We have also assumed a bubble wall velocity of $v_w = 0.05$ and a wall width of $L_w = 20/T$. Both of these values are fairly typical, and tend to maximize the baryon asymmetry generated in the phase transition.

The dependence of the baryon asymmetry relative to the value needed for big-bang nucleosynthesis (BBN), η/η_{BBN}, on $|\mu|$ and M_a is illustrated in Fig. 6.1. In this plot, we have taken the phase to be maximal, $\sin(\mathrm{Arg}(\mu)) = 1$, and have set $\tan\beta = 5$. For other values of these parameters, the baryon asymmetry scales with $\sin(\mathrm{Arg}(\mu))$ and (approximately) with $\sin 2\beta$. There are two main contributions from the CP violating currents of charginos and neutralinos to the baryon asymmetry in the MSSM. The first is proportional to the change in β going from the symmetric phase to the broken phase and exhibits a resonance at $M_2 = |\mu|$, but is highly suppressed for large values of M_a. The second contribution is independent of M_a, and falls off smoothly as $|\mu|$ becomes large. Both contributions go to zero as M_2 becomes large.

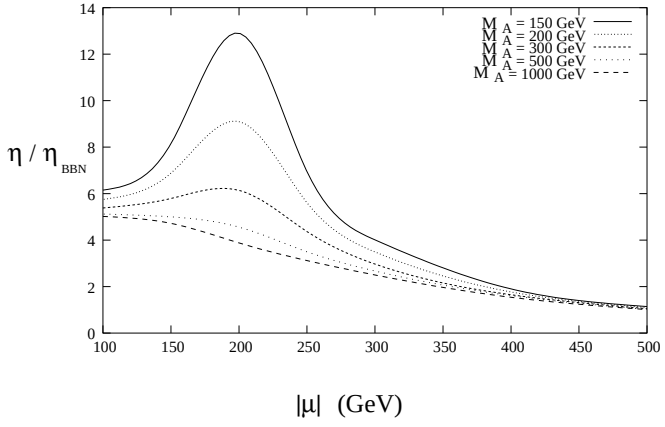

Figure 6.1: Baryon asymmetry generated by EWBG relative to that required by big-bang nucleosynthesis for $M_2 = 200$, $\tan\beta = 5$, and $\sin(\mathrm{Arg}(\mu)) = 1$.

Fig. 6.2 shows the regions in the $|\mu| - M_a$ and $M_a - \tan\beta$ planes consistent with both EWBG and the experimental bound on the electron EDM. Here, we have scanned over the

ranges

$$3 < \tan\beta < 10, \quad 100 \text{ GeV} < M_a < 1000 \text{ GeV}, \quad 100 \text{ GeV} < |\mu| < 1000 \text{ GeV}, \tag{6.15}$$

with $M_2 = 200$ GeV and the rest of the parameters as in Section 2. We find that in the allowed region, $|\mu|$ is confined to the range $110 \lesssim |\mu| \lesssim 550$ GeV, while M_a must be greater than about 200 GeV. The limits on $|\mu|$ are due to the effect of this parameter on the chargino mass. For $|\mu| \lesssim 110$ GeV, the lighter chargino has mass below the experimental bound, $m_{\chi_1} \gtrsim 103.5$ GeV [132], while for large $|\mu|$, EWBG becomes less efficient. The lower bound on M_a arises for two reasons. For small M_a the two-loop contribution to the electron EDM is enhanced, while the mass of the lightest Higgs boson is suppressed. The effect of the Higgs mass constraint can also be seen in Fig. 6.2, and results in a lower limit on $\tan\beta$. The allowed region is cut off for larger values of $\tan\beta$ since such values tend to increase the two-loop contributions to the electron EDM.

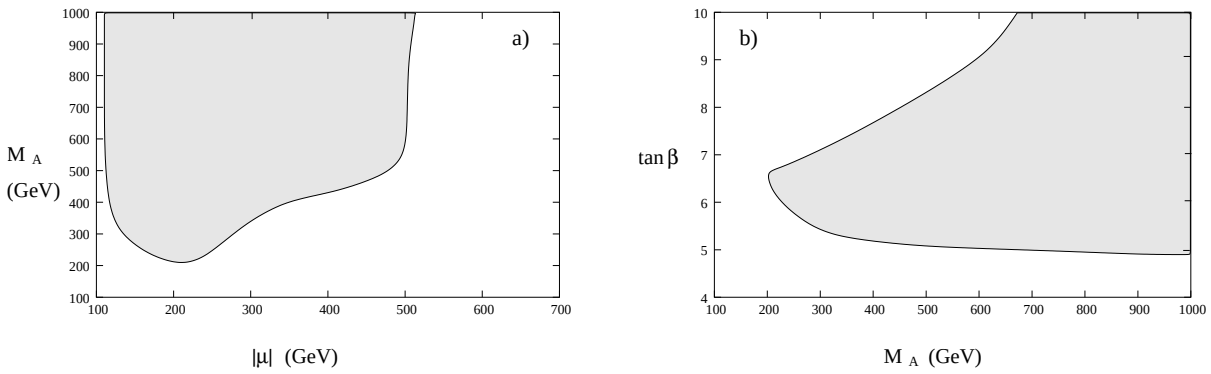

Figure 6.2: Parameter regions consistent with EWBG and the electron EDM limit. In these plots, we have taken $M_2 = 200$ GeV and varied $\text{Arg}(\mu)$ over the interval $[0, \pi]$.

From Fig. 6.2, we also see that it is possible to generate the baryon asymmetry via EWBG in the MSSM while satisfying the experimental constraints on the electron EDM and the mass of the lightest Higgs boson. Although this is reassuring, the EWBG scenario is still very strongly constrained by the electron EDM. This can be seen in Fig. 6.3, which shows the range of values of d_e obtained in our scan that are consistent with EWBG, the current electron EDM bound, and the Higgs mass limit. For $M_a < 1000$ GeV, an order of magnitude improvement of the electron EDM bound, $|d_e| < 0.2 \times 10^{-27}\, e\, cm$, will be sufficient to test this baryogenesis mechanism within the MSSM. However, we should also point out that the calculation of the baryon asymmetry from EWBG has $\mathcal{O}(1)$ uncertainties associated with the values of the bubble parameters, the wall velocity, and the various approximations used to derive the diffusion equations and the CP violating sources. Therefore the limits on EWBG presented here may be somewhat more (or less) severe than they really are. Furthermore, we have not considered the possibility of fortuitous cancellations between

different EDM contributions, for instance between the one-loop and two-loop terms (for lighter sfermions), which could further reduce the value of the electron EDM.

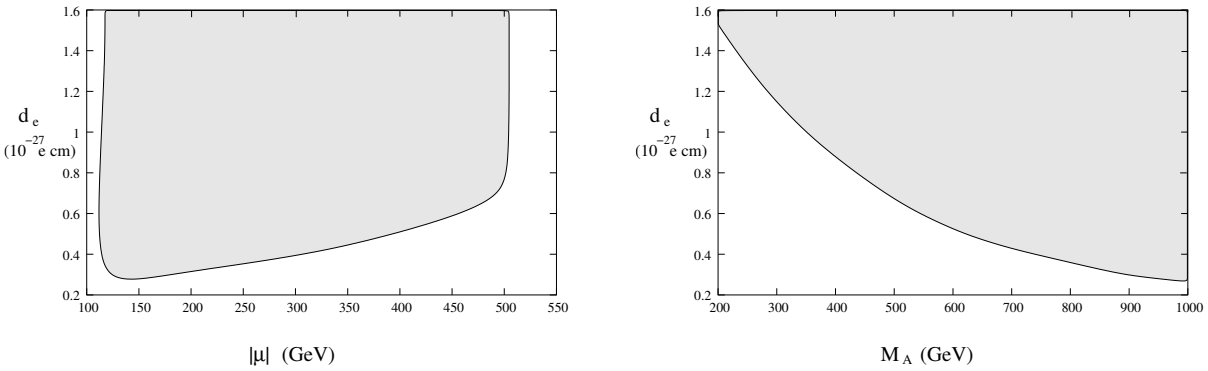

Figure 6.3: Range of values of the electron EDM for parameter sets consistent with EWBG.

6.2.2 Constraints from BR($b \to s\gamma$)

The presence of a light stop, light charginos, and a light charged Higgs boson may induce significant effects on the flavor-changing neutral currents associated with the bottom quark [133]. One of the most sensitive experimental measurements of such effects is the branching ratio of the decay of a bottom quark into a strange quark and a photon [134–138]. A realistic calculation of these effects, however, cannot be performed without knowing the flavor sector of the theory. Even for the large values of the bottom squark masses we consider in this work, of order a few TeV, the contributions coming from the interchange of gluinos and down squarks may be as large as the ones coming from the stop–chargino loops if there is additional flavour mixing beyond what is present in the SM [139].

The experimental value of the branching ratio, $BR(b \to s\gamma)$, is given by [140]

$$\mathrm{BR}(b \to s\gamma) = (3.54^{+0.30}_{-0.28}) \times 10^{-4}. \tag{6.16}$$

In the present work we will assume minimal flavour violation. The dominant contributions to $BR(b \to s\gamma)$, in addition to those already present in the SM, therefore come from loops involving the charged Higgs or charginos, and the light stop. While the loops involving the charged Higgs boson tend to increase the branching compared to the SM, the loops with charginos have a non-trivial dependence on the CP violating phase.

In Fig. 6.4 we display the value of BR($b \to s\gamma$) as a function of the phase of the Higgsino mass parameter, μ, for $M_a = 200$, 1000 GeV and $\tan\beta = 7$. The stop sector parameters have been chosen so as to be consistent with EWBG, and their precise values are listed in Eq. (6.18) in the following section. The sample chargino and neutralino mass parameters are taken to be $(|\mu|, M_1)$ =(300, 60) GeV (solid lines), (350,110) GeV (dashed lines), and (175,110) GeV (dotted lines), with $M_1 = (g_1^2/g_2^2)\, M_2$.

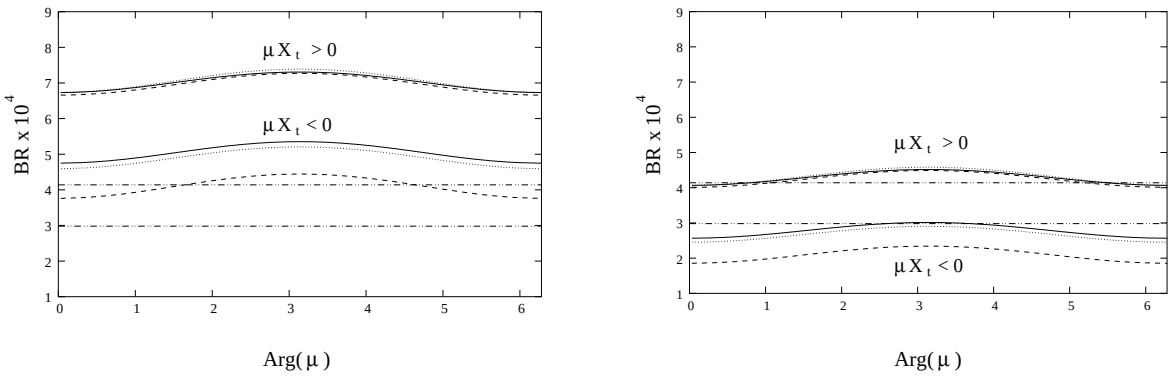

Figure 6.4: BR($b \to s\gamma$) as a function of Arg(μ) for values of the CP-odd Higgs mass $M_a = 200$ GeV (left), and $M_a = 1000$ GeV (right). The stop parameters were chosen as in section 2, and the chargino and neutralino mass parameters are given by $(|\mu|, M_1) = (350,$ 110) GeV (solid lines), (175, 110) GeV (dashed lines), and (300, 60) GeV (dotted lines). The dot-dashed bands represent the present experimental range at the 2 σ level.

As is apparent from the figure, in the absence of other sources of flavor violation a light CP-odd Higgs scalar with mass of about 200 GeV is highly restricted by $BR(b \to s\gamma)$. Negative values of $\mu\, X_t$, where $X_t = (A_t - \mu^*/\tan\beta)$, are necessary to keep the predicted branching ratio close to the experimentally allowed range.[3] This is due to a cancellation between the charged Higgs and the squark–chargino contributions to the branching ratio when $\mu\, X_t$ is negative. Otherwise these contributions interfere constructively with each other and with the SM contribution. For both signs of $\mu\, X_t$, the branching ratio is largest when Arg(μ) = π and smallest for Arg(μ) = 0. Since the branching ratio tends to be somewhat high for $M_a \sim 200$ GeV, even with $\mu\, X_t < 0$, small values of Arg(μ) are preferred in this case.

Larger values of the CP-odd Higgs mass are consistent with the measured value of BR($b \to s\gamma$) over a wide range of values of M_1, μ, and Arg(μ). For moderately large values, $M_a \lesssim 1000$ GeV, negative $\mu\, X_t < 0$ is preferred. For $M_a \gtrsim 1000$ GeV, the charged Higgs contribution decouples leaving only the stop-chargino corrections. These corrections tend to give a branching ratio that is near the upper part ($\mu\, X_t > 0$) or lower part ($\mu\, X_t < 0$) of the experimentally allowed range for $|X_t| = 700$ GeV, as we have considered here. Thus, smaller values of Arg(μ) are preferred for $\mu\, X_t > 0$, while Arg(μ) $\sim \pi$ is preferred for $\mu\, X_t < 0$. The chargino corrections can be reduced in size by taking slightly smaller values of $|X_t|$, or by invoking small flavor violation effects in the down squark sector.

[3]Recall that if the phases originate from a common gaugino phase and a U(1)$_R$ transformation is used to transfer this phase to μ and A_t, the product $\mu\, A_t$ remains real but can have either sign. See Eq. (6.14).

6.3 Neutralino Dark Matter

The dual requirements of successful EWBG and a lightest Higgs boson with mass greater than the LEP II bounds strongly constrain the parameter space of the MSSM. One of the stops must be light, with mass less than that of the top, and mostly right-handed. Furthermore, the charginos must not be too heavy, and the combination $\mu\, M_2$ must have a non-negligible phase. These conditions have important implications for neutralino dark matter.

First of all, if the lightest neutralino is to be the source of the observed dark matter, it must be lighter than the light stop so that it be stable. Secondly, in much of the parameter space of interest the light stop is only slightly heavier than the neutralino LSP implying that stop-neutralino coannihilation is significant. Finally, a phase for $\mu\, M_2$ modifies the masses of the neutralinos and their couplings to other particles, and can also affect the relative phase between the various contributions to the annihilation cross-section. The effect of CP violating phases on neutralino dark matter has been considered previously by several groups [141–143]. However, in all of these analyses the regions of MSSM parameter space considered were much different from the restricted subset required for EWBG, and in particular, none of them included a light stop.

To simplify the analysis, we shall assume throughout this work that the gaugino mass parameters, M_1 and M_2, are related by the standard unification relation, $M_2 = (g_2^2/g_1^2)\, M_1 \simeq 2\, M_1$, and have a common phase. The stop soft parameters are largely fixed by the EWBG and Higgs mass conditions. We take them to be

$$\begin{aligned} m_{U_3}^2 &\approx 0 \\ m_{Q_3} &= 1.5 \text{ TeV} \\ |X_t| &= |A_t - \mu^*/\tan\beta| \;=\; 0.7 \text{ TeV}. \end{aligned} \tag{6.17}$$

We have set $m_{D_3} = m_{L_3} = m_{E_3} = 1$ TeV as well. EWBG and the Higgs mass constraint also require $5 \lesssim \tan\beta \lesssim 10$ and $M_a \gtrsim 200$ GeV. For concreteness, we shall consider the values

$$\begin{aligned} \tan\beta &= 7 \\ M_a &= 200,\ 1000 \text{ GeV}. \end{aligned} \tag{6.18}$$

The first and second generation sfermion soft masses are taken to be very large, $m_{\tilde{f}} \gtrsim 10$ TeV. As was discussed in Section 6.2, this is necessary to avoid the electron, neutron, and ^{199}Hg EDM constraints in the presence of large phases.

6.3.1 Relic Density

We compute the relic abundance of neutralinos following the methods described in Chapter 4. In our calculation, all relevant annihilation and coannihilation processes are included as described in Ref. [144]. Besides neutralino self-annihilations, coannihilations of the light-

est neutralino with the lightest stop and the lighter chargino significantly affect our results. The complex phases enter our relic density calculation directly through the couplings and indirectly through the masses of the neutralinos and charginos. After diagonalizing of the gaugino and sfermion complex mass matrices, we calculate the annihilation cross-sections with complex couplings using the techniques outlined in Refs. [145, 146].

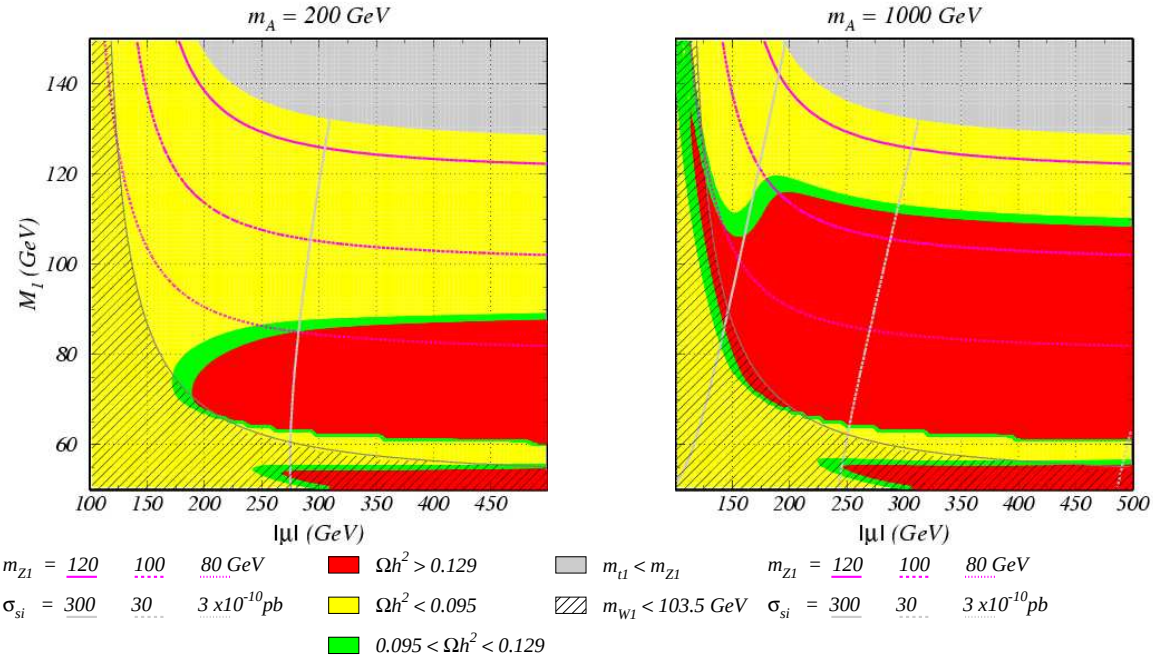

Figure 6.5: Neutralino relic density for $M_a = 200$ GeV (left) and $M_a = 1000$ GeV (right), and $\mathrm{Arg}(\mu) = 0$.

Figs. 6.5-6.7 show the dependence of the neutralino relic density on $|\mu|$ and M_1 for $\tan\beta = 7$, $M_a = 200$ GeV (left) and $M_a = 1000$ GeV (right), and three values of the μ phase: $\mathrm{Arg}(\mu) = 0,\ \pi/2,\ \pi$. Values of the phase equal to 0 or π are representative of what happens for small phases, like the ones consistent with the generation of the baryon asymmetry when $|\mu| \simeq M_2$ and $M_a \lesssim 300$ GeV where there is a resonance in the amount of baryon number produced [101]. On the other hand, large values of the phase, close to $\pi/2$, tend to be necessary to generate the baryon asymmetry outside of the resonant region, particularly for large values of M_a for which the EDM constraints become less severe.

The medium gray bands in Figs. 6.5-6.7 show the region of parameter space where the neutralino relic density is consistent with the 95% CL limits set by WMAP data. The regions in which the relic density exceeds the experimental bound, and is therefore excluded by more than two standard deviations, are indicated by the dark gray areas. The light gray areas show the regions of parameter space in which the neutralino relic density is less than the WMAP value. An additional source of dark matter, unrelated to the neutralino relic density, would be needed in these regions. Finally, in the medium-light gray region at the upper right of the plots, the lightest stop becomes the LSP, while in the hatched area at

the lower left corner the mass of the lightest chargino is lower than is allowed by LEP data [132].

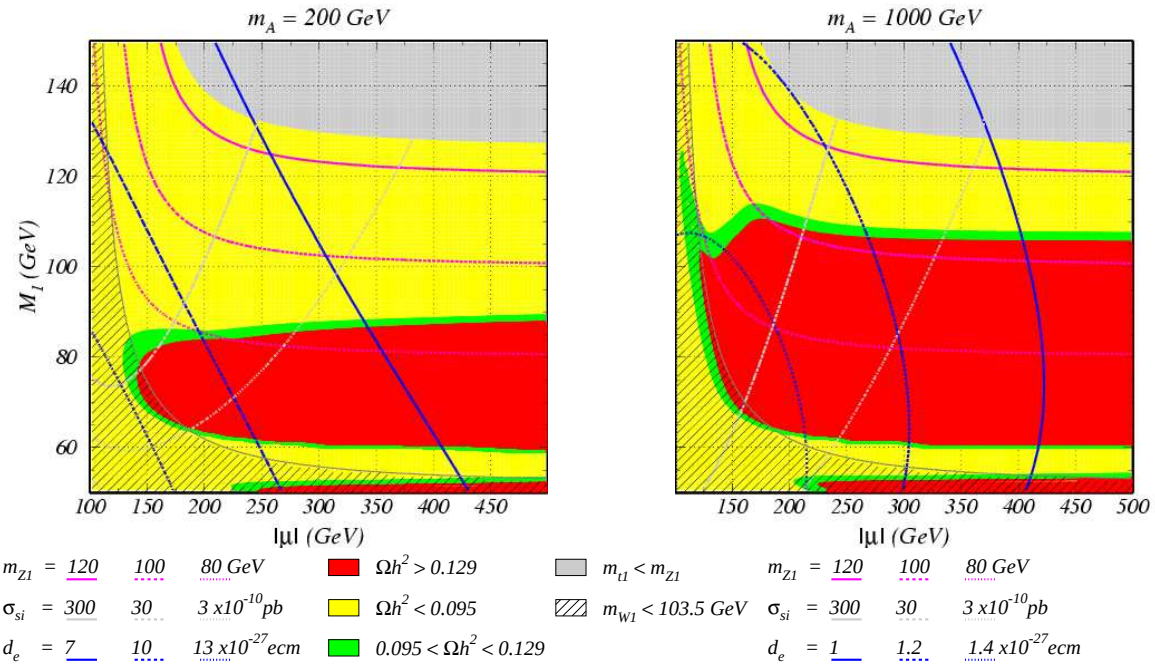

Figure 6.6: Neutralino relic density for $M_a = 200$ GeV (left) and $M_a = 1000$ GeV (right), and $\mathrm{Arg}(\mu) = \pi/2$.

Figs. 6.5-6.7 are qualitatively similar, but do show some differences due to the change in the phase of μ. Before discussing the effect of the phase, we will examine their general features. For $M_a = 1000$ GeV and for all three phase values, the region where the relic density is too high consists of a wide band in which the lightest neutralino has mass between about 60 and 105 GeV and is predominantly Bino. Above this band, the mass difference between the neutralino LSP and the light stop is less than about 20 GeV, and stop-neutralino coannihilation as well as stop-stop annihilation very efficiently reduce the neutralino abundance. For $M_a = 200$ GeV, instead, the contribution to neutralino annihilation from s-channel exchange of heavy CP-even and CP-odd Higgs bosons is enhanced by a resonance around $m_{\tilde{N}_1} \simeq 100$ GeV. This restricts the band in which the relic density is too high to the region where the lightest neutralino has mass between about 60 and 85 GeV, and is also mostly Bino. For both values of M_a, there is an area below the disallowed band in which the neutralino mass lies in the range 40-60 GeV, and the neutralino annihilation cross-section is enhanced by resonances from s-channel h^0 and Z^0 exchanges.

The relic density is also quite low for smaller values of $|\mu|$. In these regions, the neutralino LSP acquires a significant Higgsino component allowing it to couple more strongly to the Higgs bosons and the Z^0. For $M_a = 1000$ GeV, this is particularly important in the region near $(|\mu|, M_1) = (175, 110)$ GeV where the neutralino mass becomes large enough that annihilation into pairs of gauge bosons through s-channel Higgs and Z^0 exchange and t-

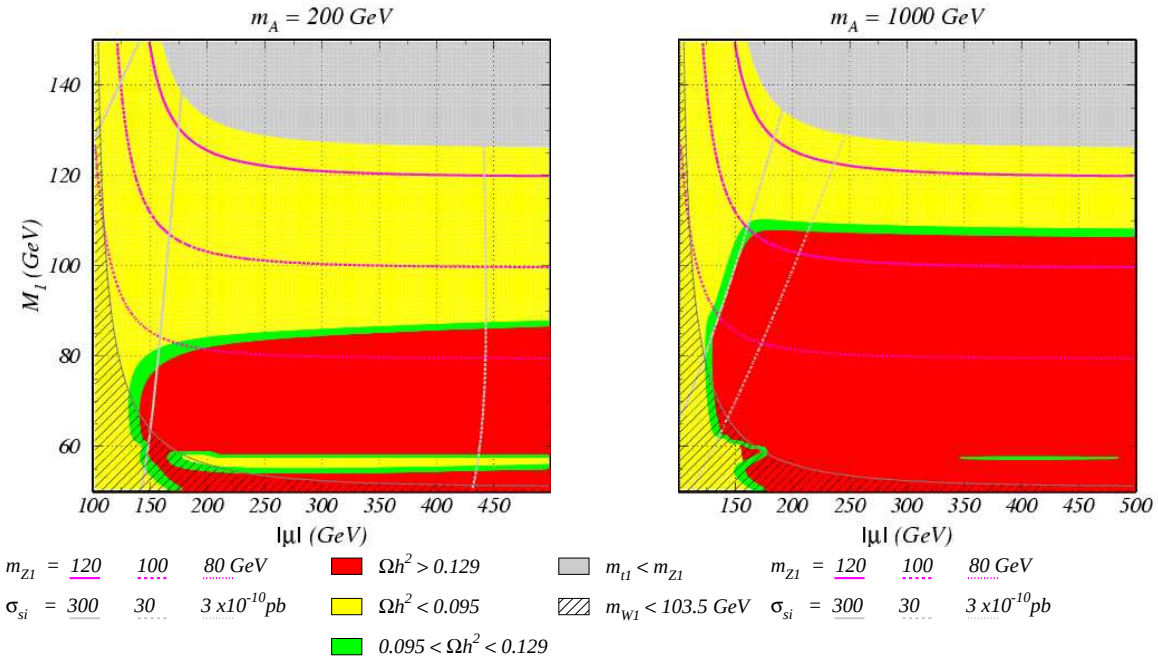

Figure 6.7: Neutralino relic density for $M_a = 200$ GeV (left) and $M_a = 1000$ GeV (right), and $\mathrm{Arg}(\mu) = \pi$.

channel neutralino and chargino exchange is allowed, and is the reason for the dip in the relic density near this point. Since the corresponding couplings to the gauge bosons depend on the Higgsino content of the neutralino, these decay channels turn off as $|\mu|$ increases. For higher M_1 values, the lightest neutralino and chargino masses are also close enough that chargino-neutralino coannihilation and chargino-chargino annihilation substantially increase the effective total annihilation cross section.

In Figs. 6.5-6.7, we have taken $M_2 = (g_2^2/g_1^2)M_1$, as suggested by universality and gauge unification. With this relation, smaller values of M_1 and μ are excluded by the lower bound on the chargino mass from LEP data [132], as indicated by the hatched regions in the figures. This constraint becomes much less severe for larger values of the ratio M_2/M_1. We also find that increasing this ratio of gaugino masses (with M_1 held fixed) has only a very small effect on the neutralino relic density.

6.3.2 Effects of CP Violating Phases

For the parameters considered in the previous section, relevant for EWBG within the MSSM, CP violating phases modify the values of the neutralino relic density but have only a mild effect on the general qualitative features of the allowed parameter space. This is somewhat misleading, however, since the value of the relic density at a given point in the $|\mu| - M_1$ plane can vary markedly with $\mathrm{Arg}(\mu)$.

The most important effect of varying $\mathrm{Arg}(\mu)$ is to shift the mass of the neutralino

LSP. The dependence of the lightest neutralino mass on this phase is shown in Fig. 6.8 for $\tan\beta = 7$ and three sample values of $(|\mu|, M_1)$: $(|\mu|, M_1) = (350, 110)$ GeV, $(300, 60)$ GeV, and $(175, 110)$ GeV. For $M_a = 1000$ GeV, these three points are representative of the regions where the annihilation cross section is dominated by stop-neutralino coannihilation [$(350, 110)$ GeV], Higgs boson s-channel annihilation [$(300, 60)$ GeV], and annihilation into pairs of gauge bosons [$(175, 110)$ GeV]. In each of the three cases, the neutralino mass increases with $\mathrm{Arg}(\mu)$, by about 3%, 7%, and 11%, respectively. Such a mass shift can significantly modify the relic density at a single point where neutralino annihilation is enhanced by a resonance or coannihilation with another species. The effect on the net distribution of relic densities, on the other hand, is fairly small; shifting the phase tends to translate this distribution down and to the left in the $|\mu|$-M_1 plane.

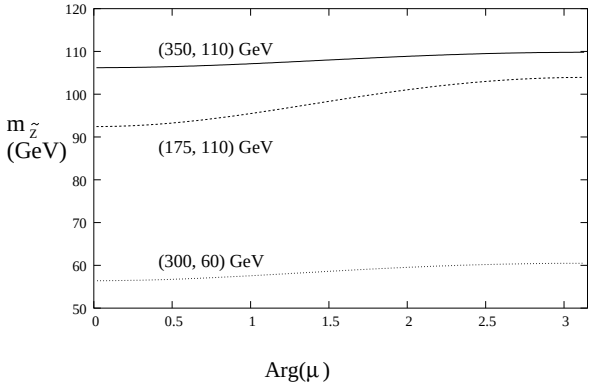

Figure 6.8: Mass of the lightest neutralino as a function $\mathrm{Arg}(\mu)$ for $\tan\beta = 7$ and three sample values of $(|\mu|, M_1)$.

The neutralino-Higgs couplings are also quite sensitive to $\mathrm{Arg}(\mu)$. The couplings of the Higgs bosons to a pair of neutralinos are given in [147], and have the form

$$\begin{aligned} \tilde{N}_1\tilde{N}_1\, h^0/H^0 &\sim -i(F\, P_L + F^* P_R) \\ \tilde{N}_1\tilde{N}_1\, A^0 &\sim -i(G\, P_L - G^* P_R) \end{aligned} \tag{6.19}$$

where $P_{L,R} = (1 \mp \gamma_5)/2$ are the usual chiral projectors. Using these couplings, the spin-summed and squared matrix elements for $\tilde{N}_1\tilde{N}_1 \to \bar{f}f$ annihilation via s-channel Higgs exchange are proportional to

$$|\mathcal{M}|^2 \propto \begin{cases} \mathrm{Re(F)}^2\,(\mathrm{s} - 4\,\mathrm{m}^2_{\tilde{\mathrm{N}}_1}) \;+\; \mathrm{Im(F)}^2\,\mathrm{s}\;; & h^0,\ H^0 \\ \mathrm{Re(G)}^2\,\mathrm{s} \;+\; \mathrm{Im(G)}^2\,(\mathrm{s} - 4\,\mathrm{m}^2_{\tilde{\mathrm{N}}_1})\;; & A^0 \end{cases} \tag{6.20}$$

In calculating the thermal average, one integrates these matrix elements over s through the range $[4\,m^2_{\tilde{N}}, \infty)$ with a Boltzmann factor. The Boltzmann suppression is strong for a non-relativistic relic particle, so the integral is dominated by the region $s \sim 4\,m^2_{\tilde{N}}$. In

particular, this means that the terms in Eq. (6.20) proportional to s have the potential to give a much larger contribution to the annihilation cross-section than those proportional to $(s - 4\,m_{\tilde{N}}^2)$.

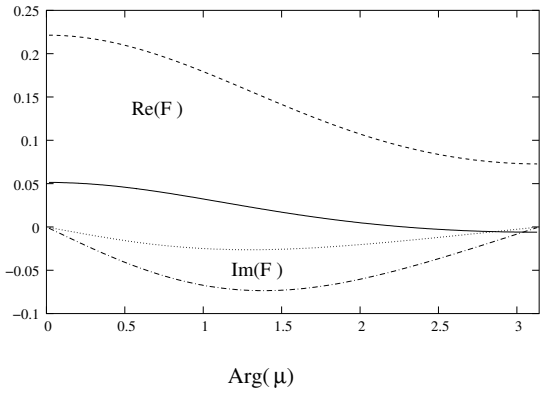

Figure 6.9: Variation of the real and imaginary parts of the $\tilde{N}_1\tilde{N}_1h^0$ coupling with Arg(μ) for $(|\mu|, M_1) = (300, 60)$ GeV (solid and dotted), and $(|\mu|, M_1) = (175, 110)$ GeV (dashed and dash-dotted).

The dependence of the $\tilde{N}_1\tilde{N}_1\,h^0$ coupling on Arg(μ) for $M_a = 1000$ GeV, and $(|\mu|, M_1) = (300, 60)$ GeV and $(|\mu|, M_1) = (175, 110)$ GeV is shown in Fig. 6.9. Both the real and imaginary parts of the couplings are larger in the $(|\mu|, M_1) = (175, 110)$ GeV case since for these values of the parameters, the neutralino LSP has a much larger Higgsino component than for $(|\mu|, M_1) = (300, 60)$ GeV, when the neutralino is mostly Bino. The couplings for $(|\mu|, M_1) = (350, 110)$ GeV, where the LSP is also mostly Bino, are very similar to those for $(|\mu|, M_1) = (300, 60)$ GeV. Setting $M_a = 200$ GeV has only a small effect on these couplings. For both points shown in Fig. 6.10, the imaginary part of the coupling vanishes when μ is real, and is largest when μ is pure imaginary, Arg(μ) = $\pi/2$. The real part of the coupling also tends to decrease with Arg(μ) due to an accidental cancellation of terms. This behavior may be seen by comparing the region $M_1 \lesssim 60$ GeV in Figs. 6.5, 6.6, and 6.7, where s-channel h^0 exchange tends to be dominant. The relic density in this region is lowest when Arg(μ) = $\pi/2$, Fig. 6.6, while in Fig. 6.7, corresponding to Arg(μ) = π, the contribution from h^0 exchange is much smaller than for other values of this phase.

The couplings of the H^0 and A^0 bosons to pairs of the lightest neutralino are shown in Fig. 6.10 for $M_a = 1000$ GeV, and $(|\mu|, M_1) = (300, 60)$ GeV and $(|\mu|, M_1) = (175, 110)$ GeV. As for the h^0 coupling, these couplings are nearly unchanged when $M_a = 200$ GeV. The couplings for $(|\mu|, M_1) = (350, 110)$ GeV are very similar to those for $(|\mu|, M_1) = (300, 60)$ GeV as well. The imaginary part of the H^0 and A^0 couplings vanishes for Arg(μ) = 0, π and is largest near Arg(μ) = $\pi/2$, while the real parts of these couplings are largest for Arg(μ) = 0, π and nearly zero when Arg(μ) = $\pi/2$. From Eqs. (6.19, 6.20), this implies that the contribution of s-channel H^0 exchange to neutralino annihilation is largest when

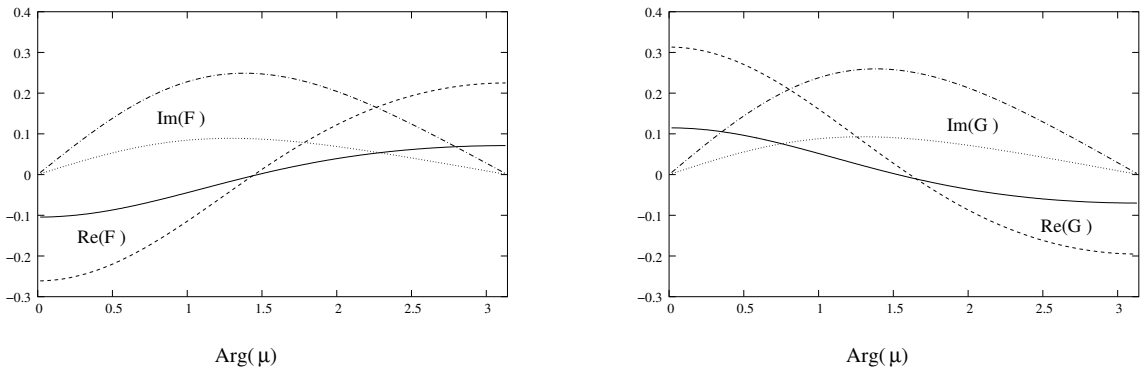

Figure 6.10: Variation of the real and imaginary parts of the $\tilde{N}_1\tilde{N}_1H^0$ (left) and $\tilde{N}_1\tilde{N}_1A^0$ (right) couplings with Arg(μ) for $(|\mu|, M_1) = (300, 60)$ GeV (solid and dotted), and $(|\mu|, M_1) = (175, 110)$ GeV (dashed and dash-dotted).

Arg(μ) $= \pi/2$, and smallest for Arg(μ) $= 0,\ \pi$, and that the opposite is true for s-channel A^0 exchange. Interestingly, the sum of the A^0 and H^0 contributions is nearly independent of the phase. We expect this to be the case whenever $M_a^2 \gg M_Z^2$, and the heavy CP-even and CP-odd Higgs states are nearly degenerate. The same effect was found in Ref. [122].

We have also investigated the phase dependence of the $\tilde{N}_1\, t\, \tilde{t}$ coupling which generates the most important contributions to stop-neutralino coannihilation. While this coupling does vary somewhat with the phase, the effect of the phase on the neutralino mass is much more important. This is because the coannihilation contribution to the relic density is suppressed by a factor approximately equal to $e^{-(m_{\tilde{t}}-m_{\tilde{N}_1})/T_f}$ [Eq. (4.21)], where $T_f \simeq m_{\tilde{N}_1}/20$ is the neutralino freeze-out temperature, making it very sensitive to the neutralino mass.

6.4 Direct Detection of Dark Matter

If relic neutralinos make up the dark matter, then they should be present in the space around us, and it might be possible to observe them directly. Indeed, the search for weakly interacting massive particles is underway by looking for their elastic scattering off nuclei, the signature for which is the recoil of the target nucleus. Several existing and future experiments are engaged in this search. These include solid-state germanium based ionization detectors such as IGEX [148], HDMS [149], CDMS [150], EDELWEISS [151] and GENIUS [152], as well as the solid crystal or liquid NaI based scintillator detectors used for example by DAMA [153] and ZEPLIN [154–157]. Other types of detection methods include xenon based detectors as used in XENON [158] and UKDMC [159], gas target projection chambers such as those used in DRIFT [160], and metastable particle detectors such as SIMPLE [161] and PICASSO [162].

The elastic scattering of neutralinos with nuclei can be described by the sum of a spin

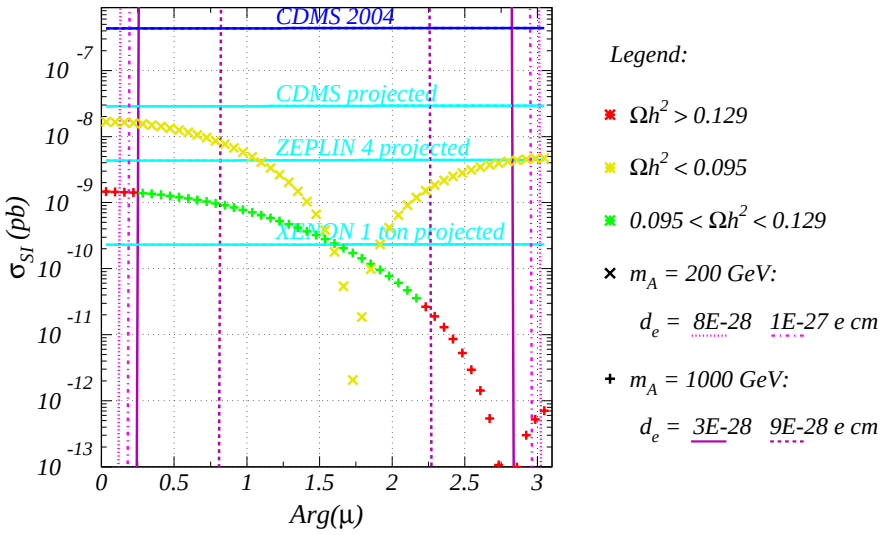

Figure 6.11: Spin-independent neutralino-proton scattering cross section as the function of Arg(μ), for $|\mu| = 350$ GeV and $M_1 = 110$ GeV, and for M_a= 200 (1000) GeV for the upper (lower) curve.

independent (SI) cross section, and a spin dependent (SD) cross section. The SI cross section is roughly proportional to the square of the atomic number of the target nucleus, whereas the SD cross section is proportional to the square of the net spin of the nucleus. Thus, for heavy nuclei, the SI term is greatly enhanced compared to the spin dependent one. For a target containing the isotope ^{127}I, the enhancement factor is more than 10^4. As a result, the experimental limits on the spin independent neutralino-nucleon cross sections are considerably stronger than the spin dependent ones.

In what follows, we will focus on the spin independent interactions. At the parton level, they are mediated by t-channel Higgs and s-channel squark exchanges. (Here, we only consider the leading scalar contribution and neglect the higher order tensor contributions originating from loop diagrams.) The differential scattering rate of a neutralino off the nucleus X_Z^A with mass m_X takes the form [163]:

$$\frac{d\sigma_{SI}}{d|\vec{q}|^2} = \frac{1}{\pi v^2}[Z f_p + (A-Z) f_n]^2 F^2(Q_r), \tag{6.21}$$

where $\vec{q} = \frac{m_X m_{\tilde{N}_1}}{m_X + m_{\tilde{N}_1}}\vec{v}$ is the three-momentum transfer, $Q_r = \frac{|\vec{q}|^2}{2m_N}$, $F^2(Q_r)$ is the scalar nuclear form factors, $\vec{v}$ is the velocity of the incident neutralino, and f_p and f_n are effective neutralino couplings to protons and neutrons respectively. The same formalism was used in Ref. [163], and the reader is directed there for further details. Since modern experiments express their limits in terms of the neutralino-proton cross section, we shall calculate and plot this quantity.

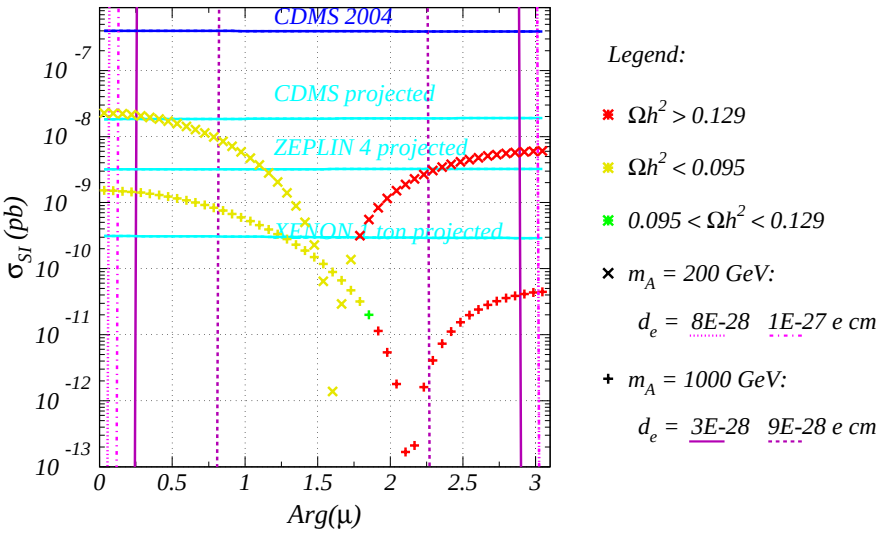

Figure 6.12: Same as Fig. 6.11, but for $|\mu| = 300$ GeV and $M_1 = 60$ GeV.

To study the dependence of the neutralino-proton cross section on the complex phases of various supersymmetric parameters, we selected three sample points in the parameter region in which the constraints from EWBG, the electron EDM and WMAP are simultaneously satisfied. Specifically, we examined values of $M_a = 200$, 1000 GeV and the same Higgsino and neutralino mass parameters chosen before, namely $(|\mu|, M_1) = (175, 110)$ GeV, (350,110) GeV, and (300,60) GeV. As emphasized above, for $M_a = 1000$ GeV these points correspond to regions where the annihilation cross section is dominated by weak processes, coannihilation with the light stop, and s-channel Higgs exchange, respectively.

Figs. 6.11–6.13 show the neutralino-proton cross section versus the phase of μ for the three sample parameter points. The most striking feature of these plots is that the cross section is suppressed for non-vanishing phases and, except for $(|\mu|, M_1) = (175, 110)$ GeV with $M_a = 1000$ GeV, nearly vanishes for a given value of Arg(μ). This behaviour follows from the phase dependence of the Higgs-neutralino couplings. In the present case, t-channel h^0 and H^0 exchange diagrams generate the most important contributions to the spin-independent neutralino-nucleon elastic scattering cross section.[4] Furthermore, these contributions depend only on the real (scalar) part of the Higgs-neutralino couplings [164, 165]; Re(F) in the notation of Eq. (6.19). The large suppression of the cross section for particular values of Arg(μ) is the result of zeroes in Re(F).

Consider first the $M_a = 1000$ GeV lines in Figs. 6.11–6.13. Since $M_a \simeq M_H \gg m_h$, the contribution of the heavier scalar Higgs is suppressed relative to the lighter state, and neutralino-proton scattering is dominated by t-channel h^0 exchange. Comparing the real

[4]We checked that the lone relatively light squark, the light stop, contributes only at the percent level via its s-channel diagram.

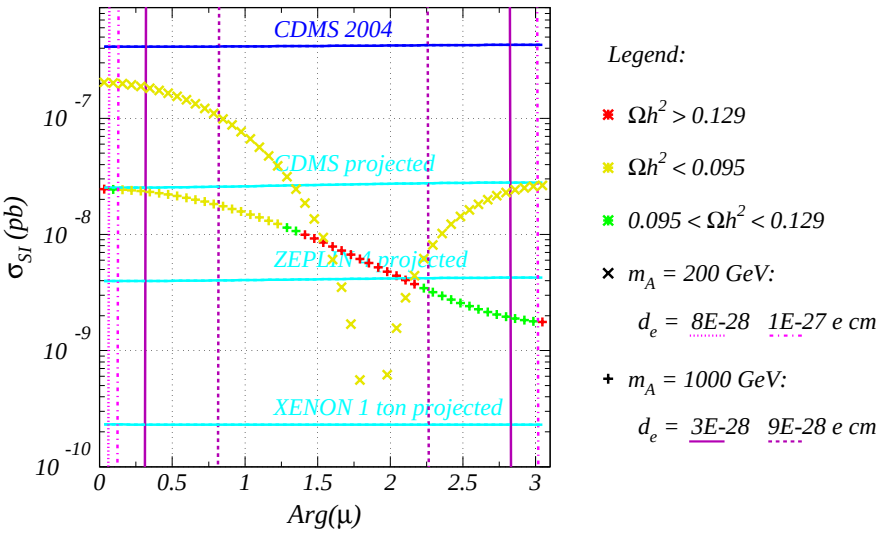

Figure 6.13: Same as Fig. 6.11, but for $|\mu| = 175$ GeV and $M_1 = 110$ GeV.

part of the h^0-neutralino coupling for $(|\mu|, M_1) = (300, 60)$ GeV, shown in Fig. 6.9, to the plot of σ_{SI} in Fig. 6.12 for $M_a = 1000$ GeV, we see that the minimum in σ_{SI} nearly coincides with the zero of the coupling. The minimum (not a zero value) in Figure 6.12 does not exactly coincide with the zero of the coupling, but is shifted closer to $\mathrm{Arg}(\mu) = \pi/2$ because the zero value of the real part of the H^0-neutralino coupling occurs close to $\mathrm{Arg}(\mu) = \pi/2$, as shown in Fig. 6.10.[5] When $(|\mu|, M_1) = (175, 110)$ GeV, the coupling of the lightest Higgs to the lightest neutralino has no zero, and σ_{SI} has no deep minimum, as shown by Fig. 6.9. For $M_a = 200$ GeV, the H^0 state is much lighter and produces a much larger contribution to σ_{SI}. In this case, the minimum of σ_{SI} is closer to $\pi/2$, near the zeroes of the H^0-neutralino coupling, as can be seen in Fig. 6.10.

The values of the electron EDM are also indicated in Figs. 6.11–6.13. Among the direct detection experiments, CDMS excludes the region above the line labeled as CDMS 2004 [166]. The lower lines indicate the projected sensitivities of future experiments: CDMS [167]; ZEPLIN [168]; and XENON [169].

In Fig. 6.14, we show the dependence of the direct dark matter detection on the phase of μ. To do this, we conducted a random scan over the following range of MSSM parameters:

$$-(80\ \mathrm{GeV})^2 < m^2_{\tilde{U}_3} < 0, \quad 100\ \mathrm{GeV} < |\mu| < 500\ \mathrm{GeV}, \quad 50\ \mathrm{GeV} < M_1 < 150\ \mathrm{GeV},$$
$$200\ \mathrm{GeV} < M_a < 1000\ \mathrm{GeV}, \quad 5 < \tan\beta < 10. \tag{6.22}$$

The parameters that were not scanned over were fixed as in Section 6.1. The result of the scan, projected on the stop mass versus neutralino mass plane, is shown in Fig. 6.14, where

[5] If the heavy Higgs state is decoupled completely, we find that the minimum of the scattering cross section coincides exactly with the zero of the h^0-neutralino coupling.

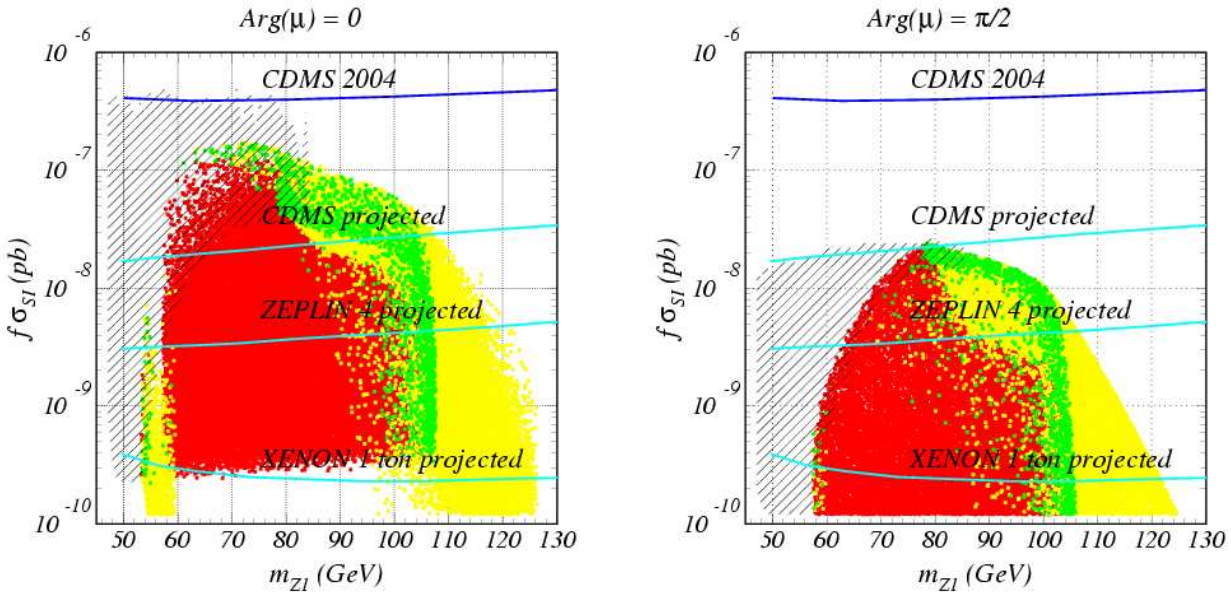

Figure 6.14: Spin independent neutralino-proton elastic scattering cross sections as a function of the neutralino mass for Arg(μ) = 0 (left) and Arg(μ) = $\pi/2$ (right). Dark gray, medium gray, and light gray dots represent parameter sets in which the neutralino density exceeds, is consistent with, or lies below the 2σ WMAP bounds. The hatching indicates the region excluded by chargino searches at LEP. The top solid line represents the 2004 exclusion limit by CDMS. The lower solid lines indicate the projected sensitivity of CDMS, ZEPLIN and XENON, respectively.

we plot $f\sigma_{SI}$ as a function of the lightest neutralino mass. The factor f is given by

$$f = \begin{cases} \Omega_{CDM}h^2/0.095 & \text{if } 0.095 \geq \Omega_{CDM}h^2 \\ 1 & \text{if } 0.095 < \Omega_{CDM}h^2 \end{cases} , \tag{6.23}$$

and accounts for the diminishing flux of neutralinos with their decreasing density [170].[6] For models marked by light gray dots the neutralino relic density lies below the 2σ WMAP bound, while models represented by medium gray dots comply with WMAP to within 2σ. Models that exceed the WMAP value by more than 2 σ are indicated by dark gray dots. The area indicated by hatching is excluded by the LEP chargino mass limit of 103.5 GeV. The solid horizontal lines in the figure indicate the current and projected future sensitivities of several direct-detection experiments.

The structure of this scatter plot can be understood by examining Figs. 6.5–6.7. As indicated in these plots by the gray direct detection contours, the spin-independent cross

[6]The experimental limits for dark matter detection rely on the standard assumptions of a dark matter flux incident on the earth, based on the observational evidence that points to a roughly spherical distribution of dark matter distribution in the galaxy, and a local dark matter velocity comparable to the speed of the sun within the galaxy.

section, σ_{SI}, decreases for increasing values of $|\mu|$. Therefore the low σ_{SI} region in Fig. 6.14 is in one-to-one correspondence with the large $|\mu|$ region in Figs. 6.5-6.7. For these large values of $|\mu|$, the lightest neutralino mass is approximately equal to M_1. Hence, increasing values of M_1 in Figs. 6.5-6.7 correspond to increasing values of $m_{\widetilde{N}_1}$ in Fig. 6.14. The same regions of enhanced annihilation, either via h^0 or A^0/H^0 resonances, or by stop coannihilation, can also be identified between these figures. In the same way, the LEP excluded, hatched area of $m_{\widetilde{\chi}_1} < 103.5$ GeV, preserves its hyperbolic shape for $m_{\widetilde{N}_1} < 85$ GeV.

At present, the region above the top solid line is excluded by CDMS. In the near future, for $\mathrm{Arg}(\mu) \simeq 0$, CDMS will probe part of the region of the parameter space where the WMAP dark matter bound is satisfied. In this region, due to their enhanced Higgsino components, neutralinos mainly annihilate to gauge bosons or, due to the small mass gap, they coannihilate with charginos. The ZEPLIN experiment will start probing the stop-neutralino coannihilation region together with the annihilation region enhanced by s-channel A^0 resonances, and XENON will cover most of the relevant parameter space. Prospects for direct detection of dark matter tend to be worse for large values of the phase of μ, $\mathrm{Arg}(\mu) \simeq \pi/2$. As seen from Figs. 6.11-6.13, this phase can lead to cancellations that suppress the direct detection cross section. In the event of such a cancellation, a detector with the sensitivity of ZEPLIN is needed to start probing the parameter space, and not even XENON will be capable of fully exploring this model.

6.5 Conclusions for the MSSM

Electroweak baryogenesis provides a mechanism to generate the baryon asymmetry that relies only on physics at the weak scale. It is therefore testable at high energy physics facilities in the near future. In this work we have examined the possibility of EWBG within the MSSM, and the implications that this on the possibility of dark matter within the model. Specifically, we have analyzed the effects of CP violating phases, as required for EWBG, in conjunction with a light stop, with mass below the top quark mass, and a light Higgs with mass below 120 GeV [94, 95]. We have shown that these phases have only a minor impact on the neutralino parameter space leading to a relic density consistent with experiment. Large phases, however, do have an important effect on direct dark matter detection rates, and induce large corrections to the electron electric dipole moment.

We have also shown that, for the phases necessary to obtain an acceptable baryon asymmetry and in the limit of heavy squarks, of order a few TeV, the predicted values of the electron electric dipole moment tend to lie within an order of magnitude below present experimental bounds. The most dangerous contribution, in the limit of very heavy squarks and sleptons, comes from two loop graphs involving charginos and Higgs bosons. Assuming no cancellations between one- and two-loop corrections, one can obtain strong bounds on the allowed parameter space. Small values of $\tan\beta$ are excluded since they lead to unacceptably small values of the Higgs mass, and large values of $\tan\beta$ tend to lead to overly large values of the electron EDM or small values of the baryon asymmetry. On the other hand, for moderate values of $\tan\beta \simeq 7$, the Higgs boson mass may be large enough

to evade the LEP bounds, even for values of M_a as small as 200 GeV.

In our analysis, we have not examined the prospects of light stop searches at hadron and lepton colliders. As discussed in Ref. [106], these become very challenging in the region where stop-neutralino coannihilation becomes relevant, both at the LHC and the Tevatron collider [171] due to the small mass difference between the stop and the neutralino. An acceptable dark matter density may be obtained for mass differences as small as 20 GeV, for which the charm particles proceeding from the stop decay are soft making the stop detection difficult.

The linear collider signatures of MSSM Baryogenesis have been discussed in Ref. [133]. A linear collider represents the best possibility for confirming this scenario since it provides the opportunity of performing precise measurements on the chargino system and hence the possibility of observing a non-zero phase of the μ parameter [172]. Precise measurements of the stop system also become easier at a linear electron-positron collider [173]. For example, the LEP collider was able to set limits on the stops even for a mass difference with the neutralino of about 1 GeV. Preliminary studies of stop searches at the linear collider [174] show that a 500 GeV ILC may be able to detect a light stop for mass differences as small as a few GeV. As we found above, in the region of parameters where stop-neutralino coannihilation leads to a value of the relic density consistent with experimental results, the stop-neutralino mass difference is never much smaller than 20 GeV, and thus an ILC will be able to explore this region efficiently.

In summary, the requirement of a consistent generation of baryonic and dark matter in the MSSM leads to a well-defined scenario, where, apart from a light stop and a light Higgs boson, one has light neutralinos and charginos, sizeable CP violating phases, and moderate values of $5 \lesssim \tan\beta \lesssim 10$. All these properties will be tested by the Tevatron, the LHC and a prospective ILC, as well as through direct dark-matter detection experiments in the near future. The first tests of this scenario will come from electron EDM measurements, stop searches at the Tevatron and Higgs searches at the LHC within the next few years.

CHAPTER 7
EWBG AND DM IN THE NMSSM

The MSSM can explain both the baryon asymmetry and the dark matter, in addition to stabilizing the gauge hierarchy and providing a unification of the gauge couplings near the Planck scale. Even so, the model has some unattractive features as well. As we discussed in Section 2.4, the LEP-II lower bound on the Higgs boson mass, of about 114 GeV, gives a strong constraint on the MSSM. Large stop masses are needed to avoid this bound, but this forces the fine-tuning of other parameters in the model to the order of 1%. The same LEP-II Higgs mass bound also constrains EWBG within the MSSM. In this case, the electroweak phase transition is strongly first order only for $m_h \lesssim 120$ GeV, only slightly above the experimental limit. On a more technical level, the MSSM also faces the *μ-problem*. Namely, the μ term, $\mu H_1 \cdot H_2$, must be included in the superpotential, with $|\mu|$ of order of the weak scale, if the electroweak symmetry is to be broken. While the μ parameter is stable under quantum corrections as a result of supersymmetry, it is difficult (although possible [175]) to explain why this dimensionful quantity should be so much smaller than M_P or M_{GUT}.

A simple way to address all three difficulties is to add a gauge singlet chiral superfield to the model. The singlet can solve the μ-problem if the μ-term is replaced by the singlet field, and the singlet field gets a VEV. Such a coupling between the Higgs fields and the singlet also generates an additional contribution to the lightest CP-even Higgs boson mass. The LEP-II Higgs mass bound becomes much easier to avoid, even without heavy stops. The bosonic component of the singlet also seems to help make the electroweak phase transition more strongly first-order [113–117], even for heavier Higgs boson masses.

In this chapter, we consider a particular singlet extension of the MSSM, the nearly minimal supersymmetry standard model (nMSSM). This model retains the attractive features of singlet extensions of the MSSM, but also manages to avoid some of the cosmological problems faced by many of these models. In Section 7.1 we will motivate this particular singlet extension, and describe its general features. Section 7.2 contains a more detailed description of the nMSSM, including an analysis of the mass spectrum at zero temperature. In Section 7.3, we examine the issue of electroweak baryogenesis in the model, and in particular, examine whether the singlet can help make the EWPT more strongly first-order. Dark matter in the model is the subject of Section 7.4, while Section 7.5 describes some of the phenomenological features of the scenario. Finally, Section 7.6 is reserved for our conclusions. The material in this chapter is based on the work [2].

7.1 A Minimal Extension of the MSSM with a Singlet Superfield

When a singlet superfield is added to the MSSM, many new dimensionful couplings become possible. To avoid re-introducing the μ problem, such terms must be forbidden by a

symmetry under which the singlet superfield is charged. In the most common formulation, the Next-to-Minimal Supersymmetric SM (NMSSM) [176], one imposes a $\mathbb{Z}_3$ symmetry under which the fields transform as $\Phi_i \to \exp(2\pi i q_i/3)\ \Phi_i$, where the charges q_i are given in Table 7.1. The most general renormalizable superpotential is then

$$\begin{aligned} W_{ren} &= \lambda\, S\, H_1{\cdot}H_2 \ +\ \kappa\, S^3 \\ &\quad +\, y_u\, Q{\cdot}H_2\, U^c \ -\ y_d\, Q{\cdot}H_1\, D^c \ -\ y_e\, L{\cdot}H_1\, E^c, \end{aligned} \tag{7.1}$$

where S is the singlet superfield and the other fields are the same as in the MSSM. Except for the cubic singlet self-coupling, this is just the MSSM superpotential with a field dependent μ-term proportional to the singlet field. Without this additional cubic term, the superpotential is invariant under an anomalous $\mathrm{U}(1)_{\mathrm{PQ}}$, whose charges are listed in Table 7.1, that gives rise to an unacceptable axion [177]. The cubic term explicitly breaks $\mathrm{U}(1)_{\mathrm{PQ}}$ down to its maximal $\mathbb{Z}_3$ subgroup, thereby removing the axion while still forbidding all dimensionful couplings. Unfortunately, this generates new difficulties. When the singlet acquires a VEV, necessarily near the electroweak scale, the $\mathbb{Z}_3$ symmetry is broken as well producing cosmologically unacceptable domain walls [178]. The domain wall problem can be avoided if $\mathbb{Z}_3$ violating non-renormalizable operators are included. However, such operators generate a large singlet tadpole that destabilizes the hierarchy [179].

	H_1	H_2	S	Q	L	U^c	D^c	E^c	W
$\mathrm{U}(1)_Y$	-1/2	1/2	0	1/6	-1/2	-2/3	1/3	1	0
$\mathbb{Z}_3 \subset \mathrm{U}(1)_{\mathrm{PQ}}$	1	1	-2	-1	-1	0	0	0	0
$\mathrm{U}(1)_R$	0	0	2	1	1	1	1	1	2
$\mathbb{Z}_5^R, \mathbb{Z}_7^R \subset \mathrm{U}(1)_{R'}$	1	1	4	2	2	3	3	3	6

Table 7.1: Charges of fields under the Abelian symmetries discussed in the text.

As shown in [180–182], both problems can be avoided in the context of an N=1 supergravity scenario. In the absence of the cubic singlet term, the superpotential of Eq. (7.1) obeys the $\mathrm{U}(1)_{\mathrm{PQ}}$, and $\mathrm{U}(1)_R$ symmetries listed in Table 7.1, and so is also invariant under the group $\mathrm{U}(1)_{R'}$ with charges $R' = 3R + \mathrm{PQ}$. This symmetry alone is enough to give the superpotential of Eq. (7.1) with no cubic term, as are the maximal $\mathbb{Z}_5^R$ and $\mathbb{Z}_7^R$ subgroups of $\mathrm{U}(1)_{R'}$. If we now demand that both the superpotential and the Kähler potential obey one of these discrete R-symmetries instead of the $\mathbb{Z}_3$ symmetry of the NMSSM, the superpotential will be of the desired form up to a possible singlet tadpole term. Using power counting arguments it may be shown that a singlet tadpole does arise, but only at the six ($\mathbb{Z}_5^R$) or seven ($\mathbb{Z}_7^R$) loop level. The loop suppression in both cases is large enough that the induced tadpole does not destabilize the hierarchy [180, 181]. Therefore, this mechanism very elegantly solves three problems: it prevents the appearance of dimensionful couplings (other than the tadpole) in the renormalizable part of the superpotential; the induced singlet tadpole explicitly breaks $\mathrm{U}(1)_{\mathrm{PQ}}$ and its discrete subgroups, thereby avoiding unacceptable axions and domain walls; and the loop suppression of the tadpole leads naturally to a singlet VEV of the order of M_{SUSY}. Following [182], we shall refer to this model as the nearly

Minimal Supersymmetric Standard Model (nMSSM).

Another interesting feature of the model is that something like R-Parity arises from the imposed R-symmetries. These symmetries forbid the appearance of all $d = 4$ B- and L-violating operators as well as the dominant higher dimensional B-violating operators that contribute to proton decay. While proton stability is ensured, there are non-renormalizable operators that make the LSP unstable. As will be shown in Section 7.2.1, the LSP of the model under study is nearly always the lightest neutralino. In the $\mathbb{Z}_7^R$ symmetric case, this symmetry forbids all $d \leq 6$ operators that could lead to the decay of such an LSP, and naïve dimensional analysis shows that it has a lifetime in excess of the age of the universe. The issue is a bit more delicate in the $\mathbb{Z}_5^R$ case since the L-violating $d = 5$ operator SSH_2L is allowed by the symmetry. We find that the lifetime of the neutralino LSP induced by this operator is greater than the age of the Universe provided the cutoff scale (by which non-renormalizable operators are suppressed) exceeds $\Lambda \gtrsim 3 \times 10^{14}$ GeV. The details of our estimate are presented in Appendix B.2. Therefore, the same symmetries that ensure a natural solution to the μ-problem stabilize the LSP, and provide the means for a sufficiently large proton lifetime.

Finally, we note that the superpotential and soft-breaking terms of the nMSSM also arise as the low-energy effective theory of minimal supersymmetric models with dynamical electroweak symmetry breaking, the so-called "Fat-Higgs "models [183]. In these models, the value of the Higgs-singlet coupling λ is not restricted by the requirement of perturbative consistency up to the grand-unification scale. Instead, the precise value of λ depends on the scale of dynamical symmetry breaking, λ being larger for smaller values of this scale. In our work, we shall focus on the case in which perturbative consistency holds up to very high energies, but we will also comment on how our results are modified if we ignore the perturbativity constraint on λ.

7.2 The nMSSM at Zero Temperature

Much of the analysis and notation in this section follows that of [181]. For simplicity, we will include only the Higgs, singlet, and third generation quark/squark fields in the superpotential. The superpotential, including the loop-generated tadpole term, is then

$$W_{nMSSM} = \lambda S H_1 \cdot H_2 \; + \; \frac{m_{12}^2}{\lambda} S \; + \; y_t Q \cdot H_2 \, U^c \; + \; \ldots \tag{7.2}$$

where $H_1^t = \left(H_1^0, H_1^-\right)$, $H_2^t = \left(H_2^+, H_2^0\right)$ denote the two Higgs superfields, S is the singlet superfield, and $A \cdot B = \epsilon^{ab} A_a B_b$ with $\epsilon^{12} = 1$.

The tree-level potential is then $V_0 = V_F + V_D + V_{soft}$:

$$\begin{aligned} V_F &= |\lambda H_1\cdot H_2 + \frac{m_{12}^2}{\lambda}|^2 + \left|\lambda S H_1^0 + y_t \tilde{t}_L \tilde{t}_R^*\right|^2 \\ &\quad + |\lambda S H_1^- + y_t \tilde{b}_L \tilde{t}_R^*|^2 + |\lambda S|^2 H_2^\dagger H_2 \\ &\quad + |y_t \tilde{t}_R^*|^2 H_2^\dagger H_2 + |y_t \tilde{Q}\cdot H_2|^2, \\ V_D &= \frac{\bar{g}^2}{8}(H_2^\dagger H_2 - H_1^\dagger H_1)^2 + \frac{g_2^2}{2}|H_1^\dagger H_2|^2 \\ V_{soft} &= m_1^2 H_1^\dagger H_1 + m_2^2 H_2^\dagger H_2 + m_s^2 |S|^2 \\ &\quad + (t_s\, S + h.c.) + (a_\lambda S\, H_1\cdot H_2 + h.c.) \\ &\quad + m_{Q_3}^2 \tilde{Q}^\dagger \tilde{Q} + m_U^2 |\tilde{t_R}|^2 + (a_t\, \tilde{Q}\cdot H_2\, \tilde{t}_R^* + h.c.). \end{aligned} \tag{7.3}$$

In writing V_D we have defined $\bar{g} = \sqrt{g_1^2 + g_2^2} = g/\cos\theta_W$.

The couplings $a_\lambda, t_s, \lambda, m_{12}^2, y_t, a_t$ can all be complex, but not all their phases are physical. By suitable redefinitions of S, H_1, and H_2, the parameters λ and m_{12}^2 can both be made real [184]. To simplify the analysis and to avoid spontaneous CP violation, we shall assume that the soft-breaking parameters a_λ, t_s, a_t and the Yukawa y_t are also real.[1] Moreover, we may take a_λ and t_s to be positive provided we allow λ and m_{12}^2 to have either sign. Real parameters are not sufficient to exclude spontaneous CP violation, however, so we must check this explicitly. We must also verify that the potential does not generate a VEV for either of the charged Higgs fields.

If none of the squark fields get VEV's, the tree-level Higgs potential becomes

$$\begin{aligned} V_0 &= m_1^2 H_1^\dagger H_1 + m_2^2 H_2^\dagger H_2 + m_s^2 |S|^2 + \lambda^2 |H_1\cdot H_2|^2 \\ &\quad + \lambda^2 |S|^2 (H_1^\dagger H_1 + H_2^\dagger H_2) + \frac{\bar{g}^2}{8}(H_2^\dagger H_2 - H_1^\dagger H_1)^2 + \frac{g_2^2}{2}|H_1^\dagger H_2|^2 \\ &\quad + t_s(S + h.c.) + a_\lambda(S\, H_1\cdot H_2 + h.c.) + m_{12}^2 (H_1\cdot H_2 + h.c.). \end{aligned} \tag{7.4}$$

We may choose an $SU(2)_L \times U(1)_Y$ gauge such that $\langle H_1^- \rangle = 0$ and $\langle H_1^0 \rangle \in \mathbb{R}^{\geq}$ at the minimum of the potential. Taking the derivative of V_0 with respect to H_2^+ and evaluating the result at the minimum, we find

$$\left.\frac{\partial V_0}{\partial H_2^+}\right|_{H_i = v_i} = {v_+}^* \left[m_2^2 + \lambda^2 |v_s|^2 + \frac{\bar{g}^2}{4}(|v_2|^2 - v_1^2) + \frac{g_2^2}{2} v_1^2 + \frac{\bar{g}^2}{8}|v_+|^2 \right], \tag{7.5}$$

where we have defined $\langle H_2^0 \rangle = v_2$, $\langle H_2^+ \rangle = v_+$, and $\langle S \rangle = v_s$. It follows that $\langle H_2^+ \rangle$ vanishes at the minimum provided $m_2^2 + \lambda^2 |v_s|^2 + \frac{\bar{g}^2}{4}(|v_2|^2 - v_1^2) + \frac{g_2^2}{2} v_1^2 > 0$.

[1] This assumption is not completely *ad hoc*. Within a minimal supergravity scenario, the soft breaking parameters are proportional to the corresponding terms in the superpotential.

If the charged Higgs VEV's vanish at the minimum, the only part of the potential that depends on the phases of the Higgs fields are the last three terms in Eq. (7.4):

$$V_{phase} = t_s\,(S + h.c.) + a_\lambda(S\,H_1^0\,H_2^0 + h.c.) + m_{12}^2(H_1^0\,H_2^0 + h.c.). \tag{7.6}$$

Recalling that a_λ and t_s are both real and positive, the potential will have an absolute minimum with $\langle S\rangle = v_s \in \mathbb{R}^{\leq}$ and $\langle H_2^0\rangle = v_2 \in \mathbb{R}^{\geq}$ provided $m_{12}^2 < 0$. While this condition is sufficient to avoid spontaneous CP violation, the result of [185] indicates that it is not necessary. We will focus on the $m_{12}^2 < 0$ case because it simplifies the analysis, and as we shall see below, it is preferred by the constraints on the scalar Higgs boson masses. However, we have also examined the $m_{12}^2 > 0$ case, and find that once we impose the experimental constraints described in following section, the parameter space with $m_{12}^2 > 0$ is very restricted, and is not consistent with electroweak baryogenesis.

With $m_{12}^2 < 0$, the field VEV's are all real and have fixed sign:

$$\langle S\rangle = v_s < 0 \qquad \langle H_1^0\rangle = v_1 > 0, \qquad \langle H_2^0\rangle = v_2 > 0. \tag{7.7}$$

We define the angle β as in the MSSM:

$$v_1 = v\cos\beta, \qquad\qquad v_2 = v\sin\beta, \tag{7.8}$$

with $v \simeq 174$ GeV. We also define $\mu = -\lambda v_s$, since this is the quantity that corresponds to the μ parameter in the MSSM. Note that μ can have either sign, depending on the sign of λ.

The minimization conditions for H_1^0, H_2^0, and S can be used to relate the scalar soft masses to the other parameters in terms of the VEV's. These give

$$\begin{aligned}
m_1^2 &= -(m_{12}^2 + a_\lambda v_s)\frac{v_2}{v_1} - \frac{\bar{g}^2}{4}(v_1^2 - v_2^2) - \lambda^2(v_2^2 + v_s^2) - \frac{1}{2v_1}\left.\frac{\partial\Delta V}{\partial H_1^0}\right|_{H_1^0=v_1}, \\
m_2^2 &= -(m_{12}^2 + a_\lambda v_s)\frac{v_1}{v_2} + \frac{\bar{g}^2}{4}(v_1^2 - v_2^2) - \lambda^2(v_1^2 + v_s^2) - \frac{1}{2v_2}\left.\frac{\partial\Delta V}{\partial H_2^0}\right|_{H_2^0=v_2}, \\
m_s^2 &= -a_\lambda\frac{v_1 v_2}{v_s} - \frac{t_s}{v_s} - \lambda^2\,v^2 - \frac{1}{2v_s}\left.\frac{\partial\Delta V}{\partial S}\right|_{S=v_s},
\end{aligned} \tag{7.9}$$

where ΔV consists of contributions to the effective potential beyond tree-level. To one-loop order

$$\Delta V = \frac{1}{(4\pi)^2}\left[\sum_b g_b\,h(m_b^2) - \sum_f g_f\,h(m_f^2)\right], \tag{7.10}$$

where the first sum runs over all bosons, the second over all Weyl fermions, g_i is the number of (on-shell) degrees of freedom, m_i is the field-dependent mass eigenvalue, and the function

$h(m^2)$ is given by (in the $\overline{DR}$ scheme)

$$h(m^2) = \frac{m^4}{4}\left[\ln\left(\frac{m^2}{Q^2}\right) - \frac{3}{2}\right]. \tag{7.11}$$

The one-loop corrections are therefore given by

$$\begin{aligned}\Delta m_i^2 &= -\frac{2}{64\pi^2}\left(\sum_b g_b m_b^2 \frac{\partial m_b^2}{\partial {H_i}^2}\left[\ln(\frac{m_b^2}{Q^2}) - 1\right]\right. \\ &\qquad \left. - \sum_f g_f m_f^2 \frac{\partial m_f^2}{\partial {H_i}^2}\left[\ln(\frac{m_f^2}{Q^2}) - 1\right]\right)\Bigg|_{H_i = v_i}.\end{aligned} \tag{7.12}$$

7.2.1 Charginos and Neutralinos

The chargino and neutralino sectors provide important phenomenological constraints on the model. The fermion component of the singlet superfield, the singlino, leads to a fifth neutralino state. Assuming the sfermions to be heavy, with masses of order a few hundred GeV, and values of λ that remain perturbative up to a grand unification scale of order 10^{16} GeV, the LSP of the model is always the lightest neutralino with a mass below about 60 GeV.

The chargino mass matrix, in the basis $(\tilde{W}^+, \tilde{H}_2^+, \tilde{W}^-, \tilde{H}_1^-)$, is

$$M_{\chi^\pm} = \begin{pmatrix} 0 & X^t \\ X & 0 \end{pmatrix}, \tag{7.13}$$

where

$$X = \begin{pmatrix} M_2 & \sqrt{2}s_\beta M_W \\ \sqrt{2}c_\beta M_W & -\lambda v_s \end{pmatrix}. \tag{7.14}$$

For the neutralinos, the mass matrix in basis $\psi_i^0 = (\tilde{B}^0, \tilde{W}^0, \tilde{H}_1^0, \tilde{H}_2^0, \tilde{S})$ reads

$$\mathcal{M}_{\tilde{N}} = \begin{pmatrix} M_1 & \cdot & \cdot & \cdot & \cdot \\ 0 & M_2 & \cdot & \cdot & \cdot \\ -c_\beta s_w M_Z & c_\beta c_w M_Z & 0 & \cdot & \cdot \\ s_\beta s_w M_Z & -s_\beta c_w M_Z & \lambda v_s & 0 & \cdot \\ 0 & 0 & \lambda v_2 & \lambda v_1 & 0 \end{pmatrix}. \tag{7.15}$$

In our analysis we take $M_1 = \frac{\alpha_1}{\alpha_2} M_2 \simeq \frac{1}{2} M_2$, which corresponds to what would be expected from universality at the GUT scale. With an eye towards electroweak baryogenesis, we allow the gaugino masses to have a common phase: $M_2 = M\, e^{i\phi}$ with M real. This phase also has a significant effect on the mass of the lightest neutralino. Since flipping the sign of λ is equivalent to shifting the gaugino phase by $\phi \to \phi + \pi$, we will consider only the $\lambda > 0$ case.

To see how the light neutralino state arises, suppose M_1 and M_2 are very large and

real so that the gaugino states decouple, leaving only the lower 3×3 Higgsino block. For $v_1 \ll v_2, v_s$, the smallest eigenvalue of this matrix is then

$$m_{\tilde{N}_1} \simeq 2\lambda v_1 v_2 v_s/(v_1^2 + v_2^2 + v_s^2), \tag{7.16}$$

and the corresponding state is predominantly singlino. More generally, the mass eigenstates are

$$\tilde{N}_i \;=\; N_{ij}\; \psi_i^0. \tag{7.17}$$

where N_{ij} is a unitary matrix such that $N^* \mathcal{M}_{\tilde{N}} N^\dagger$ is diagonal with non-negative entries [28]. We label the states in order of increasing mass so that $\tilde{N}_1$ is the lightest neutralino.

Measurements made at LEP II impose stringent constraints on the chargino and neutralino mass spectra. Since the coupling of the charginos to gauge bosons is the same as in the MSSM, the mass of the lightest chargino must satisfy $m_{\chi_1^\pm} > 104$ GeV [186]. The corresponding requirement for the neutralinos is either $(m_{\tilde{N}_1} + m_{\tilde{N}_2}) > 209$ GeV, or $\sigma(e^+e^- \to \tilde{N}_1\tilde{N}_2) \lesssim 10^{-2}$ fb. Finally, for $m_{\tilde{N}_1} < M_Z/2$, we must have $BR(Z \to \tilde{N}_1\tilde{N}_1) < 0.8 \times 10^{-3}$ [187].

It is possible to satisfy all of these constraints in the limit of large $\tan\beta$, in which case $\tilde{N}_1$ is a very light LSP; $m_{\tilde{N}_1} \lesssim 15$ GeV for $\lambda < 1.0$, $\tan\beta > 10$, and $M_2 \to \infty$. This state is mostly singlino, and couples only weakly to the gauge bosons. However, this limit also leads to an unacceptably large neutralino relic density. As we will show in Section 7.4, for heavy sfermions, the dominant annihilation channel for $\tilde{N}_1$ is s-channel Z-exchange.[2] For such a light, mostly singlino $\tilde{N}_1$, the $Z\tilde{N}_1\tilde{N}_1$ coupling is too weak for this state to annihilate efficiently.

We are thus led to consider values of $\tan\beta$ of order unity. The $\tilde{N}_1$ state now has a sizeable Higgsino component and correspondingly large couplings to the gauge bosons, so there is a danger of producing too large a contribution to the Z-width. The branching ratio of the Z to two $\tilde{N}_1$'s is given by

$$BR(Z \to \tilde{N}_1\tilde{N}_1) = \frac{g_2^2}{4\pi} \frac{(|N_{13}|^2 - |N_{14}|^2)^2}{24\cos^2_W} \frac{M_Z}{\Gamma_Z} \left[1 - \left(\frac{2\, m_{\tilde{N}_1}}{M_Z}\right)^2\right]^{3/2}. \tag{7.18}$$

Combining the branching ratio constraint with that for the relic density, we find $m_{\tilde{N}_1} \gtrsim 35$ GeV is needed if both conditions are to be met.(See Section 7.4.) As this value depends somewhat on parameters in the Higgs sector, we impose the weaker constraint $m_{\tilde{N}_1} > 25$ GeV in our analysis.

The magnitude of λ must be fairly large, $\lambda \gtrsim 0.3$, to raise the mass of the lightest neutralino above 25 GeV. ($|\lambda| \gtrsim 0.5$ for $m_{\tilde{N}_1} > 35$ GeV.) On the other hand, if λ is too large it encounters a Landau pole before the GUT scale. This is precisely what happens in the recently proposed Fat Higgs model [183], in which the Landau pole corresponds to

[2]There are also contributions to the annihilation cross-section from s-channel Higgs exchange, but these processes alone are not strong enough to produce an acceptable neutralino relic density unless the neutralino mass is close to one half of the Higgs boson masses.

the Higgs compositeness scale. We would like to maintain the property of perturbative unification in the model (in the usual sense), so we will focus most of our attention on values of λ that remain perturbative up to $M_{GUT} \sim 10^{16}$ GeV. However, with the Fat Higgs model in mind, we will also consider larger values of λ.

It is straightforward to derive the limit on λ at one-loop order. The relevant (one-loop) beta functions are [181]

$$\begin{aligned} \frac{dg_s}{dt} &= -\frac{1}{(4\pi)^2}\frac{3}{2}g_s^3, \\ \frac{dy_t}{dt} &= \frac{y_t}{(4\pi)^2}(3y_t^2 + \frac{1}{2}\lambda^2 - \frac{8}{3}g_s^2), \\ \frac{d\lambda}{dt} &= \frac{\lambda}{(4\pi)^2}(2\lambda^2 + \frac{3}{2}y_t^2), \end{aligned} \tag{7.19}$$

where $t = \ln(Q^2/M_Z^2)$. Running these up to $Q^2 = (10^{16}\ \text{GeV})^2$ and demanding $\lambda^2 < 4\pi$, we find the allowed region in the $\tan\beta$-λ plane shown in Fig. 7.1. The lower limit on $\tan\beta$ comes about because small values of this quantity imply a large $y_t(m_t)$, and this accelerates the running of λ. The figure also shows the region in which the $\tilde{N}_1$ state has mass greater than 25 GeV and satisfies the LEP II constraints listed above.

Fig. 7.2 shows the corresponding allowed region in the $|\mu| - |M_2|$ plane. The lower bounds on $|M_2|$ and $|\mu|$ are due to the chargino mass constraint. Interestingly, there is also an upper bound on $|\mu|$, which comes from the lower bound on the lightest neutralino mass. From Eqs. (7.15) and (7.16) we see that for $|v_s| \gg v$, the predominantly singlino state becomes very light. Since $\mu = -\lambda\, v_s$ and λ is bounded above by the perturbativity constraint, this translates into an upper bound on $|\mu|$. Both the phase and the magnitude of the gaugino mass M_2 have a significant impact on the mass of the light singlino state. The largest masses are obtained for $\phi = \pi$ with $|M_2| \sim \lambda\, v$, as this maximizes the constructive interference between the gaugino and Higgsino components. When $\phi = 0$ the interference is destructive, and $|M_2| \to \infty$ maximizes the mass.

Fig. 7.3 shows the range of masses of the lightest neutralino that are consistent with the constraints listed above. (The relevant input parameter sets are those listed in Table 7.2). For $\tan\beta$ and λ below the perturbative bound we see that the $\tilde{N}_1$ state has a mass below about 60 GeV, making it the LSP in the absence of a light gravitino. For $m_{\tilde{N}}$ below 50 GeV, this state is predominantly singlino, with a sizeable Higgsino component. This is because, with the assumption of gaugino mass universality, the constraint on the chargino mass puts a lower bound on $|M_1|$ that excludes a lighter predominantly Bino state. However, a mostly Bino LSP is possible if the light singlino state has mass above about 50 GeV, although the parameter space in which this can occur, consistent with perturbative unification, is severely restricted. In this event, the LSP and NLSP must be very close in mass. If λ is allowed to exceed the perturbativity bound, the situation is much less constrained; the parameter space in which the LSP is mostly Bino becomes much larger, and a Bino LSP need no longer be nearly degenerate with the NLSP.

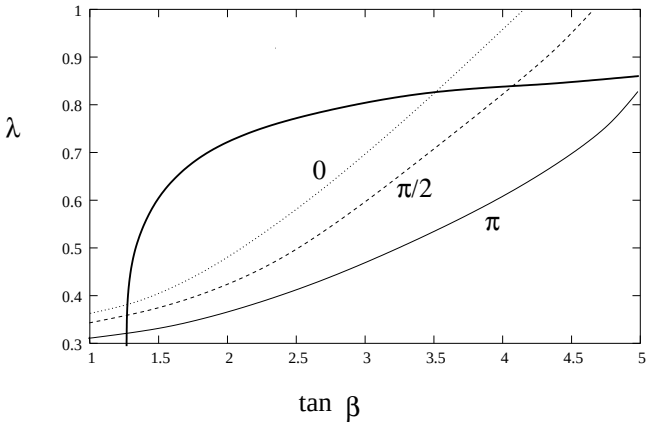

Figure 7.1: Allowed regions in the $\tan\beta - \lambda$ plane. The region consistent with perturbative unification lies below the thick solid line, while the regions consistent with the LEP II constraints (and $m_{\tilde{N}_1} > 25$ GeV) lie above the thinner lines. Among these, the solid line corresponds to a gaugino phase of $\phi = \pi$, while the dotted and dashed lines correspond to $\phi = 0,\ \pi/2$ respectively.

7.2.2 Higgs Spectrum

The LEP II lower bound on the mass of the lightest neutral CP-even Higgs boson of about 114 GeV is difficult to evade in the MSSM. This follows from the fact that, at tree-level, the mass of this state is bounded by M_Z,

$$m_h^2 \leq M_Z^2 \cos^2 2\beta, \tag{7.20}$$

which implies that large one-loop corrections are needed to increase the mass. The dominant loop contribution comes from the stops. With $\tan\beta \gg 1$, stop masses of order 1 TeV, and considerable fine-tuning of the stop mixing parameters, the mass of the lightest Higgs can be brought up to $m_h \simeq 130$ GeV [42].

The corresponding tree-level bound in the nMSSM is [182]

$$m_h^2 \leq M_Z^2(\cos^2 2\beta + \frac{2\lambda^2}{\bar{g}^2}\sin^2 2\beta), \tag{7.21}$$

which exceeds 100 GeV for $|\lambda| \sim 0.7$ and $\tan\beta \sim 2$. The same bound applies in the NMSSM [188]. This makes it possible to avoid the LEP II constraint without fine-tuning in the stop sector.

In order to discuss some of the constraints on the parameter space from the Higgs sector, we list here the tree-level Higgs masses. We have also included the one-loop mass corrections from the top and the stops given in [181] in our numerical analysis.

Since the tree-level Higgs VEV's are real, and neglecting the small CP-violating effects

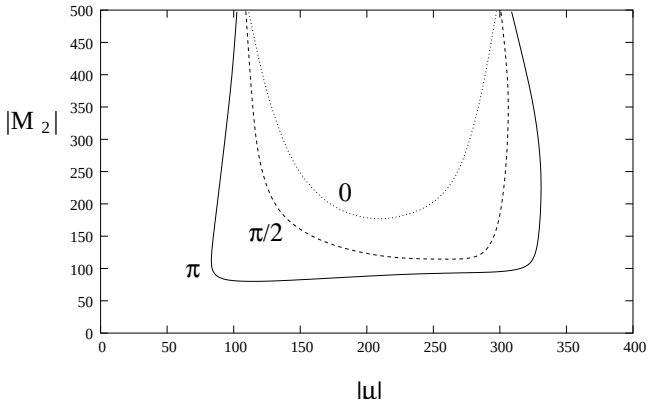

Figure 7.2: Allowed regions in the $|\mu| - |M_2|$ plane for a gaugino phase of $\phi = 0,\ \pi/2,\ \pi$, and $(\tan\beta, \lambda)$ below the perturbativity bound. The allowed region lies in the central area. Recall that $\mu = -\lambda\, v_s$ in the model.

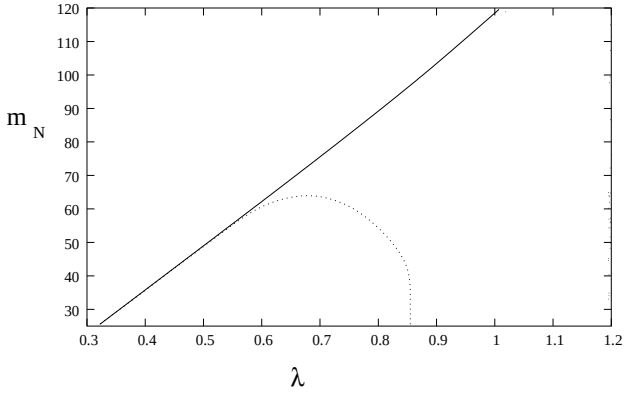

Figure 7.3: Mass of the lightest neutralino. The region to the right of the solid line is consistent with the LEP II constraints listed above. The region surrounded by the dotted line is also consistent with perturbative unification.

associated with the one-loop chargino and neutralino contributions, the Higgs fields can be expanded as

$$\begin{aligned} H_1 &= \begin{pmatrix} v_1 + \frac{1}{\sqrt{2}}(\phi_1 + i a_1) \\ \phi_1^- \end{pmatrix}, \\ H_2 &= \begin{pmatrix} \phi_2^+ \\ v_2 + \frac{1}{\sqrt{2}}(\phi_2 + i a_2) \end{pmatrix}, \\ S &= v_s + \frac{1}{\sqrt{2}}(\phi_s + i a_s). \end{aligned} \tag{7.22}$$

After electroweak symmetry breaking, the real and imaginary parts of the singlet mix with those of H_1^0 and H_2^0 to produce two neutral scalar states in addition to those of the MSSM.

In all, the physical Higgs states consist of one charged scalar, two neutral CP-odd scalars, and three neutral CP-even scalars.

For the CP-odd scalars, the combination $G^0 = -a_1\, c_\beta + a_2\, s_\beta$ is absorbed by the Z^0 while the orthogonal linear combination $A^0 = a_1\, s_\beta + a_2\, c_\beta$ mixes with a_s to give two physical scalars. The mass matrix in basis (A^0, a_s) is

$$M_P^2 = \begin{pmatrix} M_a^2 & -a_\lambda v \\ -a_\lambda v & -\frac{1}{v_s}(t_s + s_\beta\, c_\beta\, a_\lambda v^2) \end{pmatrix}, \tag{7.23}$$

where

$$M_a^2 = -\frac{1}{s_\beta\, c_\beta}(m_{12}^2 + a_\lambda\, v_s). \tag{7.24}$$

Note that Eq. (7.9) implies $m_s^2 + \lambda^2\, v^2 = -\frac{1}{v_s}(t_s + s_\beta\, c_\beta\, a_\lambda v^2)$. Therefore the singlet soft mass, m_s^2, sets the mass scale of a predominantly singlet state.

Among the charged Higgs bosons, the combination $G^+ = \phi_2^+\, s_\beta - \phi_1^{-*}\, c_\beta$ is taken up by the W^+ leaving behind a single complex charged scalar mass eigenstate, H^+, of mass

$$M_\pm^2 = M_a^2 + M_W^2 - \lambda^2 v^2. \tag{7.25}$$

It may be shown using the minimization conditions, Eq (7.9), that $M_\pm^2 > 0$ is equivalent to the condition needed to avoid a charged Higgs VEV, Eq. (7.5).

Finally, the mass matrix elements for the CP-even Higgs boson states are

$$\begin{aligned} M_{11}^2 &= s_\beta^2\, M_a^2 + c_\beta^2\, M_Z^2 \\ M_{12}^2 &= -s_\beta\, c_\beta (M_a^2 + M_Z^2 - 2\lambda^2\, v^2) \\ M_{13}^2 &= v(s_\beta\, a_\lambda + 2 c_\beta \lambda^2\, v_s) \\ M_{22}^2 &= c_\beta^2\, M_a^2 + s_\beta^2\, M_Z^2 \\ M_{23}^2 &= v\,(c_\beta\, a_\lambda + 2 s_\beta \lambda^2\, v_s) \\ M_{33}^2 &= -\frac{1}{v_s}(t_s + s_\beta\, c_\beta\, a_\lambda\, v^2) \end{aligned} \tag{7.26}$$

with the remaining elements related to these by symmetry. As for the CP-odd case, the mass of a mostly singlet state is determined by the singlet soft mass.

Large values of M_a^2 help to increase the mass of the Higgs states. This is most easily obtained with $m_{12}^2 < 0$ (see Eq. (7.24)), which is a sufficient condition to guarantee the absence of spontaneous CP violation at tree-level. We also note that the MSSM limit of the NMSSM is not possible in this model. In this limit one takes $|v_s| \gg v$, while holding λv_s fixed, thereby decoupling the singlet states from the rest of the Higgs spectrum. As discussed in Section 7.2.1, such large values of v_s lead to an unacceptably light neutralino state. On the other hand, the decoupling limit of the nMSSM discussed in [181], $|t_s| \to \infty$, is still viable. Indeed, the upper bound on the lightest neutral Higgs mass, Eq. (7.21) is saturated in this limit if $M_a^2 \to \infty$ as well.

The precise LEP II bounds on the Higgs masses depend on the couplings of the Higgs

bosons to the gauge bosons. These couplings tend to be weakened somewhat from mixing with the singlet. Let $\mathcal{O}^S$, $\mathcal{O}^P$ be the orthogonal mixing matrices relating the gauge and mass eigenstates:

$$\begin{pmatrix} S_1 \\ S_2 \\ S_3 \end{pmatrix} = \mathcal{O}^S \begin{pmatrix} \phi_1 \\ \phi_2 \\ \phi_s \end{pmatrix}; \qquad \begin{pmatrix} P_1 \\ P_2 \end{pmatrix} = \mathcal{O}^P \begin{pmatrix} A^0 \\ a_s \end{pmatrix}. \tag{7.27}$$

We label the mass eigenstates in order of increasing mass, so that S_1 is the lightest CP-even state and P_1 the lightest CP-odd state. In terms of these mixing matrices, the SVV-type couplings are

$$\begin{aligned} SZZ: &\qquad \frac{\bar{g}}{2} M_Z \left(c_\beta \, \mathcal{O}^S_{k1} + s_\beta \, \mathcal{O}^S_{k2}\right) (Z_\mu)^2 \, S_k, \\ SWW: &\qquad \frac{g}{2} M_W \left(c_\beta \, \mathcal{O}^S_{k1} + s_\beta \, \mathcal{O}^S_{k2}\right) (W_\mu)^2 \, S_k. \end{aligned} \tag{7.28}$$

Also relevant are the SPZ-type couplings

$$SPZ: \qquad \frac{\bar{g}}{2} \left[\mathcal{O}^P_{\ell 1}(s_\beta \, \mathcal{O}^S_{k1} - c_\beta \, \mathcal{O}^S_{k2})\right] \, Z^\mu \, S_k \overleftrightarrow{\partial}_\mu P_\ell. \tag{7.29}$$

The couplings of the Higgs states to fermions and neutralinos are listed in Appendix B.3.

The LEP bound on the charged Higgs boson is given in Ref. [189]. Assuming $BR(H^+ \to \tau^+\nu) \simeq 1$ this bound reads, approximately,

$$M_{H^\pm} > 90 \text{ GeV}. \tag{7.30}$$

The bounds on the CP-odd Higgs bosons depend strongly on their coupling to the Z-gauge boson and the CP-even scalars given in Eq. (7.29). If the lightest CP-odd Higgs boson, P_1, has a large singlet component this coupling can become very small, and the bound on this particle is much weaker than the LEP bound of about 90 GeV present in the MSSM [190]. This bound may be further weakened if the decay $P_1 \to \tilde{N}_1\tilde{N}_1$ is allowed kinematically. If so, this mode tends to dominate the decay width leading to a large fraction of invisible final states.

The same is true of the lightest CP-even state, S_1. The limit found in [41] depends on the strength of the SVV coupling relative to the corresponding Standard Model coupling. From Eq. (7.28) this relative factor is $|c_\beta \, \mathcal{O}^S_{11} + s_\beta \, \mathcal{O}^S_{12}|$, which can be considerably smaller than unity if the S_1 state has a large singlet component. Again, the limit is further weakened if the $S_1 \to \tilde{N}_1\tilde{N}_1$ channel is open, as this tends to dominate the decay width below the gauge boson threshold. In this case, the limit on invisible decay modes found in [191] is the relevant one.

7.3 Electroweak Baryogenesis

If Electroweak Baryogenesis (EWBG) is to generate the presently observed baryon asymmetry, the electroweak phase transition must be strongly first order. In the most promising MSSM scenario, this phase transition is dominated by a light, mostly right-handed stop [109]. Such a stop produces a large contribution to the cubic term in the one-loop effective potential that is responsible for making the phase transition first order. Even so, for Higgs masses above the LEP II bound, there is only a very small region of parameter space in which the EW phase transition is strong enough for EWBG to work [95, 101].

The prospects for EWBG in the NMSSM are more promising. The NMSSM has an additional tree-level contribution to the cubic term of the effective potential. This is sufficient to make the electroweak phase transition strongly first order without relying on the contribution of a light stop [113–117]. Since the nMSSM has a similar cubic term in the tree-level potential, we expect EWBG to be possible in this model as well.

In this section we investigate the strength to the electroweak phase transition in the nMSSM in order to find out whether a strongly first order transition is possible, and if so, try to map out the relevant region of parameter space. To simplify our analysis, we neglect the contributions from sfermions other than the stops since these are generally very small. We also fix the stop SUSY-breaking parameters to be

$$\begin{aligned} m_{Q_3}^2 &= m_{U_3}^2 = (500 \text{ GeV})^2, \\ a_t &= 100 \text{ GeV}. \end{aligned}$$

This choice of parameters leads to stops that are too heavy to have a relevant impact on the strength of the first order phase transition. We have made this choice because it allows us to emphasize the effects induced by terms in the tree-level effective potential that are not present in the MSSM. These effects turn out to be sufficient to make the phase transition strongly first order, even in the absence of light stops.

While a strongly first order electroweak phase transition is necessary for EWBG to be successful in preserving the baryon asymmetry in the broken phase, based on previous analyses of the MSSM it appears that this condition is also sufficient [102, 121]. In the MSSM, the generation of baryon number proceeds from the CP-violating interactions of the charginos with the Higgs field. The dominant source of CP violation, leading to the baryon asymmetry, is proportional to the relative phase of the μ and the gaugino mass parameters, $\mathrm{Arg}(\mu\, \mathrm{M}_2)$. The only difference in the model under study is that the μ parameter is replaced by the quantity $-\lambda\, v_s$, which is real, and CP violation is induced by the phase of the gaugino masses. Therefore, in the presence of a sufficiently strong first order phase transition, we expect a result for the baryon asymmetry generated from the chargino currents similar to the one obtained in the MSSM.

7.3.1 One-Loop Effective Potential

The finite temperature effective potential for the real Higgs scalars is

$$V(\varphi_i, T) = V_0(\varphi_i) + V_1(\varphi_i, T) + V_{daisy}(\varphi_i, T) + \dots \tag{7.31}$$

where V_n is the n-loop contribution, and the additional term, V_{daisy} is a finite-temperature effect. Also, φ_i, $i = 1, 2, s$ are the classical field variables corresponding to H_1^0, H_2^0, and S. ($\varphi_i = v_i$ at the T=0 minimum.) The tree-level part is

$$\begin{aligned} V_0(\varphi_i) &= m_1^2\,{\varphi_1}^2 + m_2^2\,{\varphi_2}^2 + m_s^2\,{\varphi_s}^2 + 2\,m_{12}^2\,\varphi_1\varphi_2 + 2\,t_s\varphi_s + 2\,a_\lambda\,\varphi_s\,\varphi_1\,\varphi_2 \\ &\quad + \frac{\bar{g}^2}{8}({\varphi_1}^2 - {\varphi_2}^2)^2 + \lambda^2\,{\varphi_s}^2({\varphi_1}^2 + {\varphi_2}^2) + \lambda^2\,{\varphi_1}^2\,{\varphi_2}^2. \end{aligned} \tag{7.32}$$

Note the cubic term, $a_\lambda\,\varphi_s\,\varphi_1\,\varphi_2$, which has no counterpart in the MSSM.

In the $\overline{DR}$ scheme, the one-loop contribution reads

$$V_1(\varphi_i, T) = \sum_b g_b\,f_B(m_b^2, T) + \sum_f g_f\,f_F(m_f^2, T), \tag{7.33}$$

where b runs over bosons, f runs over Weyl fermions, and g_i is the number of (on-shell) degrees of freedom. Explicit expressions for the functions f_B and f_F are given in Eq. (5.23). The third contribution to the potential, V_{daisy}, is a finite-temperature effect [58, 85, 86] coming from a resummation of the bosonic self-energies. It modifies the effective potential by the amount

$$V_{daisy} = -\frac{1}{12\pi}\sum_b\ g_b\ \left(\overline{m}_b^2 - m_b^2\right)^{3/2}, \tag{7.34}$$

where $\overline{m}_b^2$ is the thermal mass. The sum includes gauge bosons, although only the longitudinal modes of these develop a thermal contribution to their mass at leading order. The field-dependent mass matrices relevant to our analysis (including thermal corrections) are listed in Appendix B.1.

7.3.2 Tree-Level Analysis

To better understand the effect of the new cubic term, we have examined a simplified form of the potential which allows us to obtain analytic expressions for the critical temperature, T_c, and the field VEV's. If the cubic term plays a dominant role in making the electroweak phase transition first order, we expect this analysis to give a good qualitative description of the transition.

Our first simplifying assumption is that the ratio of the field values at the broken phase minimum remains constant up to T_c. That is, we fix $\tan\beta$, and consider variations in $\varphi = \sqrt{{\varphi_1}^2 + {\varphi_2}^2}$. To make the one-loop part of the potential more manageable, we keep only the leading φ^2T^2 terms in the low-temperature expansion, and include only the contributions of the gauge bosons and the top. Since the stops are assumed to be

heavy, the leading temperature-dependent contribution comes from the top provided λ lies below the perturbative bound, $\lambda \lesssim 0.8$. For larger values of λ the contributions from the Higgs, charginos, and neutralinos become important. We shall restrict ourselves to the perturbative regime in the present analysis.

In terms of φ, φ_s, and β, the effective potential becomes $V = V_0 + V_1$. The tree-level part is

$$V_0 = M^2\varphi^2 + m_s^2{\varphi_s}^2 + 2t_s\varphi_s + 2\tilde{a}\varphi^2\varphi_s + \lambda^2\varphi^2{\varphi_s}^2 + \tilde{\lambda}^2\varphi^4, \tag{7.35}$$

where we have defined

$$\begin{aligned} M^2 &= m_1^2\cos^2\beta + m_2^2\sin^2\beta + m_{12}^2\sin 2\beta, \\ \tilde{a} &= a_\lambda \sin\beta\,\cos\beta, \\ \tilde{\lambda}^2 &= \frac{\lambda^2}{4}\sin^2 2\beta + \frac{\bar{g}^2}{8}\cos^2 2\beta. \end{aligned} \tag{7.36}$$

Within our approximation, the one-loop part is

$$V_1 = \frac{1}{8}\left(g_2^2 + \frac{\bar{g}^2}{2} + 2y_t^2\sin^2\beta\right)\varphi^2T^2. \tag{7.37}$$

To find the minimization conditions, we shall make use of the simple (quadratic) φ_s dependence and consider only the field-space trajectory along $\frac{\partial V}{\partial \varphi_s} = 0$, at which the minimum of the potential is found. This condition allows us to eliminate φ_s in terms of φ giving

$$\varphi_s = -\left(\frac{t_s + \tilde{a}\varphi^2}{m_s^2 + \lambda^2\varphi^2}\right). \tag{7.38}$$

Inserting this back into the effective potential, we find

$$V(\varphi, T) = m^2(T)\varphi^2 - \frac{(t_s + \tilde{a}\varphi^2)^2}{m_s^2 + \lambda^2\varphi^2} + \tilde{\lambda}^2\varphi^4, \tag{7.39}$$

where $m^2(T) = M^2 + \frac{1}{8}\left(g_2^2 + \frac{\bar{g}^2}{2} + 2y_t^2\sin^2\beta\right)$.

The critical temperature, T_c, and the VEV at T_c, φ_c, are defined by the two conditions

$$\begin{aligned} V(\varphi_c, T_c) &= V(\varphi = 0, T_c), \\ \left.\frac{\partial V}{\partial\varphi}\right|_{\varphi=\varphi_c} &= 0. \end{aligned} \tag{7.40}$$

Solving for φ_c and T_c we find

$$\begin{aligned} \varphi_c^2 &= \frac{1}{\lambda^2}\left(-m_s^2 + \frac{1}{\tilde{\lambda}}|m_s\,\tilde{a} - \frac{\lambda^2\,t_s}{m_s}|\right), \\ T_c^2 &= 8\left(F(\varphi_c^2) - F(v^2)\right) \Big/ \left(g_2^2 + \frac{\bar{g}^2}{2} + 2y_t^2\sin^2\beta\right), \end{aligned} \tag{7.41}$$

where

$$F(\varphi^2) = 2\tilde{a}\left(\frac{t_s + \tilde{a}\varphi^2}{m_s^2 + \lambda^2\varphi^2}\right) - \lambda^2\left(\frac{t_s + \tilde{a}\varphi^2}{m_s^2 + \lambda^2\varphi^2}\right)^2 - 2\tilde{\lambda}^2\varphi^2.$$

Both φ_c^2 and T_c^2 must of course be positive if a solution is to exist. For $\varphi_c^2 > 0$, we need

$$m_s^2 < \frac{1}{\tilde{\lambda}}\left|\frac{\lambda^2\,t_s}{m_s} - m_s\,\tilde{a}\right|. \tag{7.42}$$

The positivity of T_c^2 requires that $F(\varphi_c^2) > F(v^2)$. Since increasing the temperature tends to decrease the field VEV, this condition will be satisfied if $F(\varphi^2)$ is a decreasing function which is the case provided

$$(m_s\,\tilde{a} - \frac{\lambda^2 t_s}{m_s})^2 < \tilde{\lambda}^2(m_s^2 + \lambda^2\varphi^2)^3. \tag{7.43}$$

It is sufficient to demand that this hold for $\varphi = \varphi_c$, which gives

$$m_s^3(m_s^2\tilde{a} - \lambda^2 t_s)^2 < \frac{1}{\tilde{\lambda}}|m_s^2\tilde{a} - \lambda^2 t_s|^3. \tag{7.44}$$

This is equivalent to the inequality in Eq. (7.42). Thus, Eq. (7.42) is the necessary condition for a first order phase transition. To satisfy this equation, m_s^2 must not be too large. This can be also seen from Eq. (7.39), which has only positive quadratic and quartic terms in the limit $\lambda^2\varphi^2 \ll m_s^2$.

7.3.3 Numerical Analysis

The results of the previous section have been examined more carefully by means of a numerical investigation of the one-loop effective potential. In this analysis, we consider only the dominant contributions which are those of the top, the stops, the gauge bosons, the Higgs bosons, the charginos, and the neutralinos. The corresponding field-dependent mass matrices, both at zero and finite temperature, are listed in Appendix B.1. For the purpose of calculating thermal masses, we assume that the remaining sfermions and the gluino are heavy enough to be neglected. We find that a strongly first order electroweak phase transition is possible within the nMSSM.

The procedure we use goes as follows. To begin, we specify the values of

$(\beta, v_s, a_\lambda, t_s, M_a, \lambda, |M_2|, \phi)$, where $M_2 = |M_2|e^{i\phi}$ is the complex Wino soft mass. These are chosen randomly from the initial ranges listed in Table 7.2. As above, the Bino mass is taken to be $M_1 = M_2/2$, and we fix the soft stop parameters to be $m^2_{Q_3} = m^2_{U_3} = (500\text{ GeV})^2$, $a_t = 100$ GeV. The subtraction scale is set at $Q^2 = (150\text{ GeV})^2$. For each parameter set we calculate the mass spectrum at zero temperature and impose the experimental constraints described in Section 7.2. At this point we do not impose any dark matter constraint other than the necessary condition $m_{\tilde{N}_1} > 25$ GeV. Since, for some parameter sets, the one-loop correction can destabilize the potential in the φ_s direction, we also check that the minimum at $(\varphi_1, \varphi_2, \varphi_s) = (v_1, v_2, v_s)$ is a global minimum at $T = 0$. Finally, we calculate φ_c and T_c using the full potential, where T_c is taken to be the temperature at which the symmetric and broken phase minima are equal in depth, and $\varphi_c = \sqrt{{\varphi_1}^2 + {\varphi_2}^2}$ is the broken phase VEV at this temperature.

$\tan\beta$	λ	v_s (GeV)	a_λ (GeV)	$t_s^{1/3}$ (GeV)	M_a (GeV)	$\lvert M_2\rvert$ (GeV)	ϕ
1–5	0.3–2.0	–750 – 0	0 – 1000	0 – 1000	200-1000	0 – 1000	0 – π

Table 7.2: Ranges of input parameters.

In this way we have found several parameter sets which satisfy all the constraints listed above, and give $\varphi_c/T_c > 0.9$, which we take as our criterion for a strongly first order transition [68, 109]. [3] Let us define

$$D = \frac{1}{\tilde{\lambda}\, m_s^2}\left(\frac{\lambda^2\, t_s}{m_s} - \tilde{a}\, m_s\right) \tag{7.45}$$

where $m_s^2 = -a_\lambda\, v_1\, v_2/v_s - t_s/v_s - \lambda^2\, v^2$ (see Eq. (7.9)), and $\tilde{a}$ and $\tilde{\lambda}$ are defined in Eq. (7.36). D is crucial in determining whether or not a first order phase transition occurs. The simplified analysis of Section 7.3.2, Eq. (7.42) in particular, suggests that $|D| > 1$ is a necessary condition for a first order transition. Fig. 7.4 shows D plotted against m_s for both λ below the perturbative bound, and for general values in the range $0.7 < \lambda < 2.0$. The region surrounded by the solid lines in this figure corresponds to parameter sets consistent with the experimental constraints. This figure shows that among the parameter sets for which a strongly first order phase transition occurs, most satisfy $|D| > 1$. On the other hand, we also find parameter sets with $|D| > 1$ that do not exhibit a strongly first order phase transition, so this condition is not a sufficient one. The low m_s region in these plots is excluded since the potential tends to become unstable in the singlet direction for small values of this quantity. This leads to the additional requirement of $m_s^2 \gtrsim (50\text{ GeV})^2$.

[3] This corresponds to $\frac{\varphi_c}{T_c} > 1.3$ for φ normalized to 246 GeV.

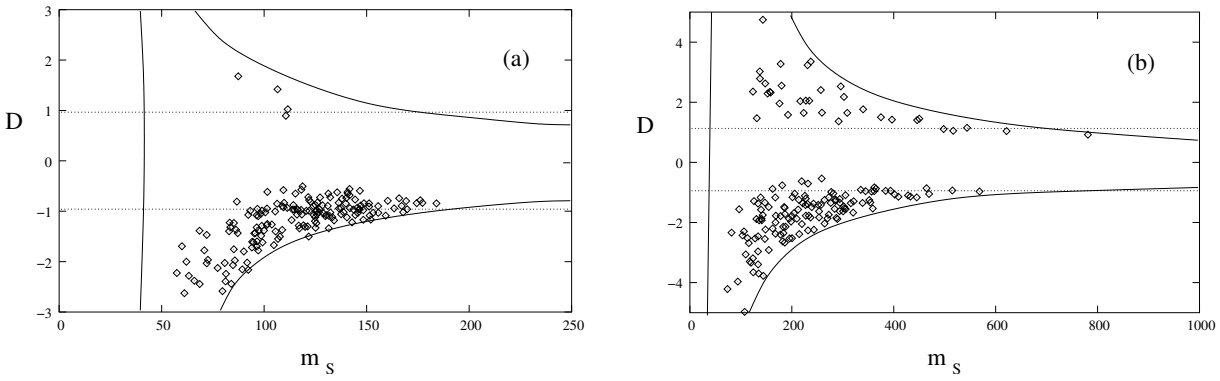

Figure 7.4: Values of D for parameter sets leading to a strongly first order phase transition for: (a) λ below the perturbative bound; (b) general values of λ in the range $0.7 < \lambda < 2.0$. The region consistent with the experimental constraints lies within the area enclosed by the solid lines.

The critical temperature for the phase transition generally falls in the range $T_c = 100-150$ GeV. Table 7.3 shows the parameter values and transition temperatures for three of the successful parameter sets. The particle spectra corresponding to these are listed in Appendix B.3. Parameter sets A and B, with $|D| \simeq 1$, both satisfy the perturbative bound while C, for which $D \simeq 6.7$, exceeds it.

Sets A and B are typical of the (perturbative) parameter sets that give a strong phase transition. As we found in Section 7.2.1, the constraints in the chargino/neutralino sector, along with perturbative consistency, force $\lambda \sim 0.5-0.8$, $\tan\beta \sim 1.5-5$, and $|v_s| \sim 150-500$ GeV. For a given v_s, the values of a_λ and t_s must then be adjusted so that $m_s^2 \gtrsim (50\text{ GeV})^2$ (Eq. (7.9)) and $|D| \gtrsim 1$ (Eq. (7.45)) if the potential is to be stable and the transition is to be strongly first order. These quantities are further constrained by the Higgs sector. We find that these requirements may be satisfied for $a_\lambda \sim 300-600$ GeV and $t_s \sim (50-200\text{ GeV})^3$. The value of M_a does not appear to have much effect on the phase transition, but tends to be fairly large, $M_a \gtrsim 400$ GeV, due to the Higgs mass constraints. While large values of M_a help to increase the masses of the lightest Higgs states, they also tend to make EWBG less efficient [101, 102, 121]. Even so, EWBG is still able to account for the baryon asymmetry provided $\tan\beta \lesssim 2$, as we tend to find here [101].

Set	$\tan\beta$	λ	v_s (GeV)	a_λ (GeV)	$t_s^{1/3}$ (GeV)	M_a (GeV)	$\lvert M_2\rvert$ (GeV)	φ_c (GeV)	T_c (GeV)
A	1.70	0.619	-384	373	157	923	245	120	125
B	1.99	0.676	-220	305	143	914	418	145	95
C	1.10	0.920	-276	386	140	514	462	145	130

Table 7.3: Sample parameter sets exhibiting a strongly first order electroweak phase transition.

7.4 Neutralino Dark Matter

As discussed above, the LSP in this model (for λ below the perturbative bound) is always the lightest neutralino, $\tilde{N}_1$, with a mass below about 60 GeV and a sizeable singlino component. This can be dangerous since a light, stable particle with very weak gauge couplings may produce a relic density much larger than is consistent with the observed cosmology. On the other hand, if the $\tilde{N}_1$ is able to annihilate sufficiently well, this state makes a good dark matter candidate [192].

For values of $\tan\beta$ and λ consistent with the perturbative limit, the LSP tends to be mostly singlino, but has a sizeable higgsino component. Since $m_{\tilde{N}_1} \lesssim 60$ GeV, s-channel Z^0 exchange is the dominant annihilation mode. There are also contributions from s-channel CP-even and CP-odd Higgs boson exchanges generated by the the $\lambda S H_1 \cdot H_2$ term in the superpotential, although these tend to be very small except near the corresponding mass poles. Since we have assumed that all sfermions are heavy, we consider only these two channels in our analysis. The relevant couplings are listed in Appendix B.2. (The matrix element for s-channel Z-exchange is given in [193].) We also neglect the possibility of coannihilation between the LSP and the NLSP. Among the parameter sets found to be consistent with the constraints, EWBG, and the perturbative bound, the NLSP is always at least 15 % (and almost always more than 25%) heavier than the LSP, implying that the coannihilation contribution is strongly Boltzmann-suppressed. Moreover, when the LSP and NLSP are close in mass the NLSP is mostly Bino, so the annihilation cross-section between the LSP and NLSP is less than or of the same order as that for the LSP with itself.

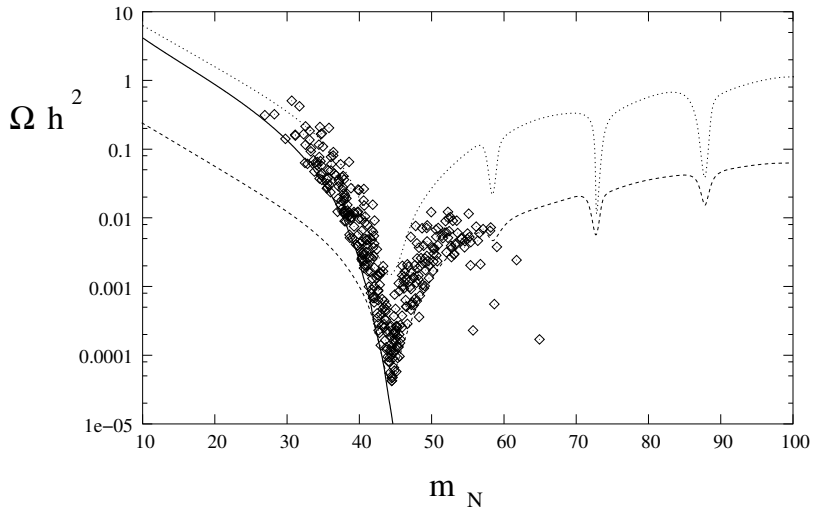

Figure 7.5: Neutralino relic density as a function of mass for two values of the mixing parameter, $||N_{13}|^2 - |N_{14}|^2| = 0.1$ (dotted), 0.5 (dashed) and typical values of the Higgs mixing parameters. The region to the right of the thick solid line is consistent with the observed Z width. The scattered points correspond to parameter sets that give a strong first order phase transition, and are consistent with perturbative unification.

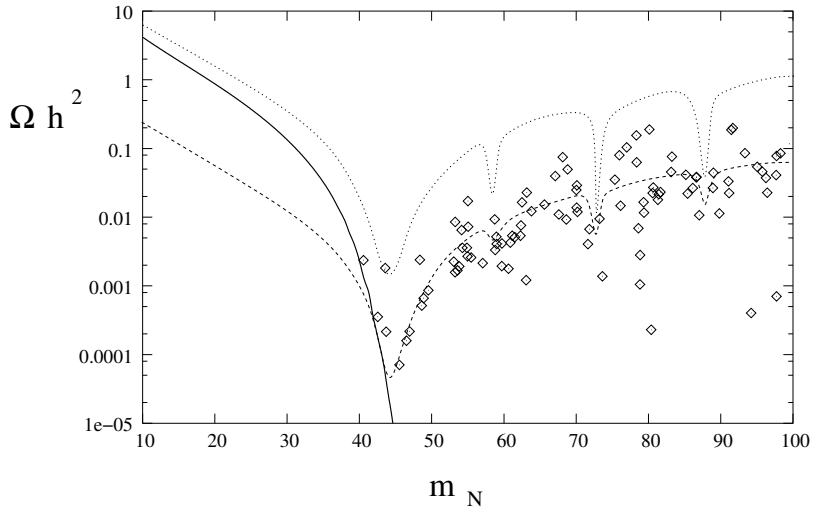

Figure 7.6: Neutralino relic density as a function of mass for two values of the mixing parameter, $||N_{13}|^2 - |N_{14}|^2| = 0.1$ (dotted), 0.5 (dashed) and typical values of the Higgs mixing parameters. The region to the right of the thick solid line is consistent with the observed Z width. The scattered points correspond to parameter sets which give a strong first order phase transition with $0.7 < \lambda < 1.2$.

The neutralino LSP relic density was computed using the methods outlined in Chapter 4. Figs. (7.5) and (7.6) show the relic densities obtained for parameter sets that satisfy the above mentioned experimental constraints, and are consistent with EWBG. A relic density consistent with the observed dark matter is obtained for neutralino masses in the range $m_{\tilde{N}_1} \simeq 30-40$ GeV. For neutralino masses greater than this, it appears to be difficult to generate a sufficiently large relic density to account for the dark matter. If we allow λ to exceed the perturbativity bound, a realistic dark matter candidate may be obtained for neutralino masses above about 65 GeV.

7.5 Phenomenological Discussion

The region of parameter space consistent with EWBG, neutralino dark matter, and the experimental bounds is quite constrained, and leads to an interesting phenomenology. We shall focus on values of $\tan\beta$ and λ that satisfy the perturbativity bound.

The dark matter condition implies that the LSP of the model is the lightest neutralino with a mass in the range $m_{\tilde{N}_1} \simeq 30-40$ GeV, and is mostly singlino. For smaller values of $|M_2|$, the next-to-lightest neutralino is predominantly bino. Otherwise it is a mostly Higgsino state. In both cases, there are always two mostly Higgsino states with masses of order $|\lambda\, v_s| \lesssim 350$ GeV. The bound on the Higgsino masses comes from the bound on $|\mu|$ found in Section 7.2.1. This bound also implies that the lightest chargino state has mass below this value.

In the Higgs sector, since M_a tends to be fairly large, one CP-even Higgs state, one

CP-odd Higgs state, and the charged Higgs end up with large masses of order M_a. The remaining CP-odd state is relatively light, and is nearly a pure singlet. For $M_a \to \infty$, the tree-level mass of this state goes to $m_P \to \sqrt{-(t_s + a_\lambda\, v^2\, s_\beta\, c_\beta)/v_s} = \sqrt{m_s^2 + \lambda^2 v^2}$, (Eq. (7.23)), which is less than 250 GeV for the values of t_s, v_s and a_λ consistent with EWBG.

The remaining pair of CP-even states also tend to be fairly light. In the $M_a \to \infty$ limit, the effective tree-level mass matrix for these states becomes

$$M^2_{S_{1,2}} = \begin{pmatrix} M_Z^2 \cos^2 2\beta + \lambda^2 \sin^2 2\beta\, v^2 & v(a_\lambda \sin 2\beta + 2\,\lambda^2 v_s) \\ v(a_\lambda \sin 2\beta + 2\,\lambda^2 v_s) & -(t_s + a_\lambda\, v^2\, s_\beta\, c_\beta)/v_s \end{pmatrix}. \tag{7.46}$$

Among the parameter ranges consistent with EWBG, the off-diagonal element of this matrix can be of the same order as the diagonal elements which leads to a strong mixing between the gauge eigenstates, although too much mixing can produce an unacceptably light mass eigenstate. The two terms in the off-diagonal matrix element tend to cancel each other. If $a_\lambda \sim -2\lambda^2\, v_s/\sin 2\beta$ then the mixing goes to zero, and the mass eigenstates consist of one SM-like state with mass below 150 GeV, and one mostly singlet state that is nearly degenerate with the lightest CP-odd state. Otherwise, the mass eigenstates are a strong admixture of S and the SM-Higgs-like linear combination $(\cos\beta\, H_1^0 + \sin\beta\, H_2^0)$. For finite M_a, the corrections to this picture are of order $a_\lambda v^2/M_a^2$.

Figs. 7.7 and 7.8 show the mass and composition of the three light Higgs states (including one-loop contributions from the top and the stops) for the representative parameter values $M_a = 900$ GeV, $t_s = (150\text{ GeV})^3$, $v_s = -300$ GeV, $a_\lambda = 350$ GeV, and $\lambda = 0.7$. These values are typical of those consistent with the constraints and EWBG. The maximum of the mass of the lightest CP-even state occurs when $\sin 2\beta = -2\lambda^2\, v_s/a_\lambda$, at which point the off-diagonal term in Eq. (7.46) vanishes. The splitting between the P_1 and S_2 states at this point is due to the finite value of M_a.

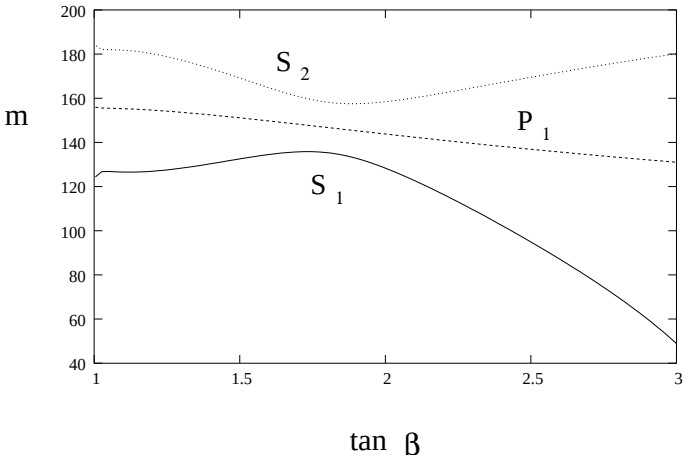

Figure 7.7: Mass and of the light Higgs bosons for typical parameter values consistent with EWBG.

The discovery of these light states is more challenging than the MSSM case for two reasons. First, all three can have sizeable singlet components which reduce their couplings

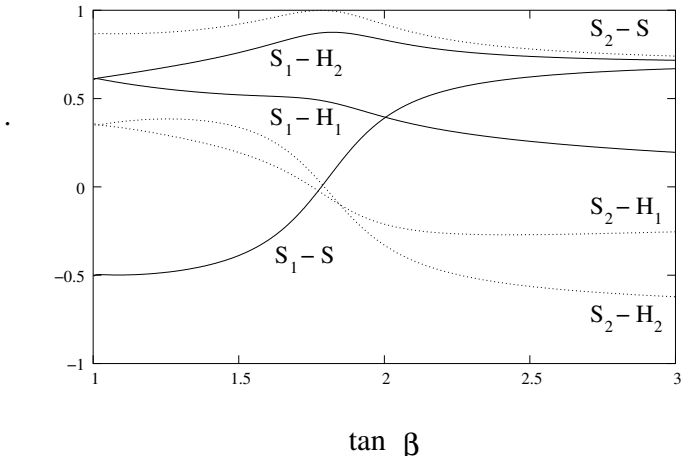

Figure 7.8: Composition of the two light CP-even Higgs bosons for typical parameter values consistent with EWBG. The solid lines correspond to the components of S_1, $\mathcal{O}^S_{1i}$, while the dotted lines are those of S_2, $\mathcal{O}^S_{2i}$, for $i = 1, 2, S$. The composition of the P_1 state is not shown because it is almost pure singlet.

to the gauge bosons and quarks, and therefore their production cross-sections. Second, these states can decay invisibly into pairs of the neutralino LSP. For Higgs masses below the gauge boson threshold this mode dominates the decay width: $BR(h \to \tilde{N}_1\tilde{N}_1) \sim 0.60 - 0.95$ for the SM-like state; $BR(h \to \tilde{N}_1\tilde{N}_1) \sim 1$ for the mostly singlet state.

Previous studies indicate that the most promising discovery mode for an invisibly decaying CP-even Higgs at the LHC is vector boson fusion (VBF) [194–196]. In [196] the authors find that, from the invisible modes alone, Higgs masses up to 150 GeV can be excluded at 95% CL with 10 fb^{-1} of integrated luminosity provided $\eta \gtrsim 0.35$, where

$$\eta = BR(h \to \text{inv}) \frac{\sigma(VBF)}{\sigma(VBF)_{SM}}. \tag{7.47}$$

Rescaling these results by the luminosity, we have

$$\mathcal{L}_{95\%} \simeq \frac{1.2 \text{ fb}^{-1}}{\eta^2}, \qquad \mathcal{L}_{5\sigma} \simeq \frac{8.0 \text{ fb}^{-1}}{\eta^2}, \tag{7.48}$$

where $\mathcal{L}_{95\%}$ and $\mathcal{L}_{5\sigma}$ are the luminosities needed for a 95% CL exclusion and a 5σ discovery respectively. For the SM-like CP-even state, we find $\eta \sim 0.5 - 0.9$ among the parameter sets consistent with EWBG. This implies that, from the invisible channels alone, less than about 5 fb^{-1} of integrated luminosity is needed to exclude this state at 95% CL, while 10–30 fb^{-1} is sufficient for a 5σ discovery. Similarly, we find $\eta = 0$–0.35 for the mostly singlet CP-even state if the mass lies below the gauge boson threshold. Thus, at least 10 fb^{-1} is needed for a 95% CL exclusion and 65 fb^{-1} for a 5σ discovery using the invisible modes. On the other hand, if this state has mass above the gauge boson threshold, the Higgs component is usually large enough that gauge boson final states completely dominate the branching

ratio. In this case, at least 8 fb^{-1} is needed for a 5σ discovery via WW and ZZ final states (where we have rescaled the results of [197]). Lastly, the light CP-odd state is nearly pure singlet and tends to decay invisibly, making it extremely difficult to observe.

7.6 Conclusions for the nMSSM

The nMSSM model elegantly solves the μ problem of the MSSM by adding a gauge singlet superfield. This model also avoids the domain wall problem of the usual NMSSM, and leads to the stability of the proton and a neutralino LSP over cosmological time scales. Like the MSSM, this model is consistent with all current experimental constraints.

We have shown that a strongly first order phase transition, necessary to preserve the baryon asymmetry produced by electroweak baryogenesis, may be naturally obtained within this model. We have also shown that the lightest neutralino provides a viable dark matter candidate and, if perturbative consistency is required up to the GUT scale, has a mass below about 60 GeV. In the region of parameters that leads to a neutralino relic density consistent with the observed one, the light CP-even and CP-odd Higgs bosons decay can decay into neutralinos providing an interesting modification to the standard Higgs physics processes.

APPENDIX A
ASPECTS OF FIELD THEORY

A.1 Notes on Notation

We list here our notational conventions for Lorentz indices, and in particular, our conventions for two- and four-component spinors. These conventions follow those of [4,28,30]. For the metric, $\eta_{\mu\nu}$, we use the mostly minus form,

$$\eta_{\mu\nu} = diag(+1, -1, -1, -1), \tag{A.1}$$

where $\mu, \nu = 0, 1, 2, 3$.

A.1.1 Two-Component Spinors

The Lorentz group is $SO(1,3)$. Its irreducible representations may be put in direct correspondence with those of $SU(2) \times SU(2)$. We can therefore label these *irreps* by a pair of half-integers, (s_1, s_2), where s_1 and s_2 label the corresponding $SU(2)$ reps. The two simplest non-trivial representations are therefore $(1/2, 0)$ and $(0, 1/2)$. These turn out to be *spinor* representations; they describe particles with half-integer spin. We denote the elements of these irreps as:

$$\begin{array}{lll} (1/2,0): & \psi_\alpha & \Rightarrow \text{“left-handed spinor”}, \\ (0,1/2): & \chi^{\dagger\,\dot\alpha} & \Rightarrow \text{“right-handed spinor”}. \end{array} \tag{A.2}$$

Here, $\alpha, \dot\alpha = 1, 2$ are the spinor indices. Also, the “dagger” on $\chi^\dagger$ is part of the name of the spinor, and does not denote any sort of conjugation. Also, since these spinors describe half-integer spin particles, they should be treated as anti-commuting *Grassmann* variables.

Under a Lorentz transformation, these spinors transform as [26]

$$\begin{aligned} \psi_\alpha &\rightarrow U_\alpha{}^\beta \psi_\beta, \\ \chi^{\dagger\,\dot\alpha} &\rightarrow \chi^{\dagger\,\dot\alpha}\,(U^{-1*})_{\dot\alpha}{}^{\dot\beta}. \end{aligned} \tag{A.3}$$

These are inequivalent representations. However, two more non-independent representations can be obtained by complex conjugation. We define

$$\begin{aligned} \chi^\alpha &:= (\chi^{\dagger\,\dot\alpha})^\dagger \rightarrow \chi^\alpha (U^{-1})_\alpha{}^\beta, \\ \psi^\dagger_{\dot\alpha} &:= (\psi_\alpha)^\dagger \rightarrow U_{\dot\alpha}{}^{\dot\beta} \psi^\dagger_{\dot\beta}. \end{aligned} \tag{A.4}$$

With these definitions, it follows that

$$\begin{aligned} \chi\psi &:= \chi^{\alpha}\,\psi_{\alpha}, \\ \psi^{\dagger}\chi^{\dagger} &:= \psi^{\dagger}_{\dot{\alpha}}\,\chi^{\dagger\,\dot{\alpha}}, \end{aligned} \tag{A.5}$$

are Lorentz invariant quantities. Now, using the fact that the two-index anti-symmetric tensors

$$\begin{aligned} \epsilon_{\alpha\beta} &= -\epsilon_{\beta\alpha} = \epsilon^{\dot{\alpha}\dot{\beta}} = -\epsilon^{\dot{\beta}\dot{\alpha}}, \\ \epsilon^{12} &= +1, \end{aligned} \tag{A.6}$$

are $SU(2)$ invariant tensors, it follows that

$$\begin{aligned} \chi_{\alpha} &:= \epsilon_{\alpha\beta}\chi^{\beta} \\ \psi^{\dagger\,\dot{\alpha}} &= \epsilon^{\dot{\alpha}\dot{\beta}}\psi^{\dagger}_{\dot{\beta}}, \end{aligned} \tag{A.7}$$

are proper $(1/2, 0)$ and $(0, 1/2)$ spinors. In exactly the same way, we can use $\epsilon^{\alpha\beta} = -\epsilon_{\alpha\beta}$ and $\epsilon_{\dot{\alpha}\dot{\beta}} = -\epsilon^{\dot{\alpha}\dot{\beta}}$ to raise and lower indices on ψ_{α} and $\chi^{\dagger}_{\dot{\alpha}}$.

Using the explicit form for the transformation matrix U (which we do not exhibit), it may be shown that the quantities

$$\begin{aligned} \chi^{\dagger}_{\dot{\alpha}}(\bar{\sigma}^{\mu})_{\dot{\alpha}\alpha}\psi_{\alpha} &:= \chi^{\dagger}\bar{\sigma}^{\mu}\psi, \\ \psi^{\alpha}(\sigma^{\mu})_{\alpha\dot{\alpha}}\chi^{\dagger\,\dot{\alpha}} &:= \psi\sigma^{\mu}\chi^{\dagger}, \end{aligned} \tag{A.8}$$

both transform as Lorentz vectors. In these expressions, the 2×2 matrices σ and $\bar{\sigma}$ are defined to be

$$\begin{aligned} \sigma^{\mu} &= (\mathbb{I}, \sigma^{i}) \\ \bar{\sigma}^{\mu} &= (\mathbb{I}, -\sigma^{i}), \end{aligned} \tag{A.9}$$

where the σ^{i} are the usual Pauli matrices. These matrices can also be related to each other by the ϵ tensors.

A.1.2 Four-Component Notation

While the two-component notation is useful because it uses only irreducible rotations representations of the Lorentz group, it becomes cumbersome when there are fermion mass terms that mix different fermions. When such terms are present, it is often more convenient to use the four-component notation.

Given the $(1/2, 0)$ and $(0, 1/2)$ spinors χ_{α} and $\xi^{\dagger\,\dot{\alpha}}$, we can form the four-component spinor Ψ according to

$$\Psi = \begin{pmatrix} \chi_{\alpha} \\ \xi^{\dagger\,\dot{\alpha}} \end{pmatrix}. \tag{A.10}$$

This corresponds to the *chiral representation*, which we shall use throughout. In terms of the *chiral projectors* $P_{L,R} = (1 \mp \gamma^5)/2$, with γ^5 given by

$$\gamma^5 = \begin{pmatrix} -\mathbb{I} & 0 \\ 0 & \mathbb{I} \end{pmatrix}, \tag{A.11}$$

we also define

$$\Psi_L := P_L \Psi = \begin{pmatrix} \chi_\alpha \\ 0 \end{pmatrix}, \qquad \Psi_R := P_R \Psi = \begin{pmatrix} 0 \\ \xi^{\dagger\,\dot{\alpha}} \end{pmatrix}. \tag{A.12}$$

The four component analogues of the σ matrices are the Dirac γ matrices,

$$\gamma^\mu = \begin{pmatrix} 0 & \sigma^\mu \\ \bar{\sigma}^\mu & 0 \end{pmatrix}. \tag{A.13}$$

Finally, we define the conjugate four-component spinor $\bar{\Psi}$ by

$$\bar{\Psi} := \Psi^\dagger \gamma^0 = (\xi^\alpha, \chi^\dagger_{\dot{\alpha}}). \tag{A.14}$$

It is now straightforward to make the correspondence between the two- and four-component notation conventions. For instance, the quantity $\bar{\Psi}\Psi$ is a Lorentz scalar, and has the expansion

$$\bar{\Psi}\Psi = \xi\chi + \chi^\dagger \xi = \bar{\Psi}_L \Psi_R + \bar{\Psi}_R \Psi. \tag{A.15}$$

Similarly, $\bar{\Psi}\gamma^\mu\Psi$ is a Lorentz vector, and has the expansion

$$\bar{\Psi}\gamma^\mu\Psi = \bar{\Psi}_L \gamma^\mu \Psi_L + \bar{\Psi}_R \gamma_\mu \Psi_R = \chi^\dagger \bar{\sigma} \xi + \xi \sigma^\mu \xi^{\dagger\,\dot{\alpha}}. \tag{A.16}$$

Notice that this term has no mixing between the different spinor representations. A more complete list of these expansions can be found in [28].

A.2 Path Integrals and the Effective Potential

Throughout this work we will make use of quantum field theory based on Feynman's path integral formalism. This formulation is the most convenient way to deal with gauge theories such as the Standard Model. To start, consider the Heisenberg picture field operator $\phi(x)$. We assume that the eigenstates of the field operators in the theory form a complete set. These eigenstates have the form

$$\phi(t, \vec{x}) \left| \hat{\phi}(t, \cdot) \right\rangle = \hat{\phi}(t, \vec{x}) \left| \hat{\phi}(t, \cdot) \right\rangle, \tag{A.17}$$

where $\hat{\phi}(x)$ is a fixed (c-number) function on spacetime. In terms of these field states, the fundamental relation for path integrals is then [6, 198]

$$\langle \phi_f t_f | \, T\{\mathcal{O}\} \, | \phi_i t_i \rangle = \mathcal{N} \int [\mathscr{D}\phi]^{\phi(t_f)=\phi_f}_{\phi(t_i)=\phi_i} \mathcal{O} \, \exp(i \int d^4x \, \mathscr{L}), \tag{A.18}$$

where $\mathcal{O}$ is a sum of products of field operators, T denotes time-ordering, and $\mathscr{L}$ is the Lagrangian for the system. Also, $\mathcal{N}$ is a normalization factor that we will specify later. The sub- and super-scripts on the measure indicate the boundary conditions for this integral.

To calculate particle scattering amplitudes, it is enough to know the expectation values of operators evaluated between the vacuum states at $t \to \pm\infty$. We define the *n-point* Green function by

$$G_n(x_1, \ldots, x_n) = \langle 0, +\infty | \, T\{\phi(x_1) \ldots \phi(x_n)\} \, |0, -\infty\rangle \tag{A.19}$$

By the LSZ procedure [7, 199], the n-point function can be converted into the scattering amplitude for a process with n incoming or outgoing ϕ particles.

The Green functions may be written in terms of a path integral using a trick. If the $t \to \pm\infty$ limit of the expectation value of the operator $\mathcal{O}$ is taken between any two field eigenstates in a slightly imaginary direction, $t \to \infty(1 + i\epsilon)$, only the projection of these eigenstates onto the vacuum survives [4]. As a result, we need not specify the boundary conditions in calculating these vacuum expectation values. Choosing the normalization factor such that the unit operator has expectation value equal to one, we find

$$\begin{aligned} \langle 0, t \to +\infty | \, T\{\mathcal{O}\} \, |0, t \to -\infty\rangle \;\; = \\ \int [\mathscr{D}\phi] \, \mathcal{O} \, \exp(i \int d^4x \, \mathscr{L}) \Big/ \int [\mathscr{D}\phi] \, \exp(i \int d^4x \, \mathscr{L}), \end{aligned} \tag{A.20}$$

where no boundary conditions are specified, but the imaginary time rotation is implied. In general, these Green functions can only be evaluated exactly when the Lagrangian is at most quadratic in all the fields. On the other hand, these Green functions may be evaluated approximately in perturbation theory using the standard Feynman diagram techniques.

A convenient way to obtain the n-point Green functions is to add a position dependent source to the action. Define the *generating functional* $Z[J]$ by [59, 200]

$$Z[J] = \int [\mathscr{D}\phi] \, \exp\left[i \int d^4x \, (\mathscr{L} + J(x)\phi(x)) \right] \Big/ \int [\mathscr{D}\phi] \, \exp(i \int d^4x \, \mathscr{L}). \tag{A.21}$$

Here, the $t \to \pm\infty$ in a slightly imaginary direction limit is implied. The name for $Z[J]$ is apt because of the fact

$$\left. \frac{\delta^n Z[J]}{\delta J(x_1) \ldots \delta J(x_n)} \right|_{J=0} = i^n \, G_n(x_1, \ldots, x_n). \tag{A.22}$$

This relation follows directly by functionally differentiating Eq. (A.21). Making a functional Taylor expansion of $Z[J]$ and using the relation above, we find

$$Z[J] = \sum_{n=0}^{\infty} \frac{i^n}{n!} \int d_1^x \ldots d_n^x G_n(x_1, \ldots, x_n) \, J(x_1) \ldots J(x_n). \tag{A.23}$$

It is also convenient to define the functional $W[J]$ by

$$W[J] = -i \ln(Z[J]). \tag{A.24}$$

It may be shown that $W[J]$ is the generating functional for *connected* Green functions $G_n^c(x_1, \ldots, x_n)$, the subset of the usual Green functions which only contain connected diagrams [200]. In other words,

$$iW[J] = \sum_{n=0}^{\infty} \frac{i^n}{n!} \int d^4x_1 \ldots d^4x_n G_n^c(x_1, \ldots, x_n)\, J(x_1) \ldots J(x_n). \tag{A.25}$$

Another interesting quantity is the *effective action*, $\Gamma[\phi_c]$. First, let us define the classical background field by

$$\begin{aligned} \phi_c(x) &= \frac{\delta W[J]}{\delta J(x)} \\ &= \langle 0, +\infty |\, \phi(x)\, | 0, -\infty \rangle_J \,, \end{aligned} \tag{A.26}$$

where the subscript indicates that the expectation value has been taken in the presence of the source J. The effective action is then defined to be the Legendre transformation of $W[J]$,

$$\Gamma[\phi_c] = W[J] - \int d^4y \frac{\delta W[J]}{\delta J(y)} J(y), \tag{A.27}$$

where J is to be regarded as a functional of ϕ_c, defined implicitly through Eq. (A.26). Differentiating $\Gamma[\phi_c]$ with respect to its argument, we obtain

$$\frac{\delta \Gamma}{\delta \phi_c(x)} = -J(x). \tag{A.28}$$

Taking the source to zero,

$$\left. \frac{\delta \Gamma}{\delta \phi_c(x)} \right|_{J=0} = 0, \tag{A.29}$$

which gives an equation for the vacuum expectation value of the field $\phi(x)$ in the vacuum.

Besides providing an equation for the vacuum expectation value of the field ϕ, it may be shown that the effective action is also the generating functional for one-particle irreducible (1-PI) Green functions,

$$\Gamma[\phi_c] = \sum_{n=0}^{\infty} \frac{1}{n!} \int d^4x_1 \ldots d^4x_n\, \Gamma_n(x_1, \ldots, x_n)\, \phi_c(x_1) \ldots \phi_c(x_n). \tag{A.30}$$

The 1-PI Γ_n's are Green functions made up of Feynman diagrams that remain connected even after cutting a single internal propagator leg. They correspond to the effective vertices in the theory after quantum corrections have been included [200].

In a theory that is translationally invariant, the vacuum expectation value for ϕ, ϕ_c, must be constant in the $J(x) \to 0$ limit. For $\phi_c = constant$, independent of x, the effective action can be put in a particularly simple form [59]:

$$\begin{aligned} \Gamma[\phi_c] &= \sum_{n=0}^{\infty} \frac{1}{n!}\, \phi_c^n\, \tilde{\Gamma}_n(p_i = 0) \left(\int d^4x \right) \\ &:= -\left(\int d^4x \right)\, V_{\rm eff}(\phi_c), \end{aligned} \tag{A.31}$$

where $\tilde{\Gamma}_n(p_i)$ is the Fourier-transform of $\Gamma_n(x_i)$. In the second line, we have defined the *effective potential*. With ϕ_c a constant, the equation for the vacuum value of ϕ becomes

$$\frac{\partial V_{\rm eff}}{\partial \phi_c} = 0. \tag{A.32}$$

Thus, the effective potential of great interest.

APPENDIX B
NOTES FOR THE NMSSM

B.1 Field-Dependent Masses

In this section we collect the field and temperature dependent mass matrices for those particles relevant to the analysis in Section 7.3. The leading thermal mass corrections were calculated following [108] for vanishing background field values; $\varphi_1 = \varphi_2 = \varphi_s = 0$. Ignoring the singlet background is reasonable here since, in the parameter space of interest, the singlet VEV is closely related to the other Higgs VEV's. To leading order, only bosons receive thermal mass corrections. These come from quadratically divergent (at T=0) loops containing particles which are light compared to the temperature, $m \lesssim 2\pi T$ for bosons and $m \lesssim \pi T$ for fermions. For the purpose of calculating thermal masses we have taken the Higgs bosons, Higgsinos, electroweak gauginos, and the SM particles to be light, while treating the rest of the particles in the spectrum as heavy. We do not expect that a different choice of spectrum would change our phase transition results since the first order nature of the transition is determined by the tree-level potential rather than the cubic one-loop term in j_B.

Gauge Bosons

At leading order, only the longitudinal components of the gauge bosons receive thermal corrections. The masses are

$$\begin{aligned} m_W^2 &= \frac{1}{2}g_2^2({\varphi_1}^2 + {\varphi_2}^2) + \Pi_{W^\pm} \\ \mathcal{M}_{Z\gamma}^2 &= \begin{pmatrix} \frac{1}{2}g_2^2({\varphi_1}^2 + {\varphi_2}^2) + \Pi_{W^3} & -\frac{1}{2}g_1 g_2({\varphi_1}^2 + {\varphi_2}^2) \\ -\frac{1}{2}g_1 g_2({\varphi_1}^2 + {\varphi_2}^2) & \frac{1}{2}{g_1}^2({\varphi_1}^2 + {\varphi_2}^2) + \Pi_B \end{pmatrix}, \end{aligned} \tag{B.1}$$

where $\Pi_i = 0$ for the transverse modes, and

$$\begin{aligned} \Pi_{W^\pm} &= \frac{5}{2}g_2^2 T^2 \\ \Pi_{W^3} &= \frac{5}{2}g_2^2 T^2 \\ \Pi_B &= \frac{13}{6}g_1^2 T^2 \end{aligned} \tag{B.2}$$

for the longitudinal modes.

Tops and Stops

$$
\begin{aligned}
m_t^2 &= y_t^2 {\varphi_2}^2 \\
\mathcal{M}_{\tilde{t}}^2 &= \begin{pmatrix} m_Q^2 + m_t^2 + D_L + \Pi_{\tilde{t}_L} & a_t\varphi_2 + \lambda\varphi_s\varphi_1 \\ a_t\varphi_2 + \lambda\varphi_s\varphi_1 & m_U^2 + m_t^2 + D_R + \Pi_{\tilde{t}_R} \end{pmatrix},
\end{aligned} \tag{B.3}
$$

where

$$
\begin{aligned}
D_L &= \frac{1}{4}(g_2^2 - \frac{1}{3}{g_1}^2)({\varphi_1}^2 - {\varphi_2}^2) \\
D_R &= \frac{1}{3}{g_1}^2({\varphi_1}^2 - {\varphi_2}^2) \\
\Pi_{\tilde{t}_L} &= \frac{1}{3}g_3^2T^2 + \frac{5}{16}g_2^2T^2 + \frac{5}{432}g_1^2T^2 + \frac{1}{6}y_t^2T^2 \\
\Pi_{\tilde{t}_R} &= \frac{1}{3}g_3^2T^2 + + \frac{5}{27}g_1^2T^2 + \frac{1}{3}y_t^2T^2.
\end{aligned} \tag{B.4}
$$

Higgs Bosons

The CP-even mass matrix elements are

$$
\begin{aligned}
\mathcal{M}_{S_{11}}^2 &= m_1^2 + \lambda^2({\varphi_2}^2 + {\varphi_s}^2) + \frac{\bar{g}^2}{4}(3{\varphi_1}^2 - {\varphi_2}^2) + \Pi_{H_1} \\
\mathcal{M}_{S_{12}}^2 &= m_{12}^2 + 2\varphi_1\varphi_2(\lambda^2 - \frac{\bar{g}^2}{4}) + a_\lambda\varphi_s \\
\mathcal{M}_{S_{13}}^2 &= a_\lambda\varphi_2 + 2\lambda^2\varphi_1\varphi_s \\
\mathcal{M}_{S_{22}}^2 &= m_2^2 + \lambda^2({\varphi_1}^2 + {\varphi_s}^2) + \frac{\bar{g}^2}{4}(3{\varphi_2}^2 - {\varphi_1}^2) + \Pi_{H_2} \\
\mathcal{M}_{S_{23}}^2 &= a_\lambda\varphi_1 + 2\lambda^2\varphi_2\varphi_s \\
\mathcal{M}_{S_{33}}^2 &= m_s^2 + \lambda^2({\varphi_1}^2 + {\varphi_2}^2) + \Pi_S
\end{aligned} \tag{B.5}
$$

where the leading thermal corrections are

$$
\begin{aligned}
\Pi_{H_1} &= \frac{1}{8}g_1^2T^2 + \frac{3}{8}g_2^2T^2 + \frac{1}{12}\lambda^2T^2 \\
\Pi_{H_2} &= \frac{1}{8}g_1^2T^2 + \frac{3}{8}g_2^2T^2 + \frac{1}{12}\lambda^2T^2 + \frac{1}{4}y_t^2 \\
\Pi_S &= \frac{1}{6}\lambda^2T^2.
\end{aligned} \tag{B.6}
$$

For the CP-odd states we have

$$\begin{aligned}
\mathcal{M}^2_{P_{11}} &= m_1^2 + \lambda^2({\varphi_2}^2 + {\varphi_s}^2) - \frac{\bar{g}^2}{4}({\varphi_2}^2 - {\varphi_1}^2) + \Pi_{H_1} \\
\mathcal{M}^2_{P_{12}} &= -m_{12}^2 - a_\lambda \varphi_s \\
\mathcal{M}^2_{P_{13}} &= -a_\lambda \varphi_2 \\
\mathcal{M}^2_{P_{22}} &= m_2^2 + \lambda^2({\varphi_1}^2 + {\varphi_s}^2) + \frac{\bar{g}^2}{4}({\varphi_2}^2 - {\varphi_1}^2) + \Pi_{H_2} \\
\mathcal{M}^2_{P_{23}} &= -a_\lambda \varphi_1 \\
\mathcal{M}^2_{P_{33}} &= m_s^2 + \lambda^2({\varphi_1}^2 + {\varphi_2}^2) + \Pi_S
\end{aligned} \tag{B.7}$$

where the thermal corrections are as above.
The charged Higgs mass matrix is

$$\begin{aligned}
\mathcal{M}^2_{H^\pm_{11}} &= m_1^2 + \lambda^2 {\varphi_s}^2 - \frac{\bar{g}^2}{4}({\varphi_2}^2 - {\varphi_1}^2) + \frac{g_2^2}{2}{\varphi_2}^2 + \Pi_{H_1} \\
\mathcal{M}^2_{H^\pm_{12}} &= -(\lambda^2 - \frac{g_2^2}{2})\varphi_1\varphi_2 - m_{12}^2 - a_\lambda \varphi_s \\
\mathcal{M}^2_{H^\pm_{22}} &= m_2^2 + \lambda^2 {\varphi_s}^2 + \frac{\bar{g}^2}{4}({\varphi_2}^2 - {\varphi_1}^2) + \frac{g_2^2}{2}{\varphi_1}^2 + \Pi_{H_2}.
\end{aligned} \tag{B.8}$$

Charginos and Neutralinos

The chargino mass matrix reads

$$M_{\chi^\pm} = \begin{pmatrix} 0 & X^t \\ X & 0 \end{pmatrix} \tag{B.9}$$

where

$$X = \begin{pmatrix} M_2 & g_2\varphi_2 \\ g_2\varphi_1 & -\lambda\varphi_s \end{pmatrix}.$$

For the neutralinos we have

$$M_{\tilde{N}} = \begin{pmatrix} M_1 & \cdot & \cdot & \cdot & \cdot \\ 0 & M_2 & \cdot & \cdot & \cdot \\ -\frac{g_1}{\sqrt{2}}\varphi_1 & \frac{g_2}{\sqrt{2}}\varphi_1 & 0 & \cdot & \cdot \\ \frac{g_1}{\sqrt{2}}\varphi_2 & -\frac{g_2}{\sqrt{2}}\varphi_2 & \lambda\varphi_s & 0 & \cdot \\ 0 & 0 & \lambda\varphi_2 & \lambda\varphi_1 & 0 \end{pmatrix}. \tag{B.10}$$

We have taken $M_1 = M_2/2$ and have allowed M_2 to be complex in our analysis.

B.2 Higgs and Neutralino Couplings

We list here the Higgs and Neutralino couplings relevant to our analysis. All fermions are written in terms of four-component spinors to facilitate the derivation of the Feynman

rules. As above, Eq. (7.17), we define the unitary matrix N_{ij} by

$$\tilde{N}_i = N_{ij}\,\psi_i^0$$

where $(\psi_i^0) = (\tilde{B^0}, \tilde{W^0}, \tilde{H_1^0}, \tilde{H_2^0}, \tilde{S})$. Similarly, as in Eq. (7.27) we define the orthogonal matrices $\mathcal{O}^S$ and $\mathcal{O}^P$ by

$$\begin{pmatrix} S_1 \\ S_2 \\ S_3 \end{pmatrix} = \mathcal{O}^S \begin{pmatrix} \phi_1 \\ \phi_2 \\ \phi_s \end{pmatrix}; \qquad \begin{pmatrix} P_1 \\ P_2 \end{pmatrix} = \mathcal{O}^P \begin{pmatrix} A^0 \\ a_s \end{pmatrix}.$$

B.2.1 Neutralino Couplings

ZNN: [28]

$$\mathscr{L}_{ZNN} = \frac{g}{2\cos\theta_W} Z_\mu \overline{\tilde{N}}_i\,\gamma^\mu(\mathcal{O}^N_{ij} P_L - \mathcal{O}^{N^*}_{ij} P_R)\tilde{N}_j \tag{B.11}$$

where

$$\mathcal{O}^N_{ij} = \frac{1}{2}\left(N_{i4}N^*_{j4} - N_{i3}N^*_{j3}\right).$$

For the Higgs-Neutralino couplings we consider only the contribution from the $\lambda S H_1 \cdot H_2$ term in the superpotential.
SNN:

$$\mathscr{L}_{SNN} = -\frac{\lambda}{\sqrt{2}} S_k \overline{\tilde{N}}_i \left(\bar{A}^k_{ij} P_L + A^k_{ij} P_R\right)\tilde{N}_j, \tag{B.12}$$

where

$$\begin{aligned} A^k_{ij} &= \mathcal{O}^S_{k1}\,Q^{45}_{ij} + \mathcal{O}^S_{k2}\,Q^{35}_{ij} + \mathcal{O}^S_{k3}\,Q^{34}_{ij}, \\ Q^{ab}_{ij} &= \frac{1}{2}\left(N^*_{ia}N^*_{jb} + N^*_{ib}N^*_{ja}\right). \end{aligned}$$

$\bar{A}^k_{ij}$ is related to A^k_{ij} by the replacement $N^*_{ij} \to N_{ij}$.
PNN:

$$\mathscr{L}_{PNN} = -i\frac{\lambda}{\sqrt{2}} S_k \overline{\tilde{N}}_i \left(\bar{B}^k_{ij} P_L - B^k_{ij} P_R\right)\tilde{N}_j, \tag{B.13}$$

where

$$B^k_{ij} = s_\beta\,\mathcal{O}^P_{k1}\,Q^{45}_{ij} + c_\beta\,\mathcal{O}^P_{k1}\,Q^{35}_{ij} + \mathcal{O}^P_{k2}\,Q^{34}_{ij},$$

As with A^k_{ij}, $\bar{B}^k_{ij}$ is related to B^k_{ij} by the replacement $N^*_{ij} \to N_{ij}$.
Finally we note that in converting these couplings into Feynman rules, one must insert an additional factor of two since the neutralinos are written as Majorana spinors [28].

B.2.2 Higgs Couplings

The relevant couplings of the Higgs scalars to the gauge bosons are given in Section 7.2.2 above. We list here the couplings of the Higgs to the third generation quarks.
$S\bar{f}f$:

$$\mathscr{L}_{S\bar{f}f} = -\frac{1}{\sqrt{2}}\, y_b\, \mathcal{O}^S_{k1}\, S_k\, \bar{b}b - \frac{1}{\sqrt{2}}\, y_t\, \mathcal{O}^S_{k2}\, S_k\, \bar{t}t. \tag{B.14}$$

$P\bar{f}f$:

$$\mathscr{L}_{P\bar{f}f} = \frac{i}{\sqrt{2}}\, y_b\, s_\beta\, \mathcal{O}^P_{k1}\, P_k\, \bar{b}\gamma^5 b + \frac{i}{\sqrt{2}}\, y_t\, c_\beta\, \mathcal{O}^S_{k1}\, P_k\, \bar{t}\gamma^5 t.$$

The couplings of the Higgs states to the other matter fermions follow the same pattern.

B.2.3 LSP Lifetime

Having listed the Higgs-Neutralino couplings, we may now present an estimate for the lifetime of the LSP in the $\mathbb{Z}_5^R$ symmetric scenario. This symmetry allows the $d = 5$ operator $\hat{S}\hat{S}\hat{H}_2\hat{L}$ in the superpotential, which can lead to the decay of the neutralino LSP. This operator generates a coupling which allows the neutralino to decay into a neutrino and a pair of off-shell neutral Higgs scalars, or an electron, a neutral Higgs scalar, and a charged Higgs scalar. We shall focus on the first mode with intermediate neutral CP-even states and a mostly singlino LSP. This gives a more stringent constraint than the charged mode, and the analysis with intermediate neutral CP-odd states is analogous. We will also assume that each of the neutral Higgs bosons subsequently decays into $\bar{b}b$. With these assumptions, we find

$$\Gamma(\tilde{N}_1 \to \nu\, \bar{b}b\, \bar{b}b) \sim \frac{\pi}{2(4\pi^2)^4} \frac{y_b^4 \left| N^*_{15} \mathcal{O}^S_{i3} \mathcal{O}^S_{j2} \mathcal{O}^S_{1i} \mathcal{O}^S_{1j} \right|^2}{\Lambda^2\, m_H^8} \left(\frac{m_{\tilde{N}}}{5}\right)^{11} \tag{B.15}$$

where Λ is the cutoff scale, m_H is the Higgs mass in the intermediate propagators, and we have set all final state momenta to $m_{\tilde{N}}/5$. Setting the mixing factor to unity, taking $m_{\tilde{N}}/m_H \sim 1$ and $\tan\beta = 2$, and demanding that $\Gamma < H_0$, we find

$$\Lambda^2 \gtrsim \left(\frac{m_{\tilde{N}}}{\text{GeV}}\right)^3 10^{23}\ \text{GeV}^2 \tag{B.16}$$

which translates into $\Lambda \gtrsim 3 \times 10^{14}$ GeV for $m_{\tilde{N}} = 100$ GeV.

B.3 Sample Mass Spectra

We list here the mass spectra for the sample parameter sets A, B, and C listed in Table 7.3.

Set	S_1 (GeV)	S_2 (GeV)	S_3 (GeV)	P_1 (GeV)	P_2 (GeV)	$H^{\pm}$ (GeV)
A	115	158	925	135	927	922
B	116	182	914	164	917	911
C	121	219	504	115	534	498

Table B.1: Higgs scalar masses.

Set	$\tilde{N}_1$ (GeV)	$\tilde{N}_2$ (GeV)	$\tilde{N}_3$ (GeV)	$\tilde{N}_4$ (GeV)	$\tilde{N}_5$ (GeV)	$\chi_1^{\pm}$ (GeV)	$\chi_2^{\pm}$ (GeV)
A	33.3	107	181	278	324	165	320
B	52.4	168	203	221	432	151	432
C	77.1	228	268	331	474	257	474

Table B.2: Neutralino and chargino masses.

Set	$\lvert N_{11}\rvert$	$\lvert N_{12}\rvert$	$\lvert N_{13}\rvert$	$\lvert N_{14}\rvert$	$\lvert N_{15}\rvert$	$\mathcal{O}^S_{11}$	$\mathcal{O}^S_{12}$	$\mathcal{O}^S_{13}$	$\mathcal{O}^P_{11}$	$\mathcal{O}^P_{12}$
A	0.13	0.10	0.11	0.37	0.91	0.46	0.74	-0.50	0.08	0.99
B	0.07	0.07	0.16	0.52	0.84	0.42	0.80	-0.44	0.07	0.99
C	0.01	0.01	0.28	0.33	0.90	0.70	0.53	0.48	0.26	0.97

Table B.3: Composition of the lightest neutralino, $\tilde{N}_1$, the lightest CP-even Higgs boson, S_1, and the lightest CP-odd Higgs boson, P_1.

REFERENCES

[1] C. Balazs, M. Carena, A. Menon, D. E. Morrissey and C. E. M. Wagner, Phys. Rev. D **71**, 075002 (2005) [arXiv:hep-ph/0412264].

[2] A. Menon, D. E. Morrissey and C. E. M. Wagner, Phys. Rev. D **70**, 035005 (2004) [arXiv:hep-ph/0404184].

[3] C. N. Yang and R. L. Mills, Phys. Rev. **96**, 191 (1954).

[4] M. E. Peskin and D. V. Schroeder, *An Introduction to Quantum Field Theory*, Addison-Wesley, Reading, USA (1995).

[5] B. Hatfield, *Quantum field theory of point particles and strings*, Addison-Wesley, Redwood City, USA (1992).

[6] L. H. Ryder, *Quantum Field Theory*, Cambridge University Press, Cambridge, UK (1985).

[7] W. Greiner and J. Reinhardt, *Field quantization*, Springer, Berlin, Germany (1996)

[8] S. Pokorski, *Gauge Field Theories*, Cambridge University Press, Cambridge, UK (1987).

[9] E. S. Abers and B. W. Lee, Phys. Rept. **9**, 1 (1973).

[10] For reviews, see: H. Georgi, "Lie Algebras In Particle Physics. From Isospin To Unified Theories," Front. Phys. **54**, 1 (1982); R. Slansky, Phys. Rept. **79**, 1 (1981).

[11] L. D. Faddeev and V. N. Popov, Phys. Lett. B **25**, 29 (1967).

[12] A. A. Belavin, A. M. Polyakov, A. S. Shvarts and Y. S. Tyupkin, Phys. Lett. B **59**, 85 (1975).

[13] R. Jackiw and C. Rebbi, Phys. Rev. Lett. **37**, 172 (1976), C. G. . Callan, R. F. Dashen and D. J. Gross, Phys. Lett. B **63**, 334 (1976).

[14] S. R. Coleman, *Aspects of Symmetry: Selected Erice Lectures*, Cambridge University Press, Cambridge, UK (1985).

[15] R. Jackiw, Rev. Mod. Phys. **52**, 661 (1980).

[16] G. 't Hooft, Phys. Rev. D **14**, 3432 (1976) [Erratum-ibid. D **18**, 2199 (1978)].

[17] J. D. Jackson, *Classical Electrodynamics*, John Wiley, New York, USA (1962).

[18] J. L. Rosner, Am. J. Phys. **71**, 302 (2003) [arXiv:hep-ph/0206176].

[19] F. Englert and R. Brout, Phys. Rev. Lett. **13**, 321 (1964); P. W. Higgs, Phys. Rev. Lett. **13**, 508 (1964), G. S. Guralnik, C. R. Hagen and T. W. B. Kibble, Phys. Rev. Lett. **13**, 585 (1964), P. W. Higgs, Phys. Rev. **145**, 1156 (1966).

[20] N. Cabibbo, Phys. Rev. Lett. **10**, 531 (1963).

[21] M. Kobayashi and T. Maskawa, Prog. Theor. Phys. **49**, 652 (1973).

[22] M. Dine, in *Flavor physics for the Millennium: TASI 2000*, ed. J. L. Rosner, World Scientific, New Jersey, USA (2001) [arXiv:hep-ph/0011376].

[23] S. R. Coleman and J. Mandula, Phys. Rev. **159**, 1251 (1967).

[24] R. Haag, J. T. Lopuszanski and M. Sohnius, Nucl. Phys. B **88**, 257 (1975).

[25] S. Weinberg, *The Quantum Theory of Fields Vol. 3: Supersymmetry*, Cambridge University Press, Cambridge, UK (2000).

[26] J. Wess and J. Bagger, *Supersymmetry and Supergravity*, Princeton University Press, Princeton, USA (1992).

[27] S. P. Martin, in *Perspectives on Supersymmetry*, ed. G. Kane, World Scientific, Singapore (1998) [arXiv:hep-ph/9709356].

[28] H. E. Haber and G. L. Kane, Phys. Rept. **117**, 75 (1985).

[29] H. P. Nilles, Phys. Rept. **110**, 1 (1984).

[30] J. D. Lykken, in *Fields, Strings, and Duality: TASI 1996*, eds. C. Efthimiou and B. Greene, World Scientific, Singapore (1997) [arXiv:hep-th/9612114].

[31] L. Girardello and M. T. Grisaru, Nucl. Phys. B **194**, 65 (1982).

[32] D. J. H. Chung, L. L. Everett, G. L. Kane, S. F. King, J. Lykken and L. T. Wang, Phys. Rept. **407**, 1 (2005) [arXiv:hep-ph/0312378].

[33] P. Van Nieuwenhuizen, Phys. Rept. **68**, 189 (1981).

[34] L. Randall and R. Sundrum, Nucl. Phys. B **557**, 79 (1999) [arXiv:hep-th/9810155].

[35] G. F. Giudice, M. A. Luty, H. Murayama and R. Rattazzi, JHEP **9812**, 027 (1998) [arXiv:hep-ph/9810442].

[36] M. Dine and W. Fischler, Phys. Lett. B **110**, 227 (1982).

[37] G. F. Giudice and R. Rattazzi, Phys. Rept. **322**, 419 (1999) [arXiv:hep-ph/9801271].

[38] G. R. Farrar and P. Fayet, Phys. Lett. B **76**, 575 (1978).

[39] M. Carena and H. E. Haber, Prog. Part. Nucl. Phys. **50**, 63 (2003) [arXiv:hep-ph/0208209].

[40] S. Dimopoulos, S. Raby and F. Wilczek, Phys. Rev. D **24**, 1681 (1981); P. Langacker and M. x. Luo, Phys. Rev. D **44**, 817 (1991); P. Langacker and N. Polonsky, Phys. Rev. D **47**, 4028 (1993) [arXiv:hep-ph/9210235]; M. Carena, S. Pokorski and C. E. M. Wagner, Nucl. Phys. B **406**, 59 (1993) [arXiv:hep-ph/9303202].

[41] R. Barate *et al.* [ALEPH Collaboration], Phys. Lett. B **565**, 61 (2003) [arXiv:hep-ex/0306033].

[42] S. Heinemeyer, W. Hollik, and G. Weiglein, Phys. Rev. D **58**, 091701 (1998) [arXiv:hep-ph/9803277]; S. Heinemeyer, W. Hollik, and G. Weiglein, Phys. Lett. B **440**, 296 (1998) [arXiv:hep-ph/9807423]; S. Heinemeyer, W. Hollik, and G. Weiglein, Eur. Phys. J. C **9**, 343 (1999) [arXiv:hep-ph/9812472]; M. Carena, M. Quiros, and C. E. M. Wagner, Nucl. Phys. B **461**, 407 (1996) [arXiv:hep-ph/9508343]; H. E. Haber, R. Hempfling, and A. H. Hoang, Z. Phys. C **75**, 539 (1997) [arXiv:hep-ph/9609331]; J. R. Espinosa and R. J. Zhang, J. High Energy Phys. **0003**, 026 (2000) [arXiv:hep-ph/9912236]; J. R. Espinosa and R. J. Zhang, Nucl. Phys. B **586**, 3 (2000) [arXiv:hep-ph/0003246]; M. Carena, H. E. Haber, S. Heinemeyer, W. Hollik, C. E. M. Wagner, and G. Weiglein, Nucl. Phys. B **580**, 29 (2000) [arXiv:hep-ph/0001002]; G. Degrassi, P. Slavich, and F. Zwirner, Nucl. Phys. B **611**, 403 (2001) [arXiv:hep-ph/0105096]; A. Brignole, G. Degrassi, P. Slavich, and F. Zwirner, arXiv:hep-ph/0112177; S. P. Martin, Phys. Rev. D **67**, 095012 (2003) [arXiv:hep-ph/0211366].

[43] E. W. Kolb and M. S. Turner, *The Early Universe*, Addison-Wesley, Redwood City, USA (1990).

[44] C. M. Will, to be published in *100 Years of Relativity: Spacetime Structure - Einstein and Beyond*, ed. A. Ashtekar, World Scientific, Singapore, [arXiv:gr-qc/0504086].

[45] D. N. Spergel *et al.* [WMAP Collaboration], Astrophys. J. Suppl. **148**, 175 (2003) [arXiv:astro-ph/0302209].

[46] J. L. Tonry *et al.* [Supernova Search Team Collaboration], Astrophys. J. **594**, 1 (2003) [arXiv:astro-ph/0305008]; A. G. Riess *et al.* [Supernova Search Team Collaboration], Astrophys. J. **607**, 665 (2004) [arXiv:astro-ph/0402512].

[47] A. A. Penzias and R. W. Wilson, Astrophys. J. **142**, 419 (1965).

[48] A. H. Guth, Phys. Rev. D **23**, 347 (1981).

[49] A. Albrecht, P. J. Steinhardt, M. S. Turner and F. Wilczek, Phys. Rev. Lett. **48**, 1437 (1982), L. F. Abbott, E. Farhi and M. B. Wise, Phys. Lett. B **117**, 29 (1982).

[50] R. A. Alpher, H. Bethe, and G. Gamow Phys. Rev. **73** 803 (1948).

[51] D. A. Kirzhnits and A. D. Linde, Phys. Lett. B **42** (1972) 471.

[52] For a review, see: S. Burles, K. M. Nollett and M. S. Turner, Astrophys. J. **552**, L1 (2001) [arXiv:astro-ph/0010171];

[53] K. A. Olive, G. Steigman and T. P. Walker, Phys. Rept. **333**, 389 (2000) [arXiv:astro-ph/9905320].

[54] J. A. Peacock, *Cosmological physics*, Cambridge University Press, Cambridge UK (1999).

[55] M. Trodden and S. M. Carroll, in *Particle Physics and Cosmology: TASI 2002*, eds. H. E. Haber and A. E. Nelson, World Scientific, Singapore (2004) [arXiv:astro-ph/0401547].

[56] J. Garcia-Bellido, Lectures given at European School of High-Energy Physics, Sant Feliu de Guixols, Barcelona, Spain, 30 May - 12 June, [arXiv:astro-ph/0502139].

[57] R. M. Wald, *General Relativity*, University of Chicago Press, Chicago (1984).

[58] J. I. Kapusta, *Finite Temperature Field Theory*, Cambridge University Press, Cambridge, UK (1993).

[59] M. Quiros, in *High Energy Physics and Cosmology: Proceedings of the 1998 ICTP Summer School*, eds. A. Masiero, G.Senjanovic, A. Smirnov, World Scientific, Singapore (1999) [arXiv:hep-ph/9901312].

[60] A. L. Maroto and J. Ramirez, arXiv:astro-ph/0409280.

[61] K. A. Olive, in *Particle Physics and Cosmology: TASI 2002*, eds. H. E. Haber and A. E. Nelson, World Scientific, Singapore (2004) [arXiv:astro-ph/0301505].

[62] G. Bertone, D. Hooper and J. Silk, Phys. Rept. **405**, 279 (2005) [arXiv:hep-ph/0404175].

[63] M. Persic, P. Salucci and F. Stel, Mon. Not. Roy. Astron. Soc. **281**, 27 (1996) [arXiv:astro-ph/9506004].

[64] Y. Mellier, Ann. Rev. Astron. Astrophys. **37**, 127 (1999) [arXiv:astro-ph/9812172].

[65] K. Griest and D. Seckel, Phys. Rev. D **43**, 3191 (1991).

[66] P. Gondolo and G. Gelmini, Nucl. Phys. B **360**, 145 (1991).

[67] J. Edsjo and P. Gondolo, Phys. Rev. D **56**, 1879 (1997) [arXiv:hep-ph/9704361].

[68] For reviews, see:
A. G. Cohen, D. B. Kaplan and A. E. Nelson, Ann. Rev. Nucl. Part. Sci. **43**, 27 (1993) [arXiv:hep-ph/9302210].; A. Riotto, *High Energy Physics and Cosmology: Proceedings of the 1998 ICTP Summer School*, eds. A. Masiero, G.Senjanovic, A. Smirnov, World Scientific, Singapore (1999) [arXiv:hep-ph/9807454]; M. Trodden, Rev. Mod. Phys. **71**, 1463 (1999) [arXiv:hep-ph/9803479]; W. Bernreuther, Lect. Notes Phys. **591**, 237 (2002) [arXiv:hep-ph/0205279].

[69] A. D. Sakharov, Pisma Zh. Eksp. Teor. Fiz. **5**, 32 (1967) [JETP Lett. **5**, 24 (1967 SOPUA,34,392-393.1991 UFNAA,161,61-64.1991)].

[70] H. Georgi and S. L. Glashow, Phys. Rev. Lett. **32**, 438 (1974).

[71] For a review, see: P. Langacker, Phys. Rept. **72**, 185 (1981).

[72] D. V. Nanopoulos and S. Weinberg, Phys. Rev. D **20**, 2484 (1979); E. W. Kolb and M. S. Turner, Ann. Rev. Nucl. Part. Sci. **33**, 645 (1983).

[73] M. Fukugita and T. Yanagida, Phys. Lett. B **174**, 45 (1986).

[74] M. A. Luty, Phys. Rev. D **45** (1992) 455.

[75] W. Buchmuller, Proceedings of the 2001 European School of High Energy Physics: Beatenberg 2001, eds. N. Ellis and J. March-Russell, CERN, Switzerland (2002) [arXiv:hep-ph/0204288].

[76] J. S. Bell and R. Jackiw, Nuovo Cim. A **60**, 47 (1969); S. L. Adler and W. A. Bardeen, Phys. Rev. **182**, 1517 (1969); W. A. Bardeen, Phys. Rev. **184**, 1848 (1969).

[77] K. Fujikawa, Phys. Rev. D **21**, 2848 (1980) [Erratum-ibid. D **22**, 1499 (1980)].

[78] F. R. Klinkhamer and N. S. Manton, Phys. Rev. D **30**, 2212 (1984).

[79] P. Arnold and L. D. McLerran, Phys. Rev. D **36**, 581 (1987).

[80] M. Dine, P. Huet and R. J. Singleton, Nucl. Phys. B **375**, 625 (1992).

[81] P. Arnold, D. Son and L. G. Yaffe, Phys. Rev. D **55**, 6264 (1997) [arXiv:hep-ph/9609481].

[82] G. D. Moore and K. Rummukainen, Phys. Rev. D **61**, 105008 (2000) [arXiv:hep-ph/9906259].

[83] A. I. Bochkarev and M. E. Shaposhnikov, Mod. Phys. Lett. A **2**, 417 (1987).

[84] G. W. Anderson and L. J. Hall, Phys. Rev. D **45**, 2685 (1992).

[85] P. Arnold and O. Espinosa, Phys. Rev. D **47**, 3546 (1993) [Erratum-ibid. D **50**, 6662 (1994)] [arXiv:hep-ph/9212235].

[86] M. E. Carrington, Phys. Rev. D **45**, 2933 (1992).

[87] M. Carena, M. Quirós and C.E.M. Wagner, *Phys. Lett.* **B380** (1996) 81.

[88] M. Laine, *Nucl. Phys.* **B481** (1996) 43; M. Losada, *Phys. Rev.* **D56** (1997) 2893; G. Farrar and M. Losada, *Phys. Lett.* **B406** (1997) 60.

[89] B. de Carlos and J.R. Espinosa, *Nucl. Phys.* **B503** (1997) 24.

[90] D. Bodeker, P. John, M. Laine and M.G. Schmidt, *Nucl. Phys.* **B497** (1997) 387.

[91] M. Carena, M. Quiros and C. E. M. Wagner, Nucl. Phys. B **524**, 3 (1998) [arXiv:hep-ph/9710401].

[92] M. Laine, K. Rummukainen, *Nucl. Phys.* **B535** (1998) 423.

[93] M. Losada, *Nucl. Phys.* **B537** (1999) 3 and *Nucl. Phys.* **B569** (2000) 125; M. Laine and M. Losada, *Nucl. Phys.* **B582** (2000) 277.

[94] M. Laine and K. Rummukainen, *Nucl. Phys.* **B597** (2001) 23 [arXiv:hep-lat/0009025].

[95] M. Quiros, Nucl. Phys. Proc. Suppl. **101**, 401 (2001) [arXiv:hep-ph/0101230].

[96] J. M. Moreno, M. Quiros and M. Seco, Nucl. Phys. B **526**, 489 (1998) [arXiv:hep-ph/9801272].

[97] A. G. Cohen, D. B. Kaplan and A. E. Nelson, Phys. Lett. B **336**, 41 (1994) [arXiv:hep-ph/9406345].

[98] I. Affleck, Phys. Rev. Lett. **46**, 388 (1981).

[99] M. Joyce, T. Prokopec and N. Turok, Phys. Rev. D **53**, 2930 (1996) [arXiv:hep-ph/9410281]; M. Joyce, T. Prokopec and N. Turok, Phys. Rev. D **53**, 2958 (1996) [arXiv:hep-ph/9410282].

[100] P. Huet and A. E. Nelson, Phys. Rev. D **53**, 4578 (1996) [arXiv:hep-ph/9506477].

[101] M. Carena, M. Quiros, M. Seco and C. E. M. Wagner, Nucl. Phys. B **650**, 24 (2003) [arXiv:hep-ph/0208043].

[102] J. M. Cline, M. Joyce and K. Kainulainen, JHEP **0007**, 018 (2000) [arXiv:hep-ph/0006119];

[103] C. Lee, V. Cirigliano and M. J. Ramsey-Musolf, Phys. Rev. D **71**, 075010 (2005) [arXiv:hep-ph/0412354].

[104] A. N. Redlich and L. C. R. Wijewardhana, Phys. Rev. Lett. **54**, 970 (1985).

[105] R. N. Mohapatra and X. m. Zhang, Phys. Rev. D **45**, 2699 (1992).

[106] C. Balazs, M. Carena and C. E. M. Wagner, Phys. Rev. D **70**, 015007 (2004) [arXiv:hep-ph/0403224].

[107] J. R. Espinosa, M. Quiros and F. Zwirner, Phys. Lett. B **307**, 106 (1993) [arXiv:hep-ph/9303317].

[108] A. Brignole, J. R. Espinosa, M. Quiros and F. Zwirner, Phys. Lett. B **324**, 181 (1994) [arXiv:hep-ph/9312296]; D. Comelli and J. R. Espinosa, Phys. Rev. D **55**, 6253 (1997) [arXiv:hep-ph/9606438].

[109] M. Carena, M. Quiros and C. E. M. Wagner, Phys. Lett. B **380**, 81 (1996) [arXiv:hep-ph/9603420].

[110] N.S. Manton, *Phys. Rev.* **D28** (1983) 2019; F.R. Klinkhamer and N.S. Manton, *Phys. Rev.* **D30** (1984) 2212.

[111] D. Bodeker, *Phys. Lett.* **B426** (1998) 351 [arXiv:hep-ph/9801430]; P. Arnold and L.G. Yaffe, hep-ph/9912306; P. Arnold, *Phys. Rev.* **D62** (2000) 036003; G.D. Moore and K. Rummukainen, *Phys. Rev.* **D61** (2000) 105008; G.D. Moore, *Phys. Rev.* **D62** (2000) 085011.

[112] K. Jansen, *Nucl. Phys.* **B Proc. Suppl. 47** (1996) 196, hep-lat/9509018; K. Rummukainen, M. Tsypin, K. Kajantie, M. Laine and M. Shaposhnikov, *Nucl. Phys.* **B532** (1998) 283; K. Rummukainen, K. Kajantie, M. Laine, M. Shaposhnikov and M. Tsypin, hep-ph/9809435.

[113] M. Pietroni, Nucl. Phys. B **402**, 27 (1993) [arXiv:hep-ph/9207227].

[114] A. T. Davies, C. D. Froggatt and R. G. Moorhouse, Phys. Lett. B **372**, 88 (1996) [arXiv:hep-ph/9603388].

[115] S. J. Huber and M. G. Schmidt, Nucl. Phys. B **606**, 183 (2001) [arXiv:hep-ph/0003122].

[116] M. Bastero-Gil, C. Hugonie, S. F. King, D. P. Roy and S. Vempati, Phys. Lett. B **489**, 359 (2000) [arXiv:hep-ph/0006198].

[117] J. Kang, P. Langacker, T. j. Li and T. Liu, Phys. Rev. Lett. **94**, 061801 (2005) [arXiv:hep-ph/0402086].

[118] C. Grojean, G. Servant and J. D. Wells, Phys. Rev. D **71**, 036001 (2005) [arXiv:hep-ph/0407019].

[119] M. Carena, A. Megevand, M. Quiros and C. E. M. Wagner, Nucl. Phys. B **716**, 319 (2005) [arXiv:hep-ph/0410352].

[120] M. Carena, M. Quiros, A. Riotto, I. Vilja and C. E. M. Wagner, Nucl. Phys. B **503**, 387 (1997) [arXiv:hep-ph/9702409];

[121] M. Carena, J. M. Moreno, M. Quiros, M. Seco and C. E. M. Wagner, Nucl. Phys. B **599**, 158 (2001) [arXiv:hep-ph/0011055].

[122] M. E. Gomez, T. Ibrahim, P. Nath and S. Skadhauge, Phys. Rev. D **70**, 035014 (2004) [arXiv:hep-ph/0404025].

[123] A. Pilaftsis, Phys. Rev. **D58** (1998) 096010 and Phys. Lett. **B435** (1998) 88; A. Pilaftsis and C.E.M. Wagner, Nucl. Phys. **B553** (1999) 3; D.A. Demir, Phys. Rev. **D60** (1999) 055006; S.Y. Choi, M. Drees and J.S. Lee, Phys. Lett. **B481** (2000) 57; M. Carena, J. Ellis, A. Pilaftsis and C.E.M. Wagner, Nucl. Phys. **B586** (2000) 92; G.L. Kane and L.-T. Wang, Phys. Lett. **B488** (2000) 383; S.Y. Choi and J.S. Lee, Phys. Rev. **D61** (2000) 015003; S.Y. Choi, K. Hagiwara and J.S. Lee, Phys. Rev. **D64** (2001) 032004; S. Y. Choi, M. Drees, J. S. Lee and J. Song, Eur. Phys. J. C **25** (2002) 307; T. Ibrahim and P. Nath, Phys. Rev. **D63** (2001) 035009; Phys. Rev. **D66** (2002) 015005; T. Ibrahim, Phys. Rev. **D64** (2001) 035009; S. W. Ham, S. K. Oh, E. J. Yoo, C. M. Kim and D. Son, hep-ph/0205244; M. Carena, J. Ellis, A. Pilaftsis and C.E.M. Wagner, Phys. Lett. **B495** (2000) 155; S. Heinemeyer, Eur. Phys. J. C **22** (2001) 521; M. Carena, J. Ellis, S. Mrenna, A. Pilaftsis and C.E.M. Wagner, Nucl. Phys. B **659**, 145 (2003) J. S. Lee, A. Pilaftsis, M. Carena, S. Y. Choi, M. Drees, J. R. Ellis and C. E. M. Wagner, Comput. Phys. Commun. **156**, 283 (2004) [arXiv:hep-ph/0307377].

[124] R. Hempfling, Phys. Rev. **D49** (1994) 6168; L. Hall, R. Rattazzi and U. Sarid, Phys. Rev. **D50** (1994) 7048; M. Carena, M. Olechowski, S. Pokorski and C.E.M. Wagner, Nucl. Phys. **B426** (1994) 269; D. Pierce, J. Bagger, K. Matchev and R. Zhang, Nucl. Phys. **B491** (1997) 3; M. Carena, D. Garcia, U. Nierste and C. E. M. Wagner, Nucl. Phys. B **577**, 88 (2000).

[125] A. Pilaftsis, Nucl. Phys. B **644**, 263 (2002) [arXiv:hep-ph/0207277].

[126] B. C. Regan, E. D. Commins, C. J. Schmidt and D. DeMille, Phys. Rev. Lett. **88**, 071805 (2002).

[127] S. Abel, S. Khalil and O. Lebedev, Nucl. Phys. B **606**, 151 (2001) [arXiv:hep-ph/0103320].

[128] A. G. Cohen, D. B. Kaplan and A. E. Nelson, Phys. Lett. B **388**, 588 (1996) [arXiv:hep-ph/9607394].

[129] J. L. Feng, K. T. Matchev and T. Moroi, Phys. Rev. D **61**, 075005 (2000) [arXiv:hep-ph/9909334].

[130] N. Arkani-Hamed, S. Dimopoulos, G. F. Giudice and A. Romanino, Nucl. Phys. B **709**, 3 (2005) [arXiv:hep-ph/0409232].

[131] D. Chang, W. F. Chang and W. Y. Keung, Phys. Rev. D **66**, 116008 (2002) [arXiv:hep-ph/0205084].

[132] LEP2 SUSY Working Group *Combined LEP Chargino Results, up to 208 GeV*, `http://lepsusy.web.cern.ch/lepsusy/www/inos_moriond01/charginos_pub.html`.

[133] H. Murayama and A. Pierce, Phys. Rev. D **67**, 071702 (2003) [arXiv:hep-ph/0201261].

[134] S. Bertolini, F. Borzumati, A. Masiero and G. Ridolfi, Nucl. Phys. B **353**, 591 (1991).

[135] R. Barbieri and G. F. Giudice, Phys. Lett. B **309**, 86 (1993) [arXiv:hep-ph/9303270].

[136] M. Ciuchini, G. Degrassi, P. Gambino and G. F. Giudice, Nucl. Phys. B **534**, 3 (1998) [arXiv:hep-ph/9806308].

[137] G. Degrassi, P. Gambino and G. F. Giudice, JHEP **0012**, 009 (2000) [arXiv:hep-ph/0009337].

[138] M. Carena, D. Garcia, U. Nierste and C. E. M. Wagner, Phys. Lett. B **499**, 141 (2001) [arXiv:hep-ph/0010003].

[139] F. Gabbiani, E. Gabrielli, A. Masiero and L. Silvestrini, Nucl. Phys. B**477** (1996) 321; K. i. M. Okumura and L. Roszkowski, JHEP **0310**, 024 (2003) [arXiv:hep-ph/0308102].

[140] R. Barate et al. [ALEPH Collaboration], *Phys. Lett.* **B 429** (1998) 169; S. Chen et al. [CLEO Collaboration], *Phys. Rev. Lett.* **87** (2001) 251807, hep-ex/0108032; K. Abe et al. [Belle Collaboration], *Phys. Lett.* **B 511** (2001) 151, hep-ex/0103042; P. Koppenburg et al. [Belle Collaboration], *Phys. Rev. Lett.* **93** (2004) 061803, hep-ex/0403004; B. Aubert et al. [BABAR Collaboration], hep-ex/0207074; hep-ex/0207076.

[141] T. Falk, K. A. Olive and M. Srednicki, Phys. Lett. B **354**, 99 (1995) [arXiv:hep-ph/9502401].

[142] P. Gondolo and K. Freese, JHEP **0207**, 052 (2002) [arXiv:hep-ph/9908390].

[143] M. Argyrou, A. B. Lahanas, D. V. Nanopoulos and V. C. Spanos, Phys. Rev. D **70**, 095008 (2004) [Erratum-ibid. D **70**, 119902 (2004)] [arXiv:hep-ph/0404286].

[144] H. Baer, C. Balázs and A. Belyaev, JHEP **0203**, 042 (2002) [arXiv:hep-ph/0202076].

[145] P. Gondolo, J. Edsjo, P. Ullio, L. Bergstrom, M. Schelke and E. A. Baltz, JCAP **0407**, 008 (2004) [arXiv:astro-ph/0406204].

[146] S. Katsanevas and P. Morawitz, Comput. Phys. Commun. **112**, 227 (1998) [arXiv:hep-ph/9711417].

[147] J. F. Gunion, H. E. Haber, G. L. Kane and S. Dawson, *The Higgs Hunter's Guide*, Addison-Wesley, Redwood City, USA (1990).

[148] I. G. Irastorza *et al.* [IGEX Collaboration], Talk given at 4th International Workshop on the Identification of Dark Matter (IDM 2002), York, England, 2-6 Sep 2002, [astro-ph/0211535].

[149] H. V. Klapdor-Kleingrothaus, A. Dietz, G. Heusser, I. V. Krivosheina, D. Mazza, H. Strecker and C. Tomei, Astropart. Phys. **18**, 525 (2003) [arXiv:hep-ph/0206151].

[150] D. Abrams *et al.* [CDMS Collaboration], Phys. Rev. D **66**, 122003 (2002) [arXiv:astro-ph/0203500].

[151] A. Benoit *et al.*, Phys. Lett. B **545**, 43 (2002) [arXiv:astro-ph/0206271].

[152] H. V. Klapdor-Kleingrothaus, Nucl. Phys. Proc. Suppl. **110**, 364 (2002) [arXiv:hep-ph/0206249].

[153] R. Bernabei *et al.*, Nucl. Phys. Proc. Suppl. **124**, 181 (2003) [arXiv:astro-ph/0205047].

[154] N. Spooner, in *Proc. of the APS/DPF/DPB Summer Study on the Future of Particle Physics (Snowmass 2001)* ed. N. Graf, eConf **C010630**, E601 (2001).

[155] D. Cline *et al.*, *Prepared for 3rd International Conference on Dark Matter in Astro and Particle Physics (Dark 2000), Heidelberg, Germany, 10-16 Jul 2000*

[156] J. Dawson *et al.*, Nucl. Phys. Proc. Suppl. **110**, 109 (2002).

[157] D. B. Cline, H. g. Wang and Y. Seo, in *Proc. of the APS/DPF/DPB Summer Study on the Future of Particle Physics (Snowmass 2001)* ed. N. Graf, eConf **C010630**, E108 (2001) [arXiv:astro-ph/0108147].

[158] E. Aprile *et al.*, Nucl. Phys. Proc. Suppl. **138**, 156 (2005) [arXiv:astro-ph/0407575].

[159] N. J. C. Spooner [UKDM and Boulby Collaborations], *Prepared for International Workshop on Technique and Application of Xenon Detectors, Kashiwa, Japan, 3-4 Dec 2001*

[160] N. Spooner, in *Proc. of the APS/DPF/DPB Summer Study on the Future of Particle Physics (Snowmass 2001)* ed. N. Graf, eConf **C010630**, P401 (2001).

[161] J. I. Collar, J. Puibasset, T. A. Girard, D. Limagne, H. S. Miley and G. Waysand, New J. Phys. **2**, 14 (2000) [arXiv:astro-ph/0005059].

[162] N. Boukhira *et al.*, Nucl. Phys. Proc. Suppl. **110**, 103 (2002).

[163] H. Baer, C. Balázs, A. Belyaev and J. O'Farrill, JCAP **0309**, 007 (2003) [arXiv:hep-ph/0305191].

[164] S. Y. Choi, S. C. Park, J. H. Jang and H. S. Song, Phys. Rev. D **64**, 015006 (2001) [arXiv:hep-ph/0012370].

[165] T. Nihei and M. Sasagawa, Phys. Rev. D **70**, 055011 (2004) [Erratum-ibid. D **70**, 079901 (2004)] [arXiv:hep-ph/0404100].

[166] D. S. Akerib *et al.* [CDMS Collaboration], Phys. Rev. Lett. **93**, 211301 (2004) [arXiv:astro-ph/0405033].

[167] L. Baudis [CDMS Collaboration], eConf **C020805**, TF02 (2002).

[168] D. B. Cline *et al.*, Nucl. Phys. Proc. Suppl. **124**, 229 (2003).

[169] E. Aprile, talk given at the 6th UCLA Symposium on Sources and Detection of Dark Matter and Dark Energy in the Universe, February 18-20, 2004 at the Marina Beach Marriott, Marina del Rey, California (http://www.physics.ucla.edu/hep/dm04/talks/aprile.pdf)

[170] J. R. Ellis, A. Ferstl and K. A. Olive, Phys. Rev. D **63**, 065016 (2001) [arXiv:hep-ph/0007113].

[171] R. Demina, J. D. Lykken, K. T. Matchev and A. Nomerotski, Phys. Rev. D **62**, 035011 (2000);

[172] S. Y. Choi, J. S. Shim, H. S. Song and W. Y. Song, [arXiv:hep-ph/9808227];
S. Y. Choi, A. Djouadi, M. Guchait, J. Kalinowski, H. S. Song and P. M. Zerwas, Eur. Phys. J. C **14**, 535 (2000) [arXiv:hep-ph/0002033];
V. D. Barger, T. Falk, T. Han, J. Jiang, T. Li and T. Plehn, Phys. Rev. D **64**, 056007 (2001) [arXiv:hep-ph/0101106].

[173] A. Bartl, S. Hesselbach, K. Hidaka, T. Kernreiter and W. Porod, arXiv:hep-ph/0306281.

[174] M. Carena, A. Finch, A. Freitas, C. Milstene, H. Novak and A. Sopczak, in preparation.

[175] See, for example, G. F. Giudice and A. Masiero, Phys. Lett. B **206**, 480 (1988).

[176] P. Fayet, Nucl. Phys. **B90** (1975) 104; H.-P. Nilles, M. Srednicki and D. Wyler, Phys. Lett. **B120** (1983) 346; J.-M. Frere, D.R.T. Jones and S. Raby, Nucl. Phys. **B222** (1983) 11; J.-P. Derendinger and C.A. Savoy, Nucl. Phys. **B237** (1984) 307; B.R. Greene and P.J. Miron, Phys. Lett. **B168** (1986) 226; J. Ellis, K. Enqvist and D.V. Nanopoulos, K.A. Olive, M. Quiros and F. Zwirner, Phys. Lett. **B176** (1986) 403; L. Durand and J.L. Lopez, Phys. Lett. **B217** (1989) 463; M. Drees, Int. J. Mod. Phys. **A4** (1989) 3635; U. Ellwanger, Phys. Lett. **B303** (1993) 271; U. Ellwanger, M. Rausch de Taubenberg and C.A. Savoy, Phys. Lett. **B315** (1993) 331; Z. Phys. **C67** (1995) 665; Nucl. Phys. **B492** (1997) 21; P.N. Pandita, Phys. Lett. **B318** (1993) 338; Z. Phys. **C59** (1993) 575; T. Elliott, S.F. King and P.L. White, Phys. Lett. **B305** (1993) 71; Phys. Lett. **B314** (1993) 56; Phys. Rev. **D49** (1994) 2435; Phys. Lett. **B351** (1995) 213; K.S. Babu and S.M. Barr, Phys. Rev. **D49** (1994) R2156; S.F. King and P.L. White, Phys. Rev. **D52** (1995) 4183; N. Haba, M. Matsuda and M. Tanimoto, Phys. Rev. **D54** (1996) 6928; F. Franke and H. Fraas, Int. J. Mod. Phys. **A12** (1997) 479; S.W. Ham, S.K. Oh and H.S. Song, Phys. Rev. **D61** (2000) 055010; D.A. Demir, E. Ma and U. Sarkar, J. Phys. **G26** (2000) L117; R. B. Nevzorov and M. A. Trusov, Phys. Atom. Nucl. **64** (2001) 1299; U. Ellwanger and C. Hugonie, Eur. Phys. J. **C25** (2002) 297; U. Ellwanger, J. F. Gunion, C. Hugonie and S. Moretti, arXiv:hep-ph/0305109; D. J. Miller and S. Moretti, arXiv:hep-ph/0403137.

[177]

[177] S. A. Abel, S. Sarkar and P. L. White, Talk given at International Workshop on Elementary Particle Physics: Present and Future, Valencia, Spain, 5-9 Jun 1995. Published in Valencia Elem.Part.Phys. (1995), [arXiv:hep-ph/9507333].

[178] S. A. Abel, S. Sarkar and P. L. White, Nucl. Phys. B **454**, 663 (1995) [arXiv:hep-ph/9506359].

[179] J. Bagger and E. Poppitz, Phys. Rev. Lett. **71**, 2380 (1993) [arXiv:hep-ph/9307317]; J. Bagger, E. Poppitz and L. Randall, Nucl. Phys. B **455**, 59 (1995) [arXiv:hep-ph/9505244] S. A. Abel, Nucl. Phys. B **480**, 55 (1996) [arXiv:hep-ph/9609323].

[180] C. Panagiotakopoulos and K. Tamvakis, Phys. Lett. B **469**, 145 (1999) [arXiv:hep-ph/9908351]; C. Panagiotakopoulos and K. Tamvakis, Phys. Lett. B **446**, 224 (1999) [arXiv:hep-ph/9809475].

[181] C. Panagiotakopoulos and A. Pilaftsis, Phys. Rev. D **63**, 055003 (2001) [arXiv:hep-ph/0008268].

[182] A. Dedes, C. Hugonie, S. Moretti and K. Tamvakis, Phys. Rev. D **63**, 055009 (2001) [arXiv:hep-ph/0009125].

[183] R. Harnik, G. D. Kribs, D. T. Larson and H. Murayama, Phys. Rev. D **70**, 015002 (2004) [arXiv:hep-ph/0311349].

[184] J. R. Ellis, J. F. Gunion, H. E. Haber, L. Roszkowski and F. Zwirner, Phys. Rev. D **39**, 844 (1989).

[185] J. C. Romao, Phys. Lett. B **173**, 309 (1986).

[186] G. Abbiendi *et al.* [OPAL Collaboration], Eur. Phys. J. C **35**, 1 (2004) [arXiv:hep-ex/0401026].

[187] [LEP Collaborations], by LEP Collaborations and ALEPH Collaboration and DELPHI Collaboration and L3 Collaboration and OPAL Collaboration and Line Shape Sub-Group of the LEP Electroweak Working Group, CERN-EP-2000-153 (2000), submitted to Phys. Rept. [arXiv:hep-ex/0101027].

[188] J. R. Espinosa and M. Quiros, Phys. Lett. B **279**, 92 (1992).

[189] [LEP Higgs Working Group for Higgs boson searches Collaboration], By LEP Higgs Working Group for Higgs boson searches and ALEPH Collaboration and DELPHI Collaboration and L3 Collaboration and OPAL Collaboration. LHWG-NOTE-2001-05, ALEPH-2001-043, PHYSICS-2001-016, DELPHI-2001-115, CERN-L3-NOTE-2689, OPAL-TN-696 (2001), [arXiv:hep-ex/0107031].

[190] [LEP Higgs Working Group Collaboration], by LEP Higgs Working Group and ALEPH collaboration and DELPHI collaboration and L3 collaboration and OPAL Collaboration. LHWG-NOTE-2001-04, ALEPH-2001-057, DELPHI-2001-114, L3-NOTE-2700, OPAL-TN-699 (2001), [arXiv:hep-ex/0107030].

[191] [LEP Higgs Working for Higgs boson searches Collaboration], by LEP Higgs Working for Higgs boson searches and ALEPH Collaboration and DELPHI Collaboration and CERN-L3 Collaboration and OPAL Collaboration. LHWG-NOTE-2001-06, ALEPH-2001-036, DELPHI-2001-116, L3-NOTE-2702, OPAL-TN-694, (2001), [arXiv:hep-ex/0107032].

[192] K. A. Olive and D. Thomas, Nucl. Phys. B **355**, 192 (1991).

[193] K. Griest, Phys. Rev. D **38**, 2357 (1988) [Erratum-ibid. D **39**, 3802 (1989)].

[194] D. Choudhury and D. P. Roy, Phys. Lett. B **322**, 368 (1994) [arXiv:hep-ph/9312347]; J. F. Gunion, Phys. Rev. Lett. **72**, 199 (1994) [arXiv:hep-ph/9309216].

[195] O. J. P. Eboli and D. Zeppenfeld, Phys. Lett. B **495**, 147 (2000) [arXiv:hep-ph/0009158];

[196] D. Cavalli *et al.*, in *Les Houches 2001, Physics at TeV Colliders*, CERN, Switzerland (2001), [arXiv:hep-ph/0203056].

[197] M. Dittmar, Pramana **55**, 151 (2000);

[198] J. Polchinski, *String Theory Vol. 1: An Introduction to the Bosonic String*, Cambridge University Press, Cambridge, UK (1998).

[199] H. Lehmann, K. Symanzik and W. Zimmermann, Nuovo Cim. **1** (1955) 205.

[200] R. H. Brandenberger, Rev. Mod. Phys. **57**, 1 (1985).